VIBRATION FATIGUE ANALYSIS AND TESTING OF NOTCHED BEAMS

A THESIS SUBMITTED TO
THE GRADUATE SCHOOL OF NATURAL AND APPLIED SCIENCES
OF
MIDDLE EAST TECHNICAL UNIVERSITY

BY

GÜRZAP İSMAİL DEMİREL

IN PARTIAL FULFILLMENT OF THE REQUIREMENTS
FOR
THE DEGREE OF MASTER OF SCIENCE
IN
AEROSPACE ENGINEERING

MAY 2019

Approval of the thesis:

VIBRATION FATIGUE ANALYSIS AND TESTING OF NOTCHED BEAMS

submitted by **GÜRZAP İSMAİL DEMİREL** in partial fulfillment of the requirements for the degree of **Master of Science in Aerospace Engineering Department, Middle East Technical University** by,

Prof. Dr. Halil Kalıpçılar
Dean, Graduate School of **Natural and Applied Sciences** _____

Prof. Dr. İsmail Hakkı Tuncer
Head of Department, **Aerospace Engineering** _____

Prof. Dr. Altan Kayran
Supervisor, **Aerospace Engineering, METU** _____

Examining Committee Members:

Assoc. Prof. Dr. Demirkan ÇÖKER
Aerospace Engineering, METU _____

Prof. Dr. Altan Kayran
Aerospace Engineering, METU _____

Prof. Dr. Erdem Acar
Mechanical Engineering, TOBB ETU _____

Assoc. Prof. Dr. Ercan Gürses
Aerospace Engineering, METU _____

Assist. Prof. Dr. Tuncay Yalçınkaya
Aerospace Engineering, METU _____

Date: 31.05.2019

I hereby declare that all information in this document has been obtained and presented in accordance with academic rules and ethical conduct. I also declare that, as required by these rules and conduct, I have fully cited and referenced all material and results that are not original to this work.

Name, Surname: Gürzap İsmail Demirel

Signature:

ABSTRACT

VIBRATION FATIGUE ANALYSIS AND TESTING OF NOTCHED BEAMS

Demirel, Gürzap İsmail
Master of Science, Aerospace Engineering
Supervisor: Prof. Dr. Altan Kayran

May 2019, 91 pages

Mechanical fatigue is an important phenomenon when the structures are exposed to dynamic, fluctuating loadings. Especially aerospace structures are commonly exposed to random vibration loadings. Even if the components are stable and durable for static requirements, vibration fatigue failures can occur due to the dynamic and fluctuating loadings. Moreover, if the loading frequency has a wide bandwidth as in random vibration loadings, the natural frequencies or resonance regions of the structures are disturbed with high probability. Therefore, in this thesis, vibration fatigue is studied both numerically and experimentally.

The main focus of this thesis study is the research of the vibration fatigue. Hence, besides the analyses, the tests are conducted. In order to study the analyses and tests, aluminum and steel rectangular cross-section beams are designed and manufactured. In order to obtain a more distinct fatigue life than other parts of the beams, the notched areas added to beam geometry. Firstly, in order to ensure the reliability of the finite element model, mesh refinement works are conducted. Then, to decide the frequency interval of the analyses, modal analyses are carried out. Moreover, in order to obtain the appropriate damping ratios of the notched beams, which are an input of frequency response analysis, modal tests are carried out. Then, frequency response analysis of the beams are conducted. After that, vibration fatigue analyses are conducted.

Furthermore, the effect of different damping ratio values is investigated in the analyses. Finally, the vibration fatigue tests of notched beams are conducted.

Keywords: Vibration Fatigue, Damping Ratio, Finite Element Method

ÖZ

ÇENTİKLİ ÇUBUKLARIN TİTREŞİMSEL YORULMA ANALİZİ VE TESTİ

Demirel, Gürzap İsmail
Yüksek Lisans, Havacılık ve Uzay Mühendisliği
Tez Danışmanı: Prof. Dr. Altan Kayran

Mayıs 2019, 91 sayfa

Mekanik Yorulma, yapılar dinamik ve dalgalı yüklere maruz kaldığında önem kazanan bir olgudur. Özellikle havacılık ve uzay yapıları yaygın olarak rastgele titreşim yüklerine maruz kalmaktadır. Parçalar statik gereksinimler için kararlı ve dayanıklı olsa bile dinamik ve dalgalı yükler nedeniyle titreşim kaynaklı yorulma hasarları oluşabilir. Dahası, yükleme frekansı rastgele titreşim yüklerinde olduğu gibi geniş bir bant aralığına sahipse, yüksek olasılıkla yapıların doğal frekansları veya rezonans bölgeleri uyarılabilir. Bu nedenle, bu tez çalışmasında titreşimsel yorulma hem sayısal hem de deneysel olarak çalışılmıştır.

Bu tez çalışmasının temel odağı, titreşimsel yorulma konusunun araştırılmasıdır. Bu nedenle, analizlerin yanısıra testler de yapılmıştır. Analiz ve test çalışmalarını incelemek için, alüminyum ve çelik dikdörtgen kesitli çubuklar tasarlanmış ve ürettirilmiştir. Çubukların belli bir bölgesine, diğer bölgelerine göre daha belirgin bir yorulma ömrü elde etmek için çentikli kısımlar çubuk geometrisine eklenmiştir. Ilk olarak, sonlu eleman modelinin güvenilirliğini sağlamak için ağ yapısı iyileştirme çalışmaları yapılmıştır. Ardından, analizlerin frekans aralığına karar vermek için modal analizler yapılmıştır. Dahası, frekans cevabı analizlerinin bir girdisi olan çentikli çubukların uygun sönümleme katsayılarını belirlemek için modal testler

yapılmıştır. Ondan sonra, çubukların frekans cevabı analizleri yapılmıştır. Daha sonra titreşim yorulma analizleri gerçekleştirilmiştir. Ayrıca, farklı sönümleme oranlarının analizlere etkisi incelenmiştir. Son olarak, çentikli çubukların titreşimsel yorulma testleri gerçekleştirilmiştir.

Anahtar Kelimeler: Titreşimsel Yorulma, Sönümleme Oranı, Sonlu Eleman Metodu

To my beloved family…

ACKNOWLEDGEMENTS

I am very thankful to my university, METU, and my thesis supervisor, Prof. Dr. Altan KAYRAN, whose valuable guidance, technical support and contributions throughout this study enabled me to complete this thesis work successfully.

I am also grateful to my workplace TÜBİTAK SAGE, my work package leader, Özlem SÖKMEN, my superior, Dr. Ümit CEYHAN, my project manager, Osman BAŞOĞLU, and my expert co-workers, Burak DURAK, Özlem Deniz OYGÜR, Özgür Sinan OYGÜR, Ercan ZENGİN, Taylan KARAAĞAÇLI, Oğuzhan KOCA, Emre OKUR, Ali Murat GÜLTEKİN, Ahmet AK, Nuri BIÇAKÇI and Hasan İNCİ. Moreover, I am also deeply thankful to my close friends and co-workers Nabi Vefa YAVUZTÜRK and Yaşar PAÇA for his continuous support and being there for me all the time.

I would like to also express my deepest gratitude to my family for their encouragements and understanding throughout this study.

TABLE OF CONTENTS

LIST OF TABLES

TABLES

LIST OF FIGURES

FIGURES

CHAPTER 1

INTRODUCTION

1.1. Fatigue

Fatigue phenomenon is related to wide range of disciplines such as biology, medical, sports, safety, transportation, computers, materials, engineering etc. Mainly it deals with the integrity of the system against to the repeated actions, mechanical loads, movements, heat energy or absorption etc. In this thesis, the mechanical vibration fatigue subject is studied.

1.2. Mechanical Fatigue

From the beginning of civilization, humankind has been aware of the fact that the repeated loads break the materials even though the load level is way below the strength of the material. The big fraction of the engineering components and structures works under repeated, fluctuating or cyclic loads. Although the level of the loading is not high enough to damage the structure or component immediately, mechanical fatigue failure may occur in the long term even if the stresses below the yield strength of the material. Mechanical fatigue damage is defined as material failure occurring primarily due to the formation of cracks resulting from fluctuating loads that create alternating stresses in the structure. The well-known method of breaking the metal wire with repeated bending is a good example of metal fatigue. While bending the wire up and down, the fluctuating compression and tension stresses are created on top and bottom of the wire as shown in Figure 1-1.

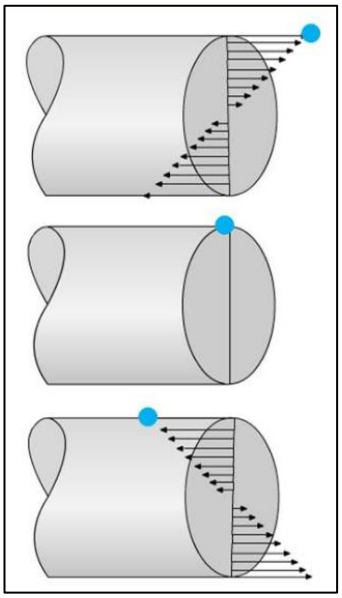

Figure 1-1: Fluctuating stresses on the bending metal wire cross-section

Among the first definitions of fatigue, one of the definitions was introduced by the International Organization for Standardization in 1964 in Geneva, American Society for Testing Materials in 1972, [1], as stated below:

"Fatigue is a process of progressive localized permanent structural changes occurring in a material subjected to conditions that produce fluctuating stresses at some point or points and that may culminate in cracks or complete fracture after a sufficient number of fluctuations."

Mechanical fatigue failure issue has been a major concern with the starts of the industry revolution. Nowadays especially the aerospace industry's increasing demands for durability, safety, reliability, long life and low cost lead in ultra-high interest in studies for improving the strength, quality, productivity, and longevity of components in aerospace engineering. Consequently, aerospace products should be designed and tested experimentally for sufficient fatigue resistance to satisfy the mechanical fatigue requirements [2]. Moreover, aerospace structures frequently encounter mechanical fatigue failures because the aerospace structures should be light in weight as much as possible. Due to the low weight requirement, the stresses in

aerospace structures are more severe than in other applications. Furthermore, aerospace structures are exposed to dynamic loads mainly due to the turbulent wind conditions in which they operate.

The fatigue process is unforeseen, as evidenced by the statistical scatter in the laboratory data in engineering [3]. Also, it is extremely difficult to accurately model the mechanical environment to which the system is exposed to over its entire service life. The environmental effects can produce complex stresses at fatigue-sensitive hot spots in the mechanical system. Due to the all uncertainties, difficulties, unpredictability and complexities, design engineers should carry on both analysis and experiments to make sure that the designed products fulfill the fatigue life requirements. Moreover, failure definitions in fatigue are subjective. It could be a crack initiation, predetermined crack length, fracture of the component or malfunction of a system. The designer should also decide on the failure criteria of the designed product.

1.3. History of Mechanical Fatigue

Over the last centuries, there are many engineering cases that are about the mechanical fatigue failures. In order to deal with this phenomenon, different techniques for fatigue analysis of structures are developed at a high rate within this time interval. The history of the mechanical fatigue phenomenon is briefly explained in the following.

The first mechanical fatigue phenomenon seems to have been reported by a German mining engineer, W. A. S. Albert who performed some repeated loading tests in 1829 on iron chain of the carrier wheeled vehicles, conveyors of the mine [3]. To make sure that the life of the conveyor chains used in Clausthal mines was enough, W. A. S. Albert designed a test machine.

The first known terrible accident of mechanical fatigue is the Versailles rail accident at 1842 in France, [4]. There were major losses of life due to fire of the follower carriages which pass over the broken engine of the train. The dramatic sketch of the accident is given in Figure 1-2.

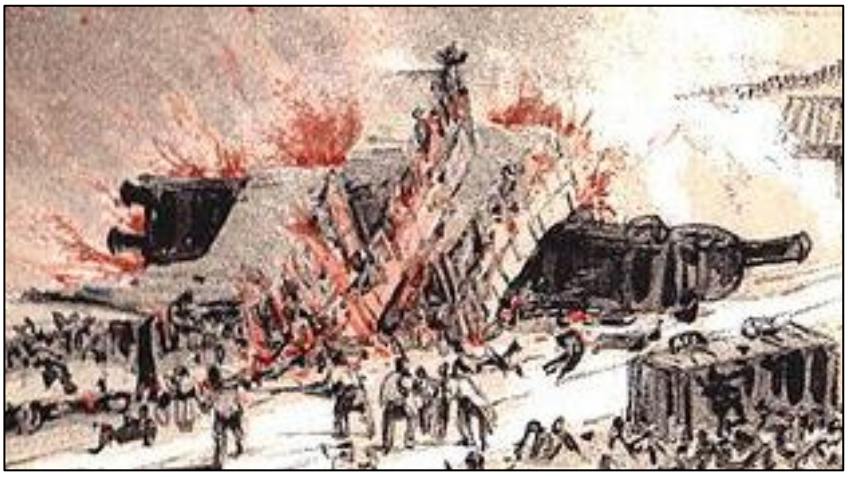

Figure 1-2: Versailles rail accident, [5]

With the development of the railway systems, fatigue failures in the railway axles became a common problem and this problem started to draw the first serious attention to the cyclic loading effects. This was the first time that many similar parts of machines had been exposed to millions of cycles at stress levels well below the yield strength, with documented service failures appearing with disturbing regularity. This theory was disparaged by W. J. Rankine in 1843. As is often done in the case of unexplained service failures, attempts were made to reproduce the failures in the laboratory. Between 1852 and 1869 the German railway engineer, August Wöhler set up and conducted the first systematic fatigue investigation [6].

In 1910, a log-log relationship for stress-cycle (S-N) curves is developed by O. H. Basquin by using Wöhler's study. In 1924, A. Palmgren propose a linear damage hypothesis and in 1945, A. M. Miner reorganized that hypothesis as a practical design tool, which is widely used as cumulative damage theory as explained in following chapters, [7].

A big tank which was full with molasses collapsed due to the mechanical fatigue in 1919. This disaster called as “The Boston Molasses Disaster” in the history. Near the manhole cover, the fatigue crack initiation and propagation to the critical size is main believed reason, [8]. The newspaper clipping of the disaster is given in Figure 1-3.

The Boston Daily Globe EXTRA

VOL XCV—NO. 16 BOSTON, THURSDAY MORNING, JANUARY 16. 1919—SIXTEEN PAGES PRICE TWO CENTS

MOLASSES TANK EXPLOSION INJURES 50 AND KILLS 11

SCENE OF RUIN AND DESOLATION IN NORTH END AFTER DESTRUCTION OF PURITY DISTILLING COMPANY TANK AND NEARBY STRUCTURES

Death and Devastation In Wake of North End Disaster

Buildings Demolished, Sticky Mass Floods Streets— Loss $500,000

Red Cross Women, Firemen and Sailors Do Heroic Work In Aiding Victims

LIST OF DEAD

DEAD AT NORTH GROVE STREET MORGUE

Figure 1-3: The newspaper clipping of The Boston Molasses Disaster, [9]

The "COMET" aircraft was in service in 1948 by Havilland, United Kingdom. This aircraft was the first commercial aircraft and it had very clean aerodynamic design. However, after the few years of flight, the COMET encountered mechanical fatigue problems. Two COMET aircraft had accidents in 1954, [10]. One of the illustrations is given in Figure 1-4.

Figure 1-4: COMET aircraft crash illustration, [11]

In 1980, at the North Sea, the off-shore hotel platform “Alexander L. Kielland” capsized. 123 lives had been lost when one of the five column legs separated from the rest of the structure. One of the lower tubular bracings attached to this column had fatigue fracture failure, [12]. The photograph of the capsizing is given in Figure 1-5.

Figure 1-5: North Sea Alexander L. Kielland Oil Rig Collapse, [13]

In 1984, Campbell and Lahey conducted a survey of serious aircraft accidents involving fatigue fracture, [14]. Between 1927 and 1984, the reported total serious aircraft fatigue accident number is 1885. Also these accidents resulted in total 558 destroyed aircraft and 2240 fatalities.

In aerospace engineering, one of the most well-known accidents is the Aloha Airlines Flight 243 in 1988, [15]. One Boeing 737 aircraft belonging to Aloha Airlines is exposed to explosive decompression caused by mechanical fatigue at 24000 ft after 89680 flight cycles. In this accident, surprisingly there is one fatality only and 65 people got injured. The dramatic picture of the accident is given in Figure 1-6.

Figure 1-6: The Aloha Airlines Flight 243 accident, [2]

In June of 1998, 101 people were killed due to the train crash which is called as "Eschede Train Disaster". The mechanical fatigue was due to mono-block train wheel which was manufactured by single-cast. After the disaster, the wheel is modified to include a rubber damping ring which is 20 mm thick between the metal wheel rim and the wheel main body, [16]. The photograph of the disaster is given in Figure 1-7.

Figure 1-7: The photograph of the Eschede Train Disaster, [17]

Nowadays, the fatigue life analysis and test techniques of designed products are quite developed. There are many empirical, analytical, experimental and computational methods developed by the engineers and scientists to analyze the fatigue failure event.

1.4. Scope of the Thesis

Mechanical fatigue analyses and experiments can be carried out in time domain or frequency domain as explained in the following chapters. Today's delicate and advanced aerospace engineering structures are exposed to random vibration loads as well as other loads such as maneuvering or temperature etc. The random vibration loads can be examined and processed well in frequency domain rather than the time domain, [44]. One of the sample random vibration load graph is given in Figure 1-8.

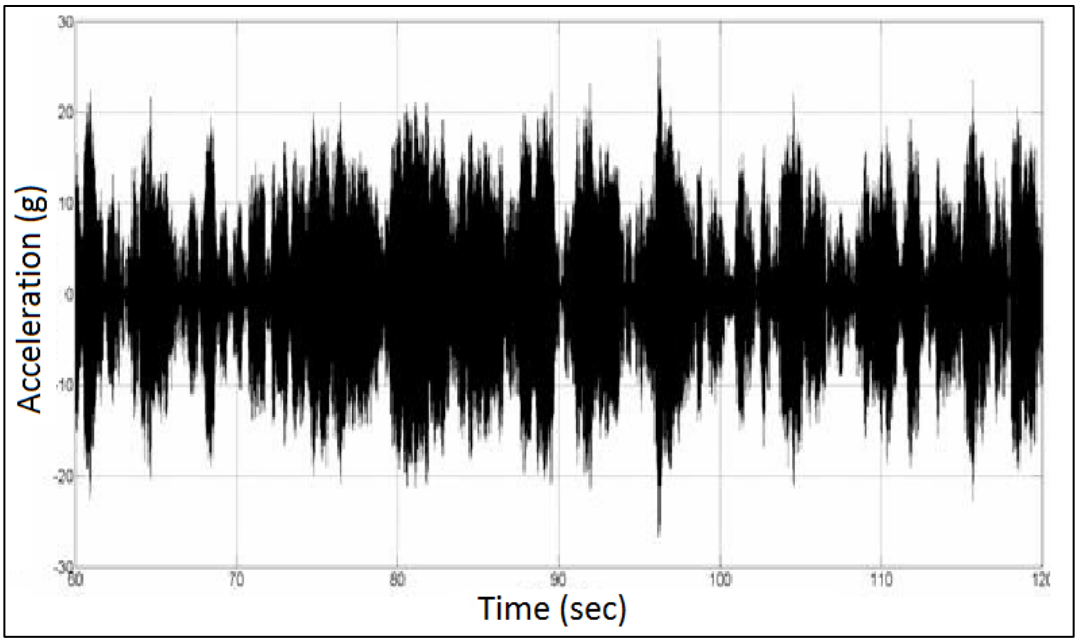

Figure 1-8: Sample random vibration load data, [18]

As seen in the Figure 1-8, the random vibration load data is very complicated because of the nature of it. It is very difficult and impractical to modify and process the random data in time domain. Instead of time domain, frequency domain fatigue analysis is suitable for handling the random vibration load data. For this reason, the frequency domain mechanical fatigue analysis is studied in this thesis.

This study contains the frequency domain mechanical fatigue analysis, which is also named as vibration fatigue analysis, of notched cantilever beams. Vibration fatigue tests of the beams are also conducted within the scope of the study. In chapter 1, definition of mechanical fatigue, some selected examples from the history of mechanical fatigue, literature survey and damage theories of mechanical fatigue are given. In chapter 2, theory of random vibration fatigue is introduced. Chapter 3 consists of vibration fatigue analysis and test of aluminum notched beams. Chapter 4 presents the vibration fatigue analysis and test of steel notched beams. And finally, chapter 5 is the result and the conclusion section.

1.5. Literature Survey

Time and frequency domain fatigue analysis techniques are studied by Bishop and he draws attention to the point that, when the loading frequency coincides with the natural frequencies of mechanical system, time domain approach comes short of the dynamic response of the structure in the resonance region [19]. In order to overcome the inefficiency of the dynamic behavior in the resonance region, the frequency domain approach should be preferred because in time domain, the transient dynamic analysis must be carried out to analyze the dynamic response of the structure in the resonance region and it is too much time consuming and impractical.

The damage accumulation rules are studied by Lio, [20]. Random vibration fatigue theory and Morrow's plastic work interaction damage rule is studied particularly. It is shown that the application of random vibration fatigue theory works very accurate with Morrow's plastic work interaction damage rule. However, iterations are required to find the material characteristics. Hence, Palmgren-Miner's rule is more favored in practice, and this method is explained in the following chapters, [21].

Also Fatemi and Yang state that the Palmgren-Miner LDR (linear damage rule) is dominantly used because more than 50 other fatigue damage models can be used in specific phenomenological factors. They state that the many damage models are

developed but none of them enjoys universal acceptance except the Palmgren-Miner rule, [22].

The frequency domain mechanical fatigue analysis is investigated by Halfpenny. Until that time, all the current methods were reviewed and the Dirlik method is recommended for frequency domain stress cycle counting, [23]. Also Bishop and Woodward state that the Dirlik method should be preferred, [19, 24, 42, 43].

1.6. Damage Theories

In this section, the types of fatigue analysis approaches are explained. As mentioned in previous sections, the mechanical fatigue is very sensitive to the type and amplitude of the loading because it substantially affects the stress-strain response of the structures. The types of approaches are Stress-Life, Strain-Life and Crack propagation. The Stress-Life (S-N) method is used when the stresses are below the yield strength of the material of the structures. The Strain-Life (E-N) method is used when the stresses are above the yield strength of the materials of the structures. The S-N method should be used until the crack initiation, because in the crack propagation region, this method is not sufficient. The E-N method should be used when there is plastic deformation. The Crack propagation approach or the Linear Elastic Fracture Mechanics (LEFM) is used when the components or structures are exposed to crack propagation. In this study, the S-N method is explained in detail but the E-N and LEFM methods are briefly discussed because the vibration fatigue analysis theory uses the S-N method.

1.6.1. Stress-Life (S-N) Method

The S-N method is the oldest and the most widely used fatigue damage approach because it is more practical than other methods and there are many stress versus life information for different materials in the literature. This method is valid in the elastic region of the material's strength. In other words, all stresses, even the local stresses, are lower than the yield strength of the material. Moreover, due to the nature of the materials and low stresses, the high cycle fatigue phenomenon is valid. In high cycle

fatigue, the number of stress cycles is more than 10^4 approximately, [3]. This regime can be associated with lower loads and longer life, or high number of cycles to produce fatigue failure. As the loading amplitude is decreased, the number of cycles for fatigue failure increases.

As mentioned previously following the well-known work of Wöhler in the 1850's, engineers have employed curves of stress versus cycles to fatigue failure, which are often called S-N (stress versus number of cycles) curves or the Wöhler's curves, [25]. These curves are extracted from the unnotched specimens. The principal S-N curves is the plot of alternating stress, S_a, versus the number of cycles to fatigue failure, N. Typical S-N curve of a metal material is given in Figure 1-9.

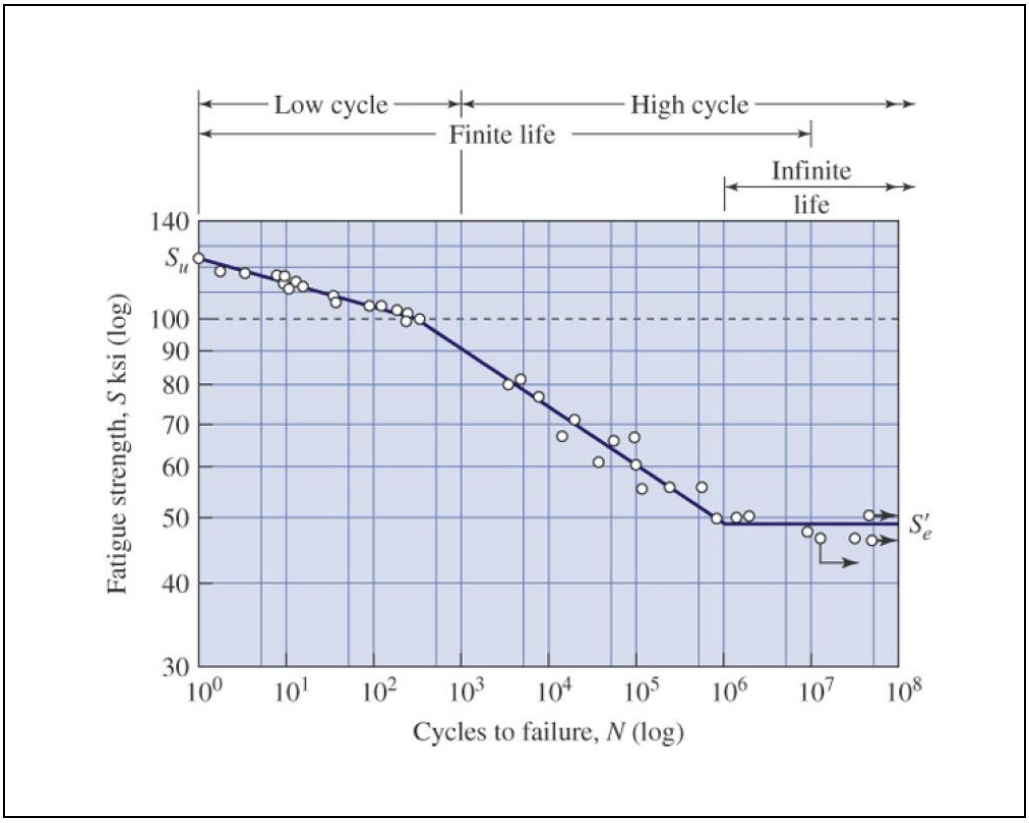

Figure 1-9: Typical S-N curves of the metal materials, [3,26]

The relations between the stress and cycles can be illustrated as in Figure 1-10, where S_a is the alternating stress amplitude, S_r is the stress range, S_{max} is the maximum stress amplitude, S_{min} is the minimum stress amplitude, S_m is the mean stress. Stress ratio R

is the ratio of the minimum stress amplitude to the maximum stress amplitude. The zero mean fluctuating stress graphs has an R value of -1 but the non-zero mean fluctuating stress graphs has R values different from -1.

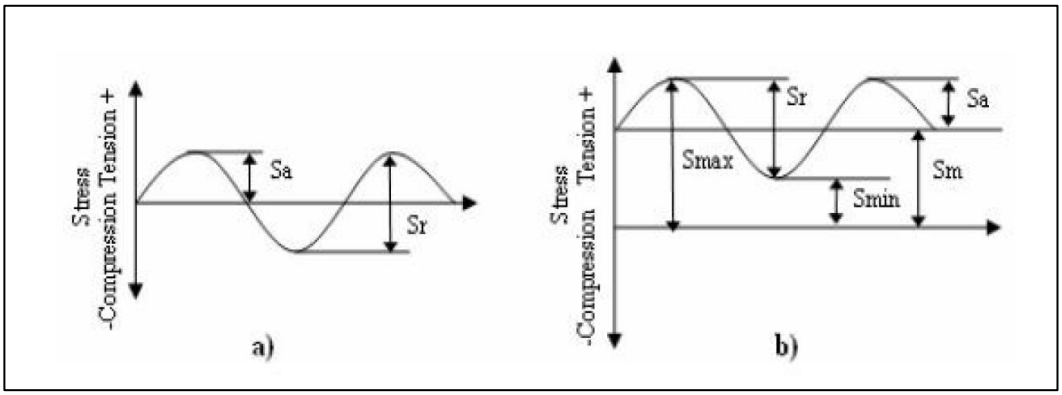

Figure 1-10: Stress cycles, a) zero mean, b) non-zero mean, [7]

In Figure 1-10 stress range S_r is constant but in nature most of the stress histories have non-constant S_r. The fatigue damage of the stress history can be calculated by first extracting stress cycles utilizing stress cycle counting methods. In time domain, mostly used cycle counting method is the Rainflow cycle counting method, [46], which has the illustration as shown in Figure 1-11.

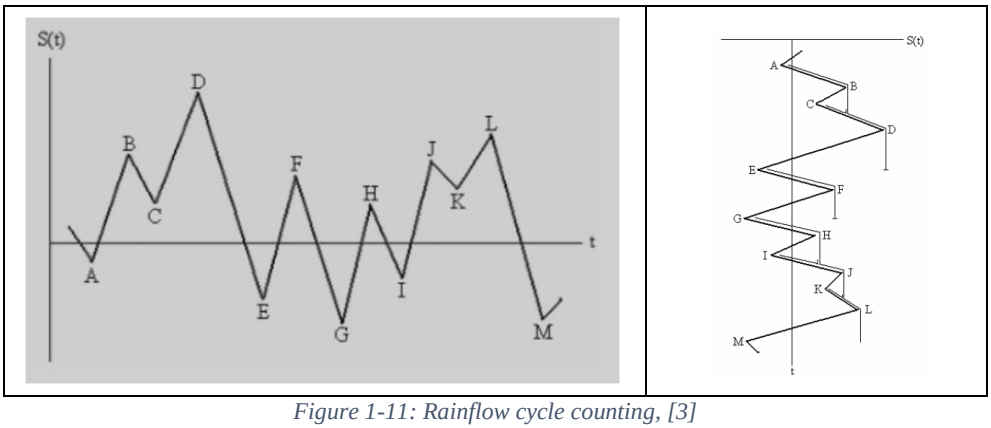

Figure 1-11: Rainflow cycle counting, [3]

However, since the frequency domain fatigue analysis and testing is investigated in this thesis study, the frequency domain cycle counting methods are investigated instead of Rainflow cycle counting method in time domain. The most widely used

frequency domain stress cycle counting method is the Dirlik method in vibration fatigue analysis which is explained in the following chapters, [40].

After the stress cycle counting is carried out, the fatigue damage can be determined by using the S-N curves of the materials utilizing the Miner's rule.

Metal materials used in fatigue phenomenon can be categorized as ferrous materials and nonferrous materials. Ferrous materials have iron. However if the materials do not include iron such as aluminum, copper, magnesium etc., they are called as nonferrous materials. For some ferrous materials, the S-N curve levels out in the high cycle regime. In other words, there is a limit stress level which is called as the endurance limit or the fatigue limit. If the stresses are below the endurance limit of the ferrous material, it can be assumed that no fatigue damage occurs or the structure has infinite life. One sample ferrous material S-N curve is given in Figure 1-12.

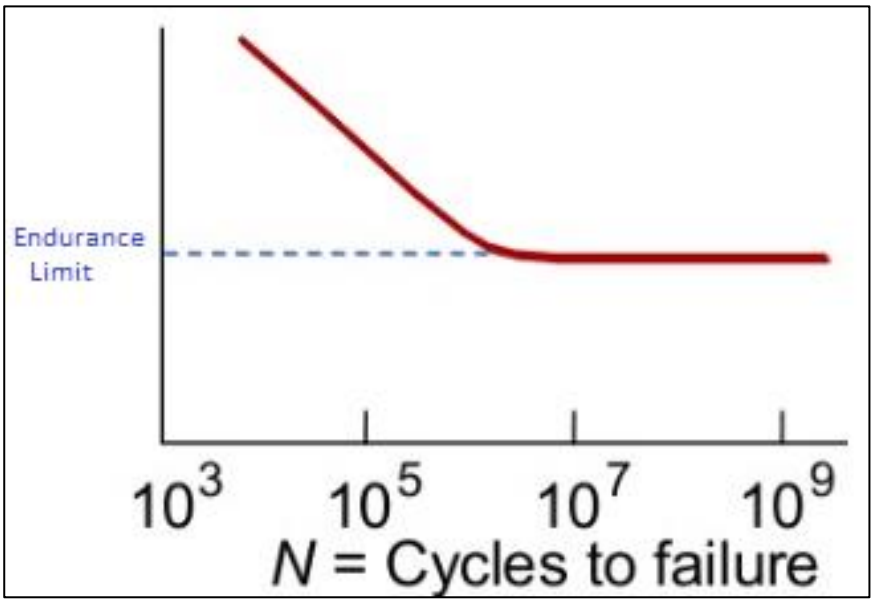

Figure 1-12: A typical S-N curve of the ferrous metal material

However, nonferrous materials are assumed have no endurance limit or infinite life even if the stresses much lower than the yield strength of the material. A sample S-N curve of the nonferrous material is given in Figure 1-13.

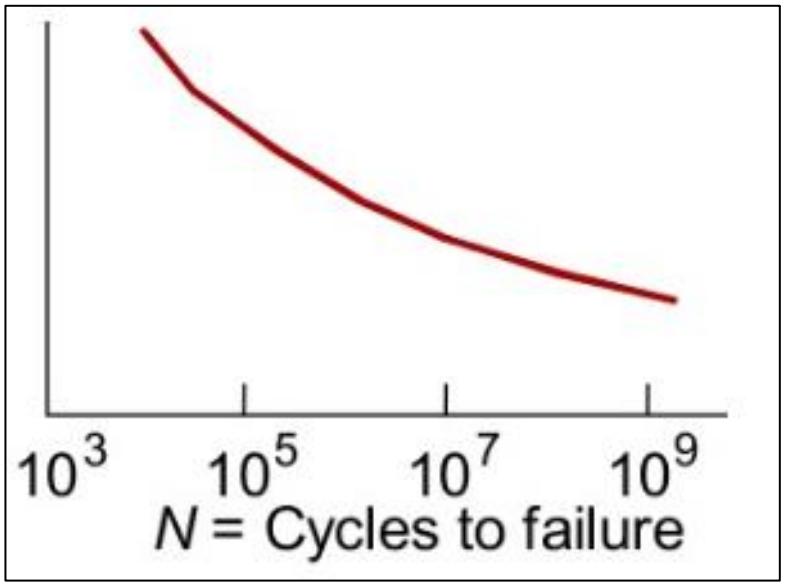

Figure 1-13: A sample S-N curve of the nonferrous metal material

For some applications, the line in finite-life region, which is above the endurance limit, can be assumed as straight line as shown in Figure 1-12. The straight line can be formulated from basic mathematic as,

$$N = C * S^{-b} \tag{1.1}$$

where b indicates the inverse slope of the line and called as Basquin exponent, C is related to the interception with the stress or the Y axis in the S-N curve graphs, [27].

While using the S-N curve of the materials, the mean stress effect should be investigated, [1]. If the mean stress is zero, as shown in Figure 1-10(a), then one can use the S-N curve directly because the S-N curves are mostly determined the rotating specimens which are exposed to bending stresses with zero mean. However, most loadings create non-zero mean stress profiles in the structures, as shown in Figure 1-10(b). The modification should be carried out in order to correct the fatigue life of the structures with non-zero mean stress profiles, [28].

Many structures carry some form of residual stresses or dead loads before the service load stresses are applied. For example the welding process, cold-rolling, shot-peening all create residual stresses. Fatigue life of the structures gets smaller as the mean stress

becomes more tensile, and to a lesser extent increases when the mean stress is compressive. The most promising mean stress effect correction method among others is the Modified Goodman rule, [28]. The formula of the Modified Goodman rule is given by,

$$S_{al} = S_0 * \left[1 - \left(\frac{S_m}{S_u}\right)^{m1}\right] \tag{1.2}$$

where; S_m is the mean stress, S_u is the ultimate tensile strength, S_0 is the allowable stress amplitude at zero mean stress (for the stated N, usually 10^7), S_{al} is the allowable stress amplitude for a given life when the mean stress is S_m and m1 is an arbitrary constant, [28]. If tests at more than one mean stress are available m1 can be calculated. Otherwise the most conservative assumption is to put m1=1, reverting to the Goodman formula, and there is experimental support for not exceeding a value of 2 (the Gerber parabola). Some references such as the Engineering Science Data Units (ESDU) sheets suggest a figure of approximately 1.5 for most steels, [28].

When the stress history is not constant amplitude, then the Palmgren-Miner rule can be implemented, [39, 45]. A sample non-constant amplitude load case is given in Figure 1-14.

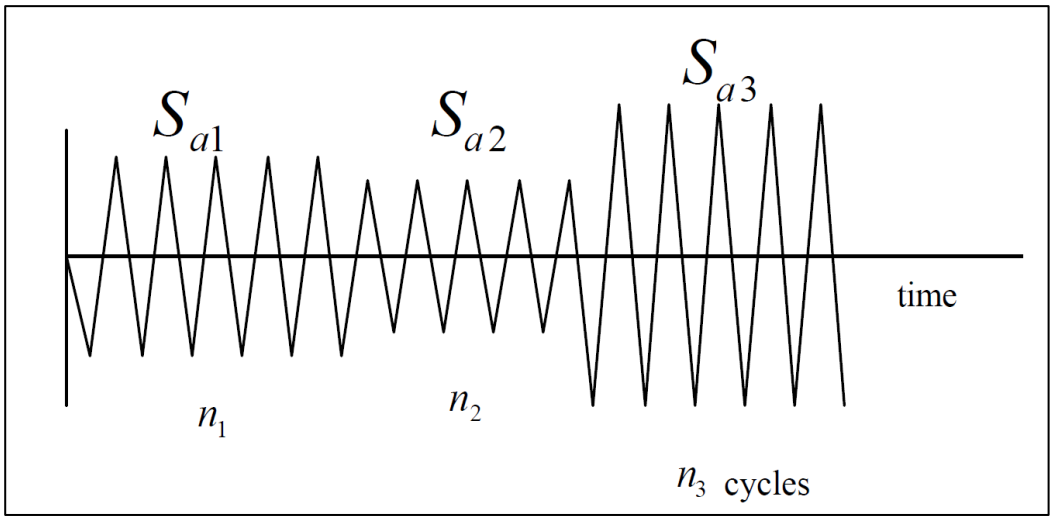

Figure 1-14: A sample non-constant amplitude load case, [28]

Palmgren-Miner rule is one of the most widely used cumulative damage models for failures caused by fatigue. The Palmgren-Miner rule states that failure occurs when the linearly cumulated damage fraction (D) reaches 1 and if there are k different stress levels and the number of cycles to failure at the i^{th} stress level (S_{ai}) is N_i, then the damage fraction is given by,

$$D = \sum_{i=1}^{k} \frac{n_i}{N_i} \tag{1.3}$$

where n_i is the number of applied load cycles of S_{ai}, [28]. The limitations of Palmgren-Miner rule are listed below;

• It assumes that all cycles of a given magnitude do the same amount of damage, whether they occur early or later in the life.

• Since the Palmgren-Miner rule assumes that the cumulative damage is composed of linearly accumulated damages, the strains and stresses should stay in the elastic region.

• Palmgren-Miner rule assumes that the presence of a stress cycle of amplitude S_2 does not affect the damage caused by a stress cycle of amplitude S_1.

• The rule governing the damage caused by a stress cycle of amplitude S_1 is the same as that governing the damage caused by a stress cycle of amplitude S_2.

1.6.2. Strain-Life (E-N) Method

This method is similar to the S-N method but it uses strain cycles instead of stress cycles. Moreover, the S-N method can be used in elastic region only but the E-N method can be used in both the elastic and the plastic region. The E-N method is more valid and favorable in these days because plastic strain changes the properties of a material, especially when the material experience plastic deformation. The E-N curves of the material fatigue strength include the plastic region fatigue information too. However, for different materials E-N curves are not available like the S-N curves. Due to the lack of E-N curve information and necessity of specific material E-N curve tests, still the most used method is the S-N method in fatigue analysis. Moreover, the

developed vibration fatigue methods include the S-N method. Consequently, in this thesis study, the S-N method is used instead of the E-N method.

1.6.3. Crack Propagation (LEFM)

This method deals with the processes after the crack initiation stage. Generally, in the aerospace munitions, the crack propagation stage is not allowed. The fatigue lives of the munitions are accepted from beginning of the service life to crack initiation time or critical crack size occurring time. It depends on the judgement of designer engineers. Therefore, in this thesis study, the LEFM method is not used.

CHAPTER 2

THEORY OF RANDOM VIBRATION FATIGUE

Vibration is the oscillating motion of a particle or body about a fixed reference point. Such a motion may be simple harmonic or non-sinusoidal. In other words, they are sinusoidal and non-sinusoidal, respectively. It can also occur in various modes, such as bending, torsional or translational modes, and since the vibration can occur in more than one mode simultaneously, its analysis can be difficult in time domain. Moreover, the mechanical fatigue analyses and tests can be carried out in time domain and frequency domain, [41]. Since the aerospace structures are mostly exposed to random vibration loading, the frequency domain methods are more appropriate as explained before.

2.1. Frequency Domain Fatigue Analysis

The frequency domain fatigue analysis is the most suitable domain for random vibration fatigue analysis. The data which are impractical to handle in time domain can be handled easily in the frequency domain, [38]. Also, if the resonance region of the mechanical system is excited, the time domain analysis comes short in terms of dynamic behavior in the resonance region, [19].

In the frequency domain the input is given in the form of a PSD of the loading and the structure is modelled by a linear frequency response function relating the input loading to the output stress at a particular location in the structure. The output from the model is expressed as a PSD; in this case it is the PSD of stress, [28]. The sample time and frequency domain demonstration is given in Figure 2-1.

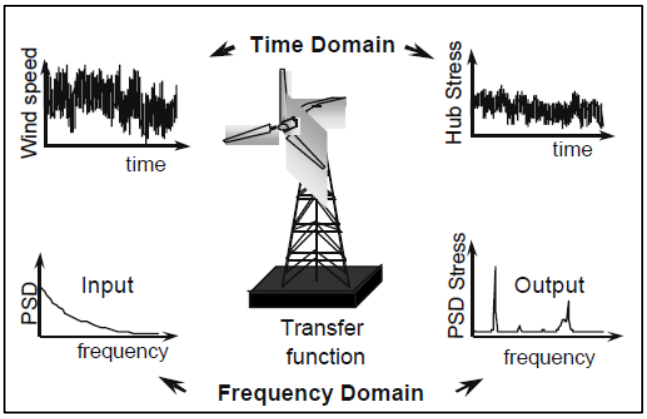

Figure 2-1: Sample frequency and time domain illustrations, [28]

The transition between the time and the frequency domain is done using the Fourier transformation. The pair of Fourier transform equations is given in Equation 2.1 and 2.2.

$$F(w) = \int_{-\infty}^{+\infty} f(t) * e^{-jwt} * dt \tag{2.1}$$

$$f(t) = \frac{1}{2*\pi} * \int_{-\infty}^{+\infty} F(w) * e^{jwt} * dt \tag{2.2}$$

By using the Fourier transformation, a complex random signal in time domain can be converted into the frequency domain and back to the time domain easily. The sample illustration of the Fourier transformation is given in Figure 2-2.

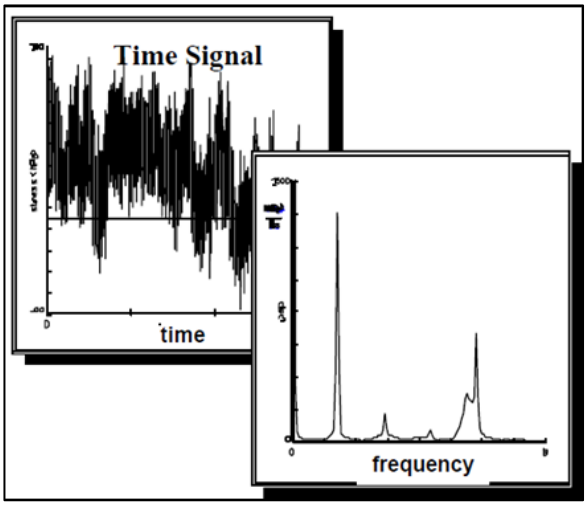

Figure 2-2: Fourier transformation of the random process from time domain to the frequency domain, [28]

The Fourier transformation can be used with continuous time signals. However, in the digital world, the time histories are recorded in a discrete form. Therefore, discrete Fourier transformation is usually needed. Hence, discrete Fourier transformation was developed in 1965 by Cooley and Tukey and it is called as Fast Fourier Transformation (FFT), [21].

The FFT of the time domain signal to the frequency domain is given by Equation 2.3.

$$y(f_n) = \frac{2T}{N} * \sum_{k=0}^{N-1} y(t_k) * e^{-i*\left(\frac{2*\pi*k}{N}\right)*k} \quad (2.3)$$

The inverse of FFT from frequency domain to time domain is given in Equation 2.4.

$$y(t_k) = \frac{1}{T} * \sum_{n=0}^{N-1} y(f_n) * e^{i*\left(\frac{2*\pi*k}{N}\right)*k} \quad (2.4)$$

In Eqs. (2.3) and (2.4), T is the period of the function $y(t_k)$ and N is the number of data points, [21].

2.2. Frequency Response Function

The frequency response function (FRF) is basically the mathematical relationship between the harmonic input and output of the dynamic structural systems. FRF gives the amplitude and phase information of the output as a function of frequency and it is unique for the particular mechanical system. The linear structure responds to a sinusoidal force with a sinusoidal displacement at the same frequency. Therefore, one can predict the frequency response of the system by multiplying the load and the FRF in frequency domain calculations as shown in Equation 2.5.

$$Input * FRF = Frequency\ Response \quad (2.5)$$

2.3. Power Spectral Density (PSD)

PSD is used to characterize the strength of stationary random process in the frequency domain. In order to get the PSD profiles of the random vibration loading, Fast Fourier Transform (FFT) of the random load history is taken and then PSD profile is obtained by taking the modulus of the squared FFT and divided by the 2T, where T stands for

the sample period which can also be defined as $1/f_s$ and f_s being the sampling frequency of the recorded signal, as shown in Equation 2.6. Moreover Figure 2-3 shows a typical PSD profile which has only the amplitude and frequency information. All phase and time information is discarded, [29].

$$PSD = \frac{1}{2*T} * |FFT|^2 \tag{2.6}$$

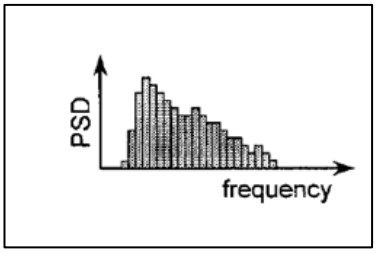

Figure 2-3: PSD illustration, [28]

The area under each spike in Figure 2-3 represents the mean square of the sine wave at that frequency of interest. The phase relationships between the waves cannot be determined anymore. Some general examples of PSD profiles for different type of load histories are given in Figure 2-4.

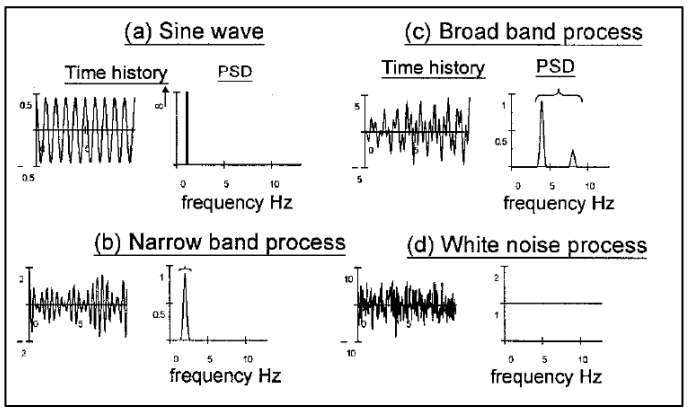

Figure 2-4: Different type of load histories and their PSD profiles, [28]

2.4. Moments of PSD profiles

The moments of the PSD profiles are needed for the frequency domain cycle counting. The relevant spectral moments are computed from a one sided PSD [G(f)] in the units of Hertz using Equation 2.7.

$$m_n = \int_0^{\infty} f^n * G(f) * df = \sum_{k=1}^{m} f_k^n * G_k(f_k) * \delta f \quad (2.7)$$

where, δf is the frequency increment, f is the frequency and G(f) is the response PSD. The nth moment of area of the PSD (m_n) is calculated by dividing the curve into small strips, as shown in Figure 2-5. The nth moment of area of the strip is given by the area of the strip multiplied by the frequency raised to the power n. The nth moment of area of the PSD is then found by summing the moments of all the strips. In theory, all possible moments are required to fully characterize the original process. However, in practice, m_0, m_1, m_2 and m_4 are sufficient to compute all of the information required for the subsequent fatigue analysis, [28].

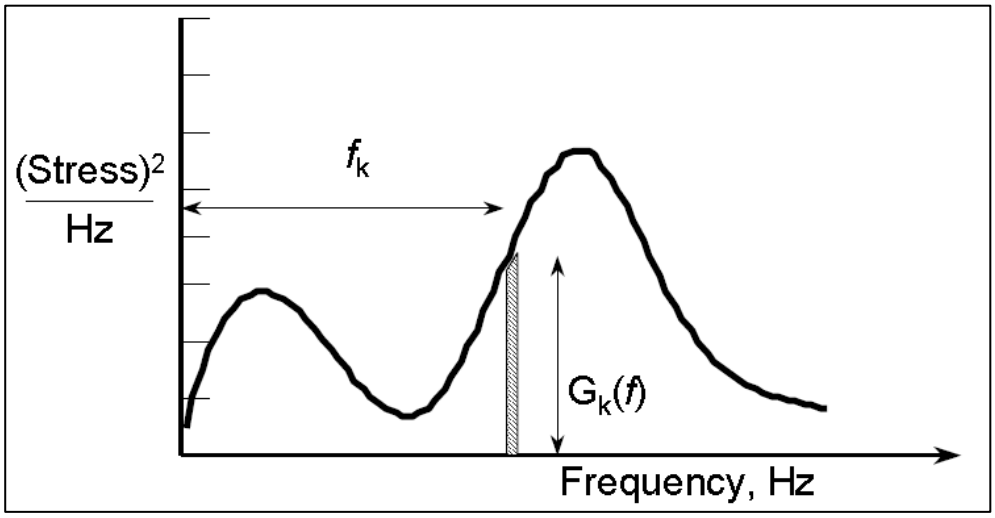

Figure 2-5: Calculation of the PSD moments, [29]

2.5. Expected Zeros, Expected Peaks and Irregularity Factor

Random stress histories can be well manipulated and described by using the statistical parameters. This is due to the fact that any sample time history can only be regarded as one sample from an infinite number of possible samples that occur for the random processes. Two of the most important statistical parameters are the number of zero crossings and number of peaks in the signal. Figure 2-6 shows a one second piece cut out from a typical wide band signal. E[0] represents the number of (upward) zero crossings, or mean level crossings for a signal with a non-zero mean. E[P] represents

the number of peaks in the same sample. These are both specified for a typical 1 second sample. The irregularity factor (γ) is defined as the number of upward zero crossings divided by the number of peaks, [28].

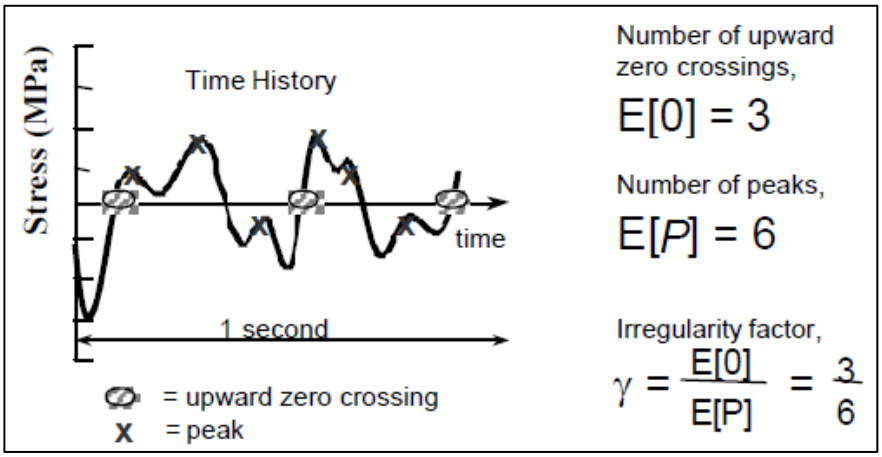

Figure 2-6: Expected zero, expected peak and the irregularity factor, [28]

The first valid effort for estimating fatigue damage from PSDs was studied by S.O. Rice in 1954. Rice discovered the important relationships for the number of upward mean crossings per second (E[0]) and the peaks per second (E[P]) in a random signal expressed only in terms of their spectral moments, m_n , [28]. In terms of spectral moments, upward mean or zero crossing is given by Equation 2.8, number of peaks is given by Equation 2.9 and the irregularity factor is given by Equation 2.10.

$$E[0] = \sqrt{\frac{m_2}{m_0}} \tag{2.8}$$

$$E[P] = \sqrt{\frac{m_4}{m_2}} \tag{2.9}$$

$$\gamma = \frac{E[0]}{E[P]} = \sqrt{\frac{m_2^2}{m_0 * m_4}} \tag{2.10}$$

2.6. Probability Density Function (PDF)

Mathematically, the most convenient way of storing the stress range histogram is in the form of PDF of the stress range, [7]. It is easy to transform from a stress range

histogram to a PDF or backwards. In order to calculate the expected fatigue damage, E(D), firstly the PDF of the stress ranges, p(S), should be determined. A typical calculation of the PDF is shown in Figure 2-7 where dS shows the width of stress.

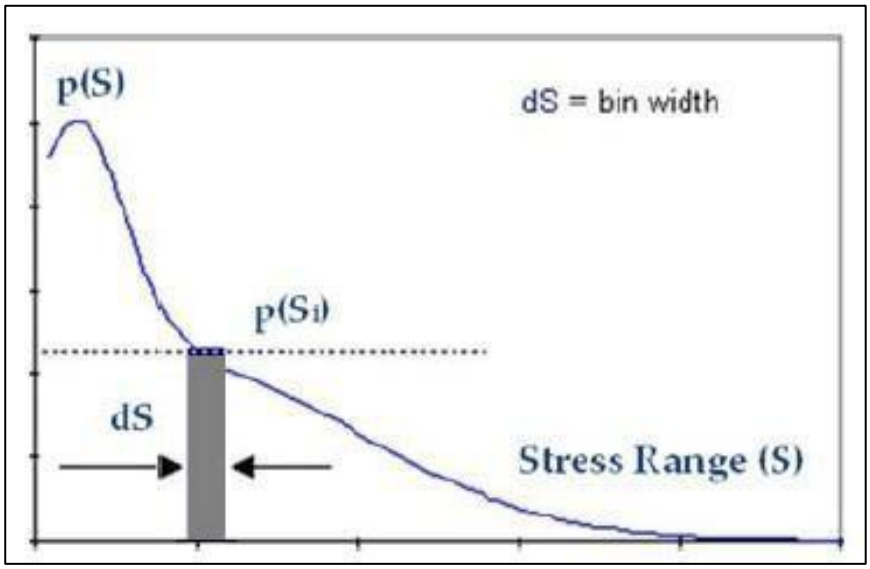

Figure 2-7: Calculation of the PDF from the stress range histogram, [29]

The bin widths, dS, and the total number of cycles in the histogram, S_t, are required in order to obtain PDF from a stress range histogram. By using the PDF, the reverse calculation can also be done. Multiplication of the bin width with the value of the PDF at the stress level ($p(S_i)$* dS) gives the probability that the stress is in the range S_i-dS/2 and S_i+dS/2. Multiplying the probability of the stress range p(S)*dS with the total number of cycles (S_t) in the histogram, total number of cycles, N(S), for a given stress level, S, can be obtained, as shown by Equation 2.11.

$$N(S) = p(S) * dS * S_t \quad (2.11)$$

2.7. Stress Cycle Counting Method from PSD in the Frequency Domain

Dirlik's empirical formula for the cycle counting is the most superior in terms of accuracy, [19]. Dirlik has derived an empirical closed form expression for the determination of the PDF of the cycle counting of stress ranges, which was obtained using extensive computer simulations to model the signals using the Monte Carlo

technique, [30]. The fatigue damage (D) is calculated after the cycle counting by the Dirlik's method and given by Equation 2.12, where m and A are material properties which are the fatigue strength exponent obtained from the material S-N curve and the fatigue strength coefficient respectively as given by Eqn (1.1) where m corresponds to b and A corresponds to C in Eqn (1.1).

$$D = \left(\frac{1}{2^m * A}\right) * \int_0^\infty S^m * N(S) * dS \tag{2.12}$$

In Equation 2.12, histogram formula N(S) for stress cycles range is given by Equation 2.13, where ν_p and τ are the rate of peaks (number of expected peaks per unit time) and the exposure time, respectively.

$$N(S) = \nu_p * \tau * p(S) \tag{2.13}$$

The best correlation for p(S) proposed by Dirlik is given by Equation 2.14.

$$p(S) = \frac{\frac{D_1}{Q} * e^{\frac{-Z}{Q}} + \frac{D_2 * Z}{R^2} * e^{\frac{-Z^2}{2*R^2}} + D_3 * Z * e^{\frac{-Z^2}{2}}}{2 * \sqrt{m_0}} \tag{2.14}$$

where, S is the stress range and other parameters in Equation 2.13 and 2.14 are given by Table 2-1.

Table 2-1: Parameters in Equation 2.13 and 2.14

$D_1 = \frac{2*(x_m - \gamma^2)}{1+\gamma^2}$, $D_2 = \frac{1-\gamma-D_1+D_1^2}{1-R}$, $D_3 = 1 - D_1 - D_2$, $Q = \frac{1{,}25*(\gamma - D_3 - D_2 * R)}{D_1}$
$R = \frac{\gamma - x_m - D_1^2}{1-\gamma-D_1+D_1^2}$, $Z = \frac{S}{2*\sqrt{m_0}}$, $x_m = \frac{m_1}{m_0} * \sqrt{\frac{m_2}{m_4}}$, $\nu_p = \sqrt{\frac{m_4}{m_2}}$, $\gamma = \frac{m_2}{\sqrt{m_0 * m_4}}$

2.8. Random Vibration Fatigue Analysis Flowchart

In this thesis study, MSC Patran pre-post processor is used for the finite element model (FEM) preparation. Furthermore, the frequency response analysis is done by using the MSC Nastran finite element solver. The fatigue analysis tool, nCode, is used for the random vibration fatigue analysis and post processing of the analysis results.

Initially, the stress frequency response to unit load input, which is acceleration in this thesis study, is calculated. Then, the load PSD profile should be supplied to the fatigue analysis. The analysis engine in nCode utilizes the stress profile corresponding to the unit load input in order to extract the stress PSD profile of the entire elements in the model. Stress cycle counting in the frequency domain is done by the analysis engine in nCode, using the Dirlik's method described in the previous section. Finally, the analysis engine in nCode determines the fatigue life and damage caused by the loading via the fatigue life modeler in the engine. It should be noted that in all calculations, there must be consistency in the units. For example if the PSD of the acceleration loading has the unit g^2/Hz, then the unit input acceleration for the frequency response analysis should be 1 g or 9810 mm/s^2. Moreover, if the PSD of the acceleration loading has unit as (mm/s^2)^2/Hz, then the unit input acceleration for the frequency response analysis should be 1 mm/s^2.

After the determination of damage (D) by the Dirlik's method, one can then find fatigue life (1/D), [34]. The failure occurs when the cumulative damage (D) reaches to value of 1.

Basic flowchart of the random vibration fatigue analysis is given in Figure 2-8.

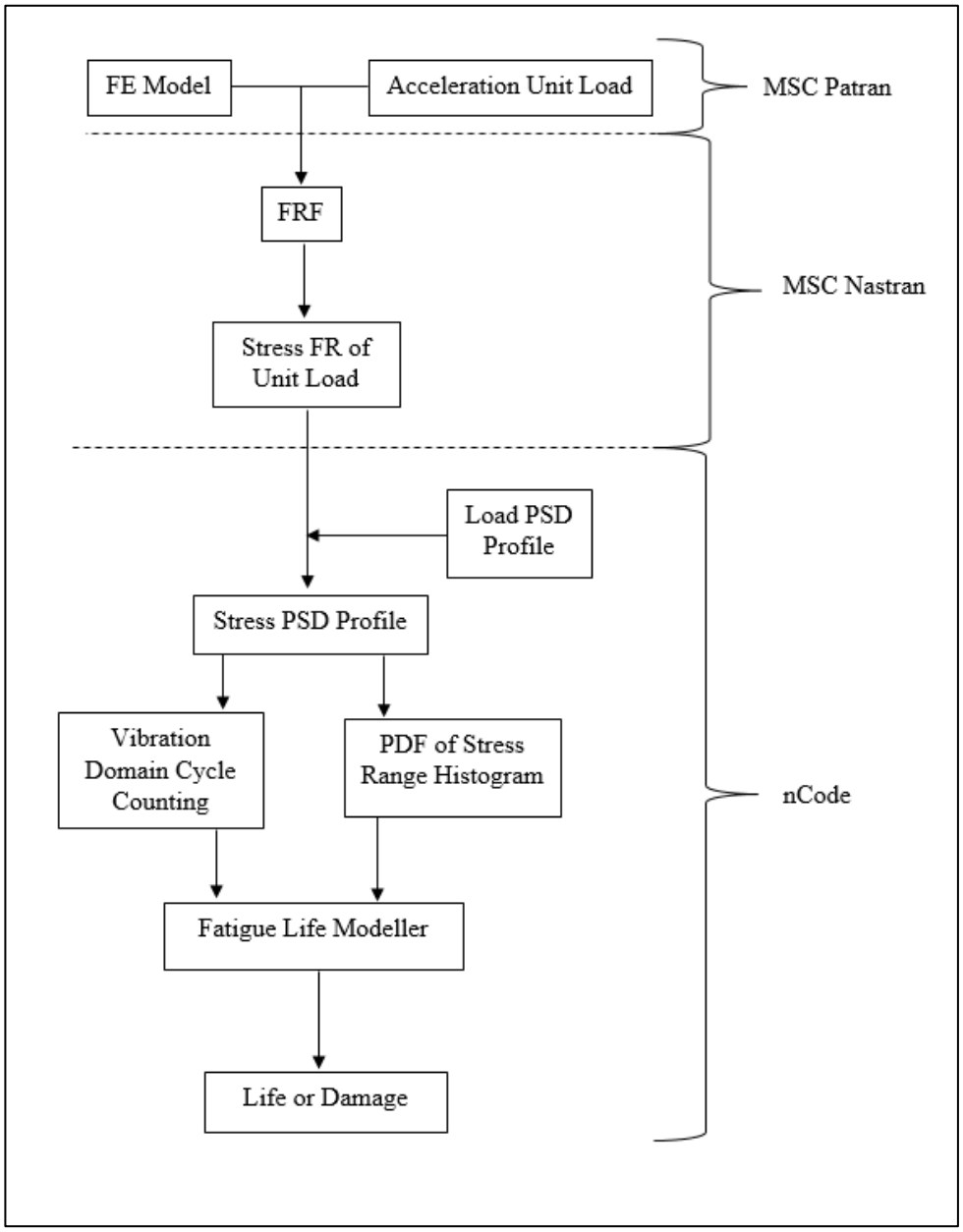

Figure 2-8: Basic flowchart of the random vibration fatigue analysis

CHAPTER 3

VIBRATION FATIGUE ANALYSIS AND TEST OF ALUMINUM NOTCHED BEAMS

Aluminum notched rectangular cross-section beams are designed in order to conduct the random vibration mechanical fatigue analysis and tests. Before the fatigue analyses, to decide on the frequency range of interest, preliminary modal analysis is carried out. Then, to extract the modal damping ratios of the beam, modal test is performed. Finally, the random vibration fatigue analysis is performed and for comparison, vibration fatigue testing is also carried out.

3.1. Aluminum Notched Beams

The rectangular cross-section notched aluminum beam is designed in order to perform the vibration fatigue analyses and tests. The notched region is designed so that fatigue failure occurs in the notched region first so the control of the random vibration fatigue analysis and test is easy. The material properties of the material of the notched beam are given in Table 3-1.

Table 3-1: The mechanical material properties of Aluminum, [35]

Density	2710 kg/m^3
Elastic Modulus	68.3 GPa
Poisson's Ratio	0.33

The geometry and 2-D drawing of the notched beam is given in Figure 3-1.

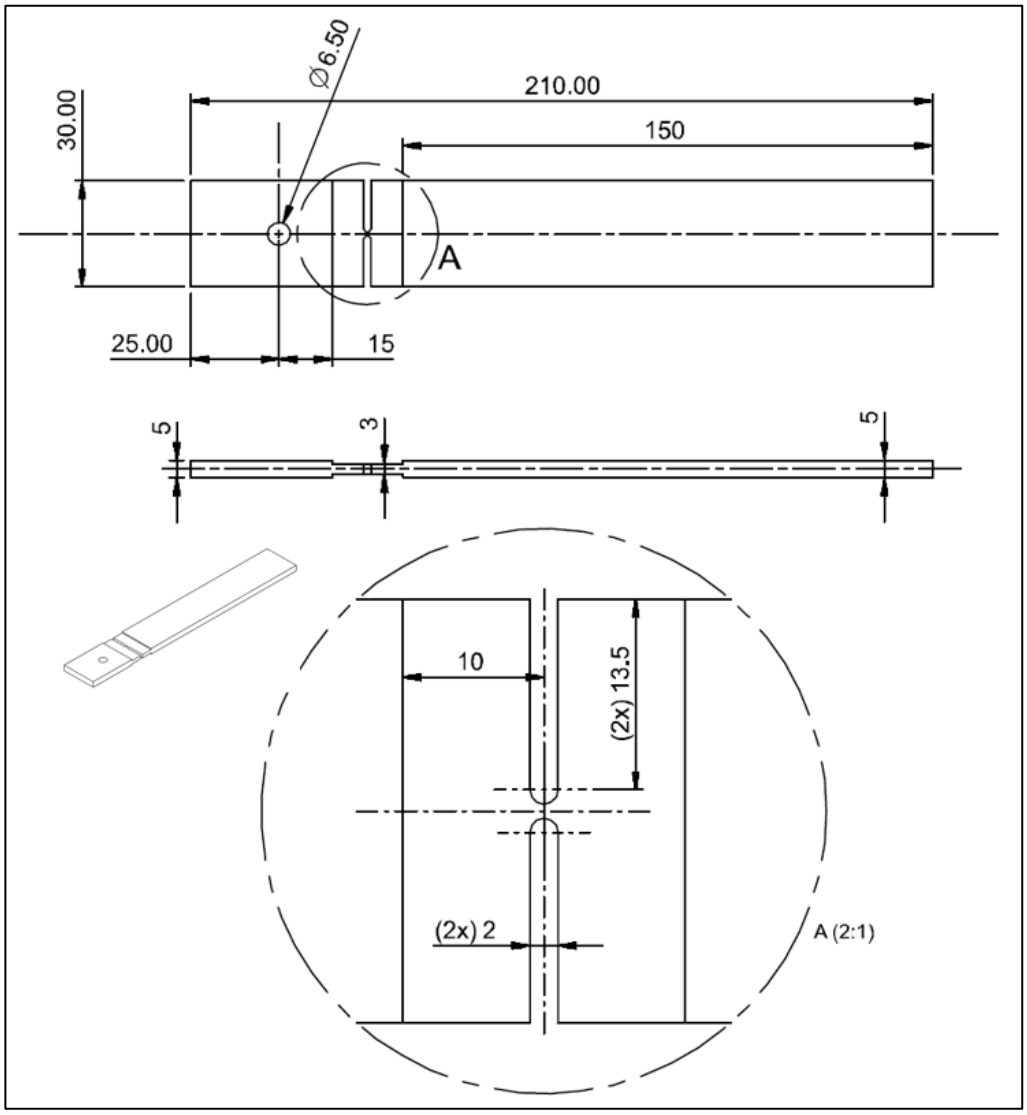

Figure 3-1: Geometry and 2-D drawing of the aluminum notched beam, [mm]

It should be noted that the notched beam is designed to connect it to both the vibration table and the modal shaker. The 6.5 mm diameter hole is designed for the connection to the modal shaker. However, as test program progressed the modal shaker is not used at all.

3.2. Preliminary Modal Analysis

The designed aluminum notched beam is planned for fatigue analyses and tests. In order to decide the frequency interval of the test and the analysis, preliminary modal

analysis should be carried out. Moreover, with the information of preliminary modal analysis, the misplacement of test devices (e.g. sensors) can be prevented.

The modal analysis is performed using the MSC Nastran finite element solver and MSC Patran finite element pre-post processor. The used finite element types in the finite element model are TET4 and HEX8. Figure 3-2 gives the description of the finite elements used in the finite element model.

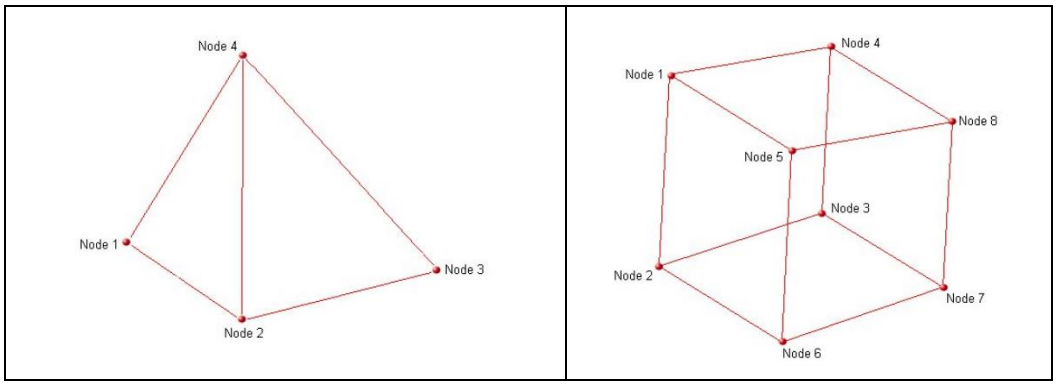

Figure 3-2: Solid type TET4 (left) and HEX8 (right) finite elements, [36]

Before starting the fatigue analysis, the mesh refinement work has been performed. Mesh refinement work assures the reliability of the finite element model. The refinement work is conducted for an out-of-plane inertial loading of the notched beam of magnitude 1 g or 9810 mm/s^2. The beam is cantilevered from left side of the beam for a length of 25 mm as shown in Figure 3-3.

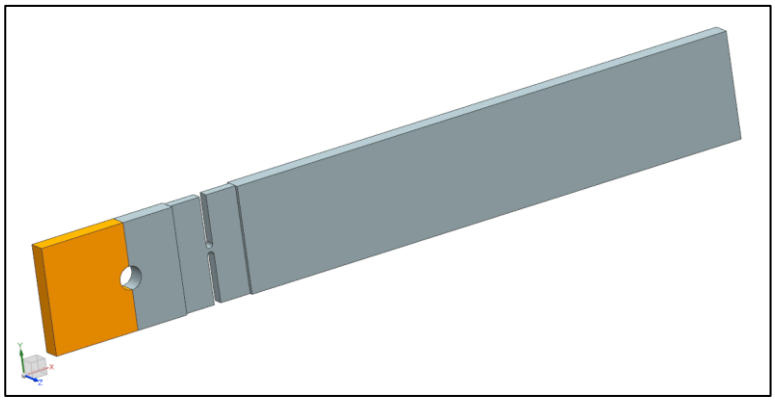

Figure 3-3: Displacement boundary condition of notched beam ( )

The result of the mesh refinement work is given in Table 3-2 and Figure 3-4. According to the results of the mesh refinement study, the edge length of the mesh is selected as 0.125 mm around the notched side of the beam utilizing HEX8 elements and 5 mm for the rest of the beam utilizing TET4 type solid finite elements.

The reason for using hexagonal elements rather than tetrahedron elements around the notched region is the quality of elements. Also, it is commonly known that the HEX8 elements give more reliable results compared to TET4 elements. Moreover, hexagonal elements are very robust but computationally more expensive than tetrahedron elements. Hence, in the finite element model of the notched beam, the notched region is meshed with HEX8 and the rest of the beam is meshed with TET4 elements.

Table 3-2: Mesh refinement work table result

Mesh number	Mesh edge length around the notch (mm)	Maximum stress around notch (MPa)	Deviation (%)
1	8	34.2	-
2	4	30.5	10.82
3	2	31.5	3.17
4	1	32.8	3.96
5	0.5	38.3	14.36
6	0.25	40.6	5.67
7	0.125	40.9	0.73

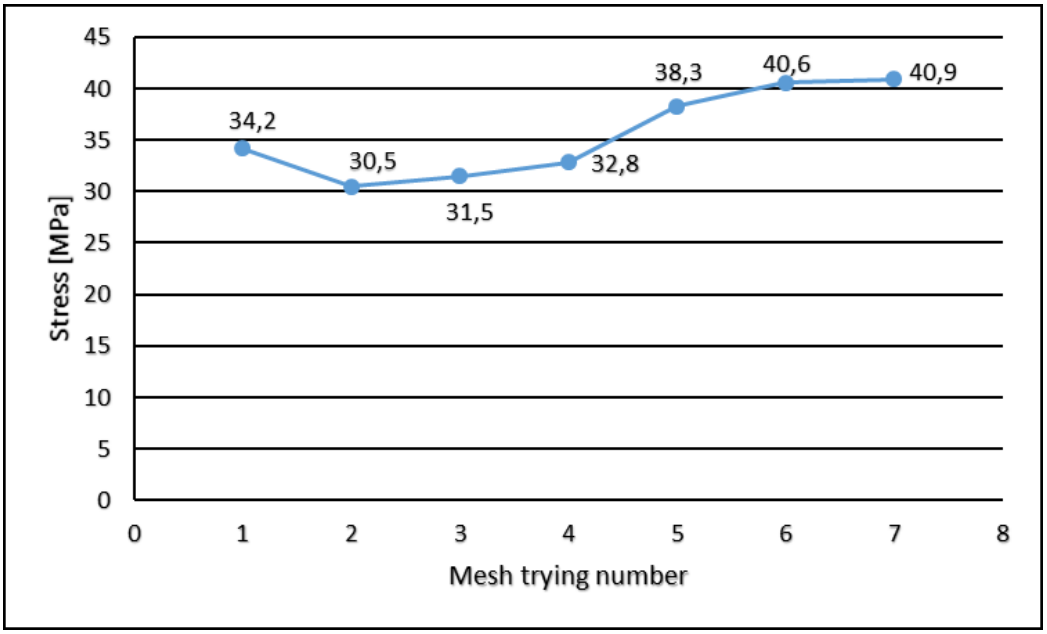

Figure 3-4: Mesh refinement work graphical result

After the mesh refinement work, mesh number 7 is selected. Also, all of the analyses in this thesis study are conducted with the same mesh structure in order to maintain the consistency. Figure 3-5 gives the finite element mesh of the notched aluminum beam and Figure 3-6 gives the detailed view of the finite element mesh of the notched region.

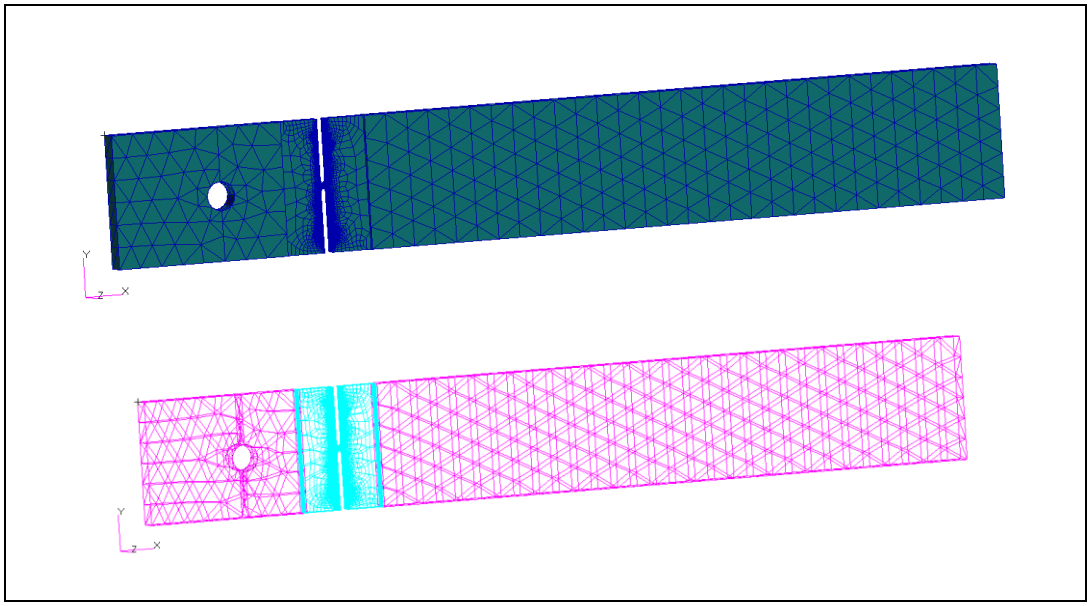

Figure 3-5: Finite element mesh of the aluminum beam

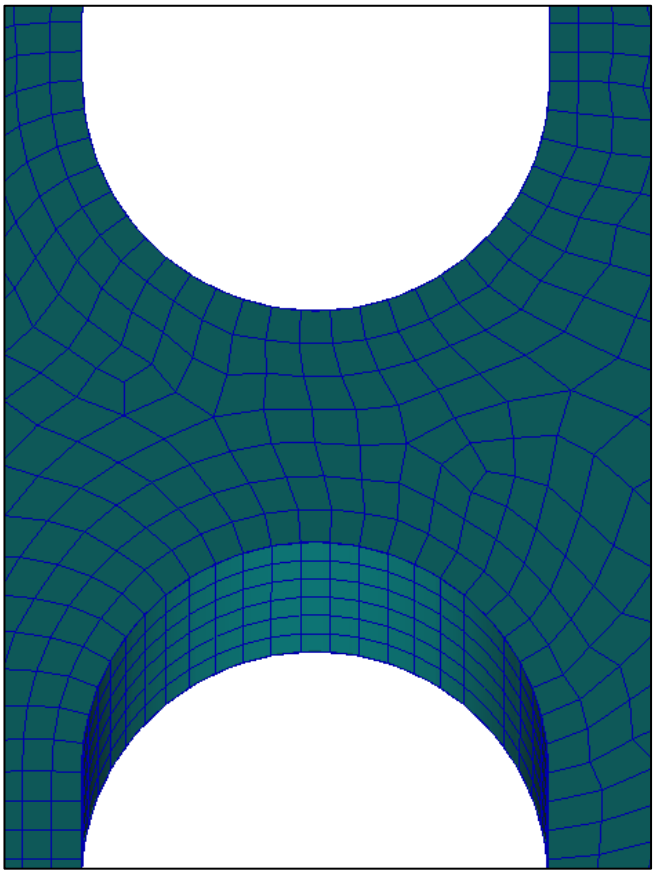

Figure 3-6: Finite element mesh around the notched region

In order to show an example of the von Mises stress distribution of the notched beam, Figure 3-7 and Figure 3-8 are given.

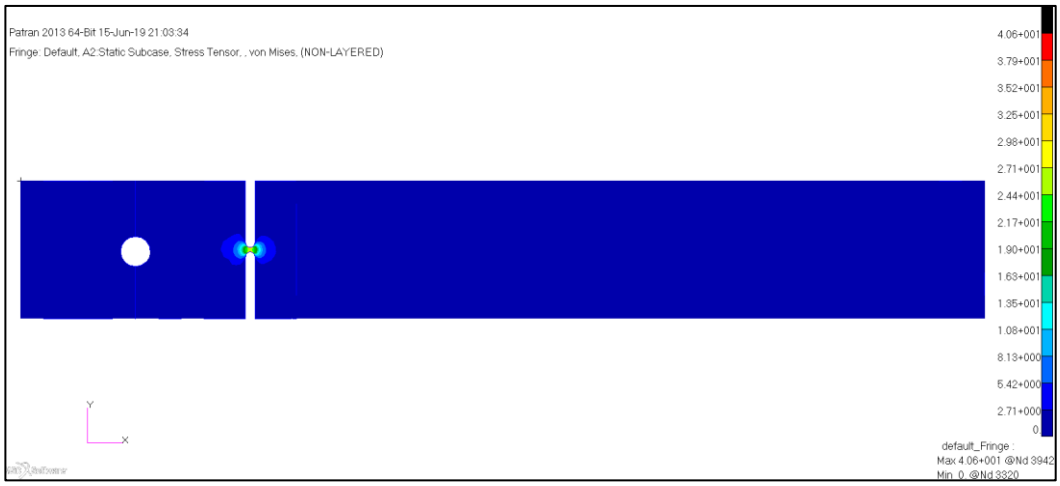

Figure 3-7: The von Mises stress distribution of the notched beam with mesh number 7

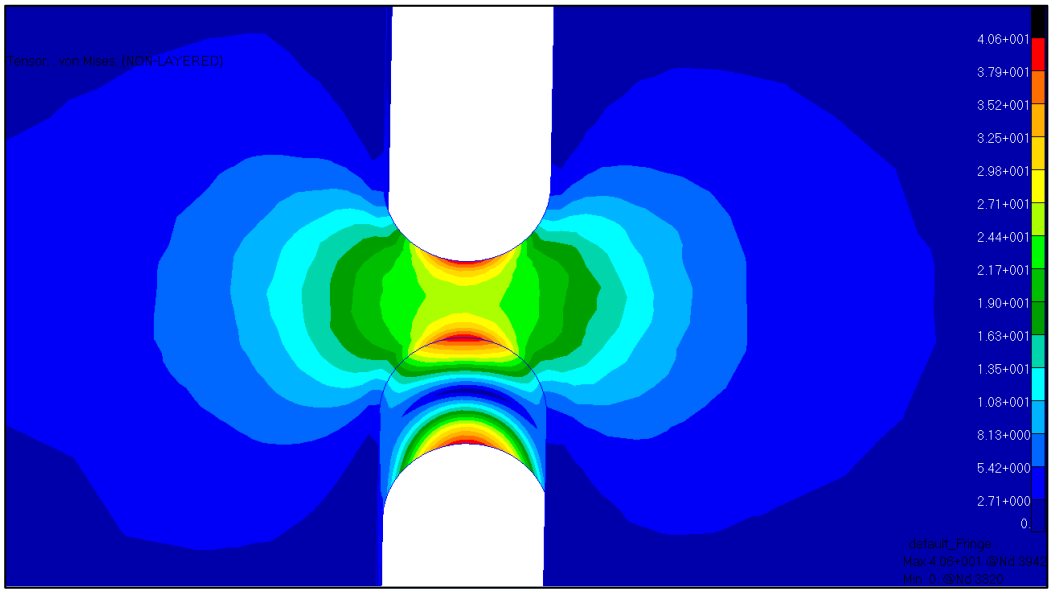

Figure 3-8: The detailed stress distribution of the Figure 3-7 on the notch

The main aim of the preliminary modal analysis is to determine the frequency of interest. Hence, the modal effective mass fraction output is requested from the modal analysis. The modal effective mass fraction provides the information about the significance of the modes in dynamic behaviors of structures. For this specific beam geometry, the participation of 80-90% cumulative modal effective mass fraction is thought to be sufficient for the dynamic behavior of the notched beam. In MSC Nastran, the modal effective mass fraction output is requested by the "meffmass" command which is inserted to the MSC Nastran input file.

The modal effective mass fraction results of the modal analysis are given in Table 3-3. Modal effective mass indicates the mass participation of each mode in each of the 6 rigid body motions (T1: x translation, T2: y translation, T3: z translation, R1: x rotation, R2: y rotation, R3: z rotation). Modal effective mass fraction is modal effective mass divided by the rigid body active mass and adds up to 1 when all modes are included. The most effective degree of freedom to excite is the out-of-plane displacement according to Figure 3-1. It corresponds to the z direction in the analysis coordinate frame. Moreover, it corresponds to T3 degree of freedom in the .f06 file of the MSC Nastran finite element solver.

Table 3-3: Modal effective mass fraction results for the out-of-plane displacement (z translation, T3)

Mode No.	Frequency (Hz)	Fraction	Cumulative
1	23.753	2.094E-09	2.094E-09
2	39.637	6.808E-01	6.808E-01
3	341.129	3.911E-09	6.808E-01
4	664.104	1.480E-01	8.288E-01
5	1916.791	5.727E-02	8.861E-01

According to the Table 3-3, mode 1 and 3 has very little effect on the out-of-plane (z translation) dynamic behavior of the beam, however modes 2, 4 and 5 are dominant ones, because they are the out-of-plane modes. 89% cumulative modal effective mass fraction is considered to be sufficient for the analysis and the tests. Based on the modal effective mass fraction results, the frequency interval is decided to be 1 Hz to 2048 Hz. However, since the vibration test table used in the present thesis study allows tests from 4 Hz up to 2000 Hz, the frequency interval is decided to be 4 Hz-2000 Hz.

The first 5 mode shapes of the beam are given in Figure 3-9, Figure 3-10, Figure 3-11, Figure 3-12 and Figure 3-13 respectively.

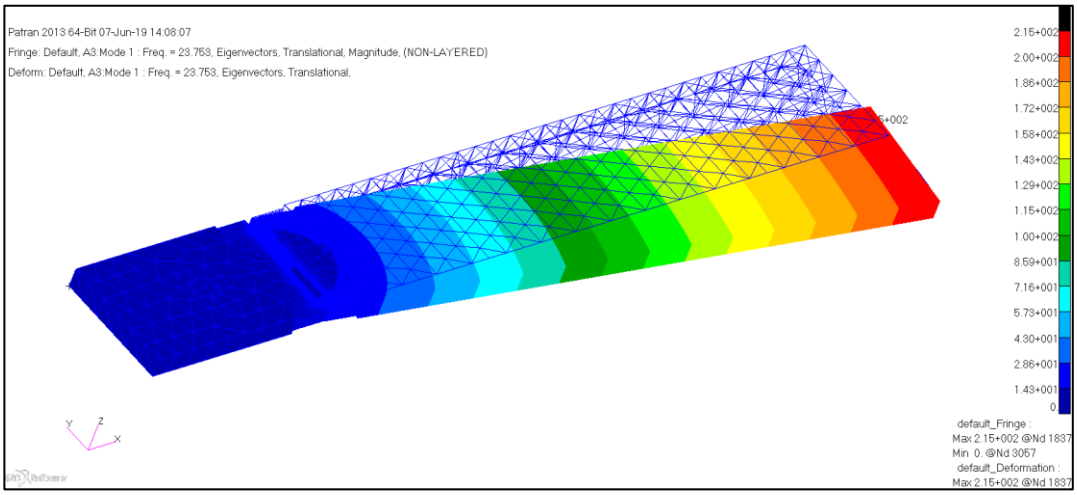

Figure 3-9: 1st mode shape of the beam- 1st in-plane bending

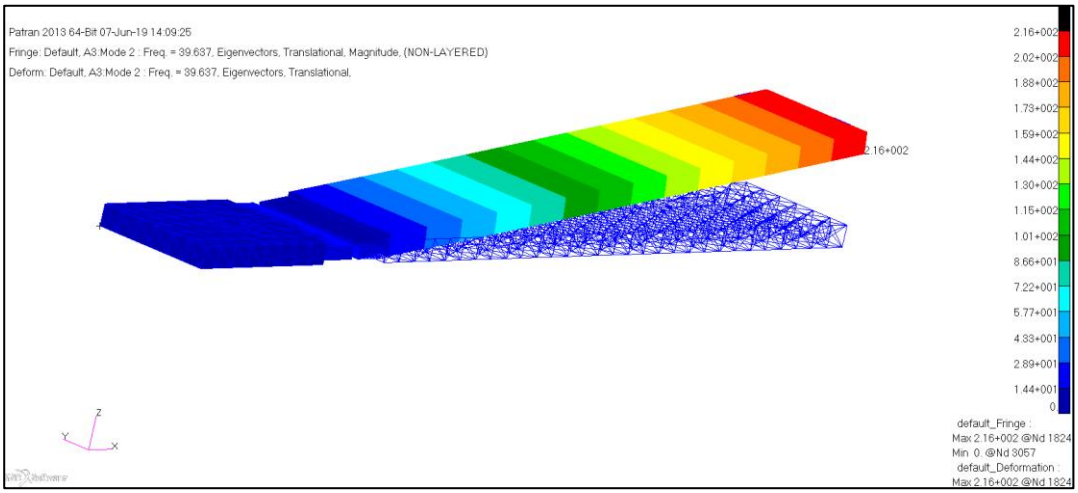

Figure 3-10: 2nd mode shape of the beam- 1st out-of-plane bending

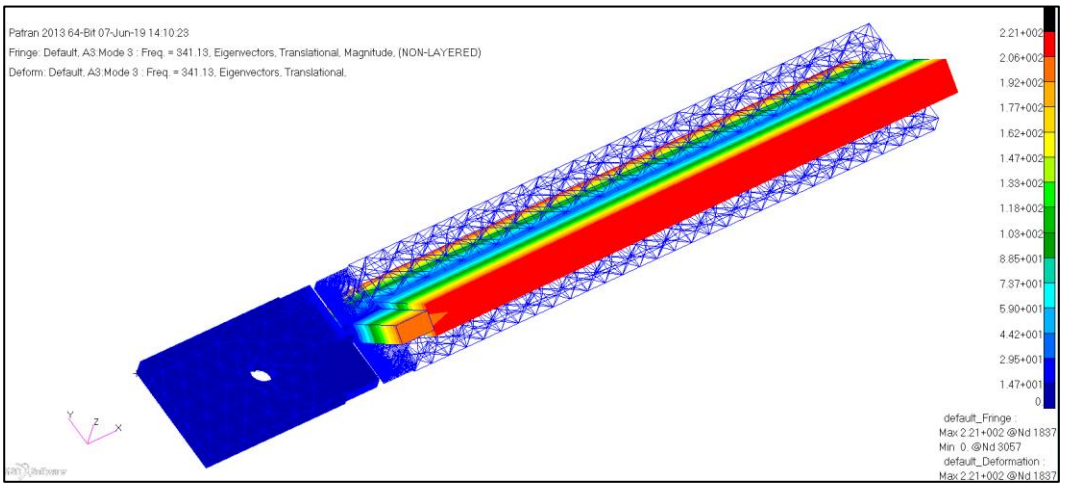

Figure 3-11: 3rd mode shape of the beam- 1st torsion

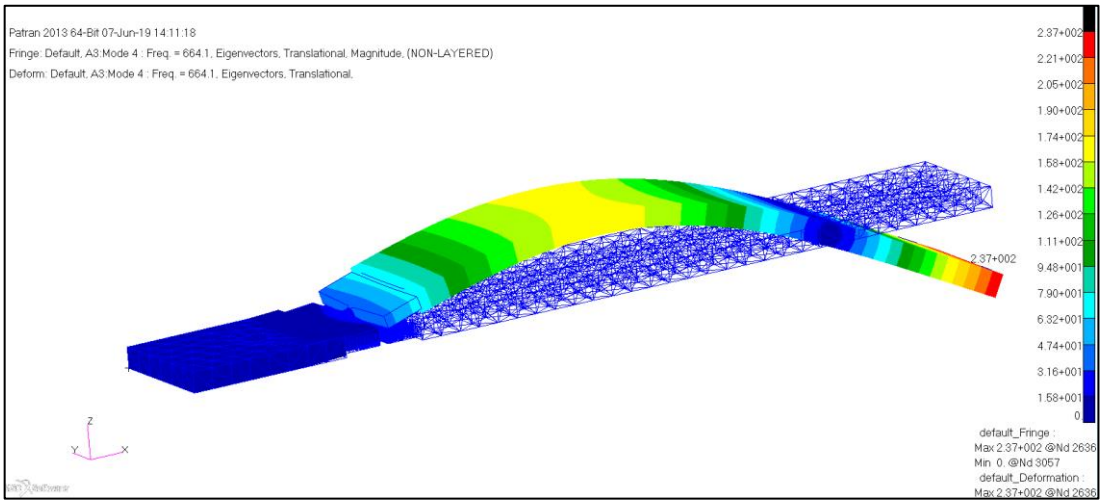

Figure 3-12: 4th mode shape of the beam- 2nd out-of-plane bending

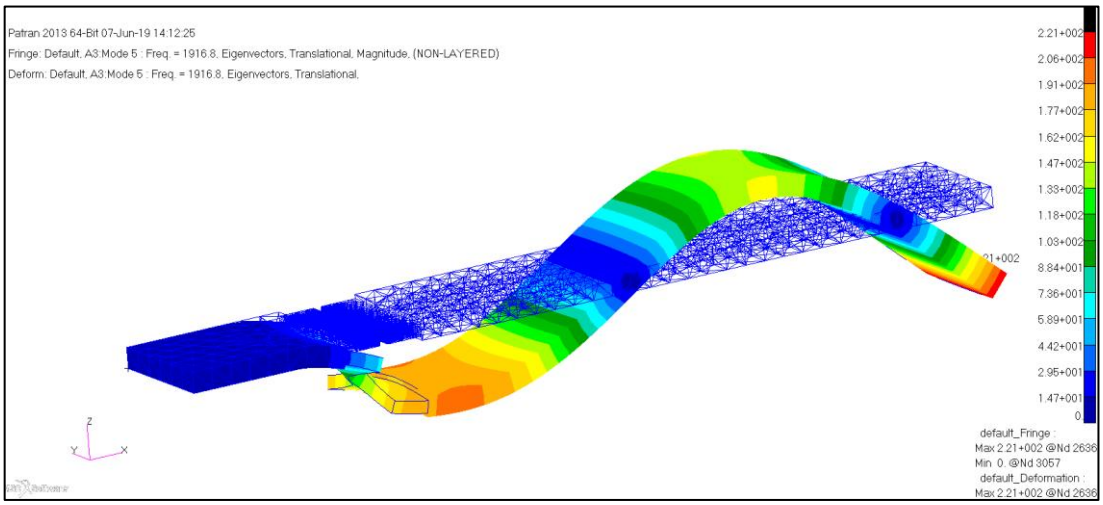

Figure 3-13: 5th mode shape of the beam- 3rd out-of-plane bending

Among the first 5 modes of the beam, only the 2nd, 4th and 5th modes are out-of-plane (T3: z-translation) displacement modes. Mode 1 is the in-plane displacement mode and mode 3 is the in-plane twisting mode and they are ineffective on the out-of-plane z-translation according to the modal effective mass fraction results. Therefore, modes 1 and 3 are ignored for the rest of this thesis study.

3.3. Modal Test of the Notched Beam

The modal damping ratios of the beam should be determined by carrying out with modal testing because the fatigue analysis results are very sensitive to the damping values, [29]. Without including the damping, in the resonance regions the notched beam encounters unrealistically high stresses. However, in reality, there is the damping in the dynamic systems. Therefore, the modal testing is carried out with impact hammer, accelerometers and clamp in order to extract the modal damping rations of the beam. The test setup, impact hammer and the accelerometers used are shown in Figure 3-14, Figure 3-15, Figure 3-16 and Figure 3-17.

Figure 3-14: The modal test setup

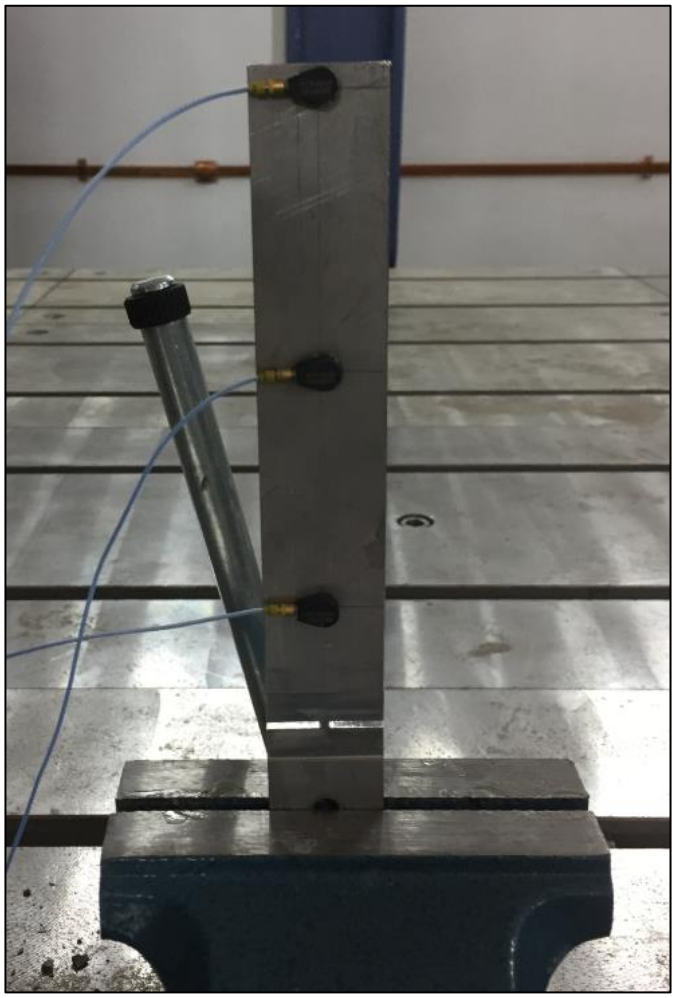

Figure 3-15: The modal test setup

Figure 3-16: The impact hammer (calibration is valid until 26.01.2022)

Figure 3-17: One of the accelerometers (calibration is valid until 20.11.2019)

The modal damping ratio result of the modal test is given in Table 3-4. The used software is LMS Test.Lab and this program uses the half-power bandwidth method while calculating the damping ratios. The damping ratio calculation is given by Equation 3.1, [47]. The coefficients in Eqn. 3.1 is given by Figure 3-18.

$$\zeta = \frac{\omega_2 - \omega_1}{2 * \omega_n} \tag{3.1}$$

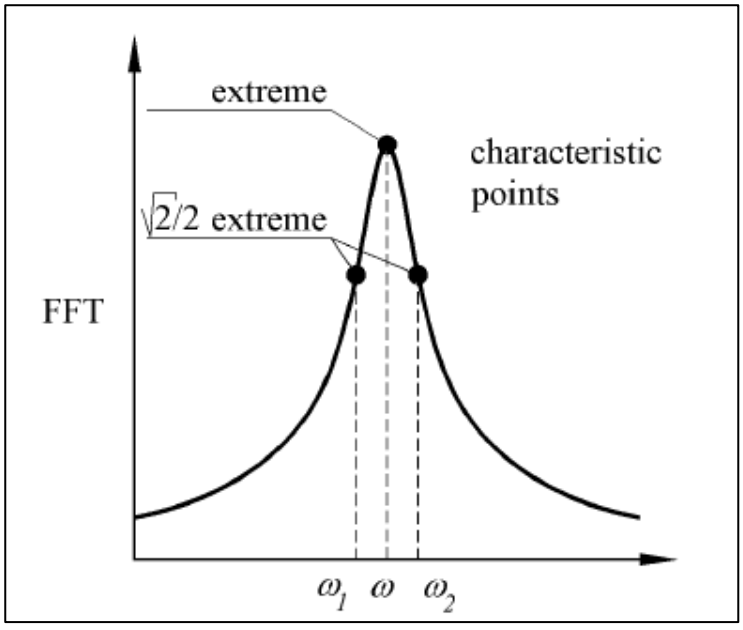

Figure 3-18: Half-power bandwidth method, [48]

Table 3-4: The modal damping ratio results

Mode no.	Frequency, [Hz]	Damping ratio, (ζ), [%]
2	38.490	1.14
4	635.053	0.48
5	1762.752	0.46

Table 3-5 compares the modal analysis and test results. As Table 3-5 shows, modal analysis and test results are in agreement, below 10%. Slight deviation between the analysis and test results could be due to the differences in the analysis and test boundary conditions since the boundary conditions cannot be applied perfectly in test the environment. Also, the material properties of the material used for the notched beam may differ slightly from those used in analysis.

Table 3-5: The deviations of analysis and test natural frequencies

Mode no.	Analysis Result [Hz]	Test Result [Hz]	Deviation [%]
2	39.64	38.49	2.90
4	664.10	635.05	4.37
5	1916.79	1762.75	8.04

3.4. Frequency Response Analysis of the Notched Beam

In order to perform the vibration fatigue analysis of the notched beam, the magnitude of the stress PSD profile to unit load input should be determined. For this purpose, finite element model of the notched beam is prepared according to the output of the mesh refinement work given in Table 3-2. The finite element mesh of the notched beam is given in Figure 3-5 and Figure 3-6. In order to extract the frequency response corresponding to the unit acceleration loading, the base acceleration load (1 mm/s^2) in the z-direction is applied to the region 25 mm from the left side of the beam as shown in Figure 3-1 and Figure 3-19. Since the frequency interval is from 4 Hz to 2000 Hz,

a field is created in MSC Patran utilizing the information given in Table 3-6. The field created is used in the frequency response analysis of the notched beam.

Table 3-6: Acceleration table

Frequency [Hz]	4	2000
Amplitude [mm/s^2]	1	1

The modal damping ratios of the notched beam, given in Table 3-4, are introduced into the analysis via the MSC Patran GUI utilizing the "Modal Damping" table. While inserting the modal damping ratios into the analysis, the values should multiplied by 2 because in the analysis "Structural Damping" (G) is selected as the damping, [37]. The relationship between the "Damping Ratio" (ζ) and the "Structural Damping" (G) is given by Equation 3.2. Table 3-7 gives the "Structural Damping" (G) values entered into the frequency response analysis.

$$G = 2 * \zeta \tag{3.2}$$

Table 3-7: Structural Damping Ratios (G) of the notched beam

Mode no.	**Natural Frequency**	**ζ [%]**	**G [%]**
2nd	39.64	1.14	2.28
4th	664.10	0.48	0.96
5th	1916.79	0.46	0.92

The prepared finite element model of the notched beam and the applied load and boundary conditions are given in Figure 3-19.

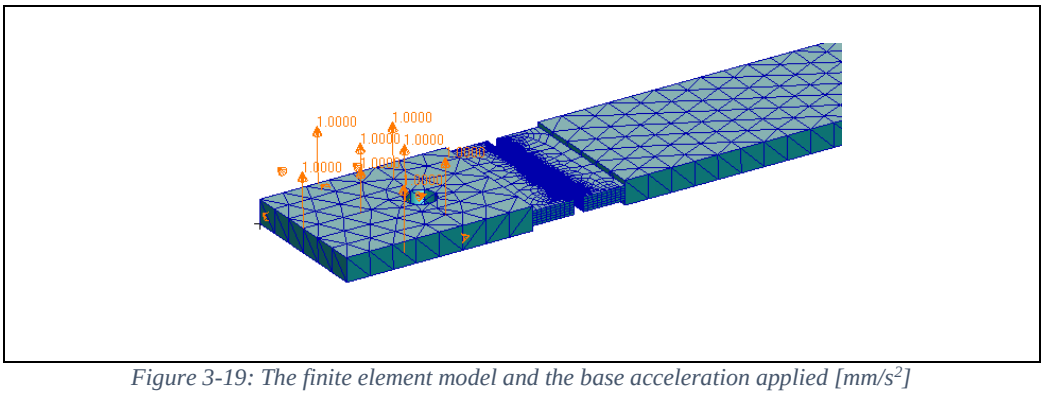

Figure 3-19: The finite element model and the base acceleration applied [mm/s^2]

The frequency response analysis to unit acceleration load input is performed with the MSC Nastran solution sequence 111. The stress frequency response of the notched beam to unit load is used in the vibration fatigue analysis for all nodes in the finite element model. In order to show an example, the stress frequency response of the notched beam to unit load is extracted from the node which is the middle node at the top element at notched region, as shown in Figure 3-20.

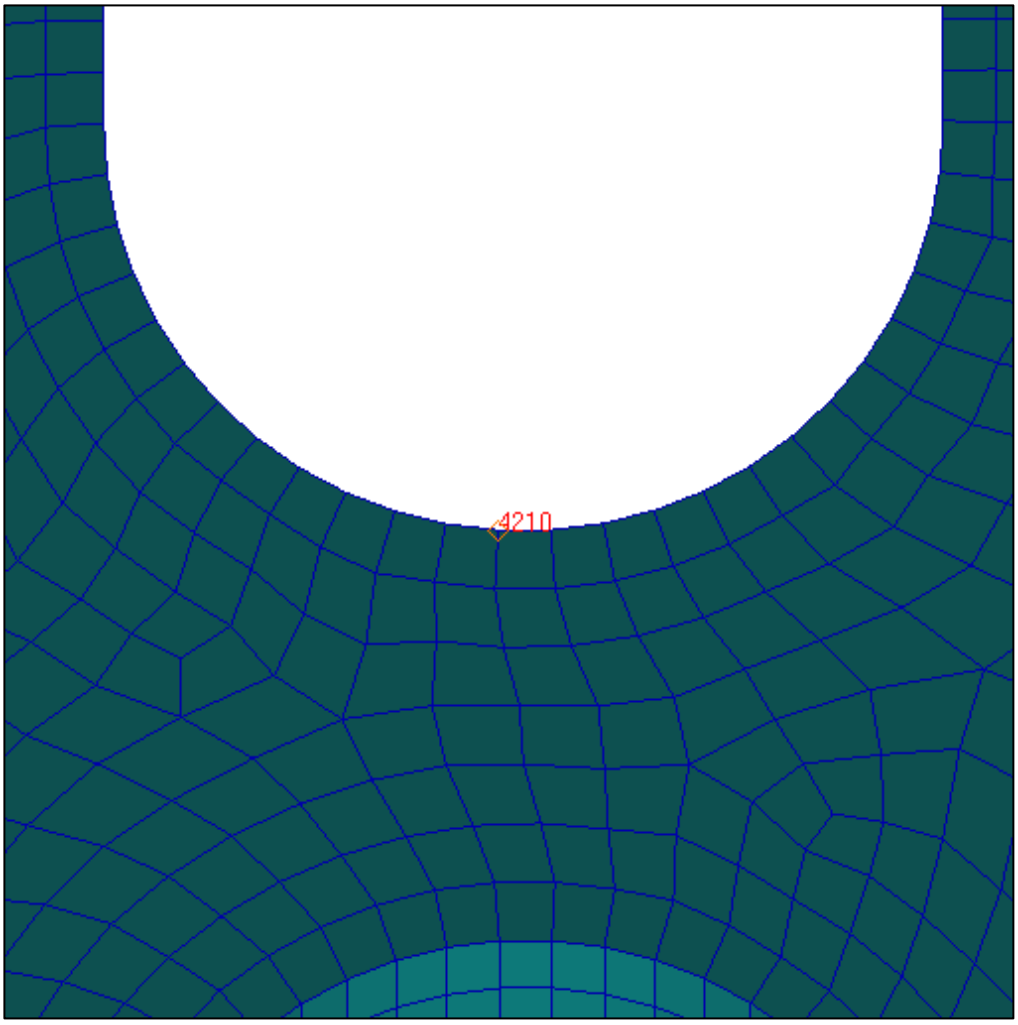

Figure 3-20: The finite element node (4210) where the von Mises stress frequency response is calculated

The von Mises stress frequency response of the node 4210 in the analysis model is given in Figure 3-21. As expected, the resonance regions of the stress frequency response and the natural frequencies are consistent.

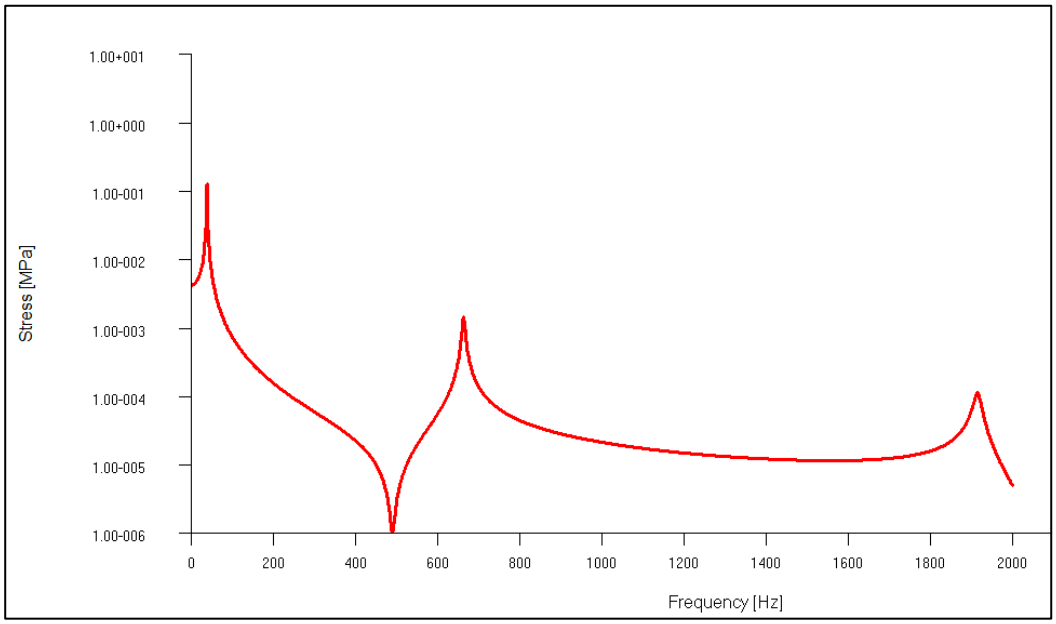

Figure 3-21: The von Mises stress response of the node 4210 corresponding to the unit load

3.5. Vibration Fatigue Analysis

Following the completion of the frequency response analysis corresponding to unit base vibration input for all nodes in the finite element model, the vibration fatigue analysis is conducted. For the vibration fatigue analysis, nCode DesignLife program is used as the fatigue analysis solver. In the vibration fatigue analysis, the beam is held horizontally, however, the mean stress effect of the gravity is neglected in this thesis study. The workspace of the fatigue analysis of the nCode DesignLife program is given in Figure 3-22.

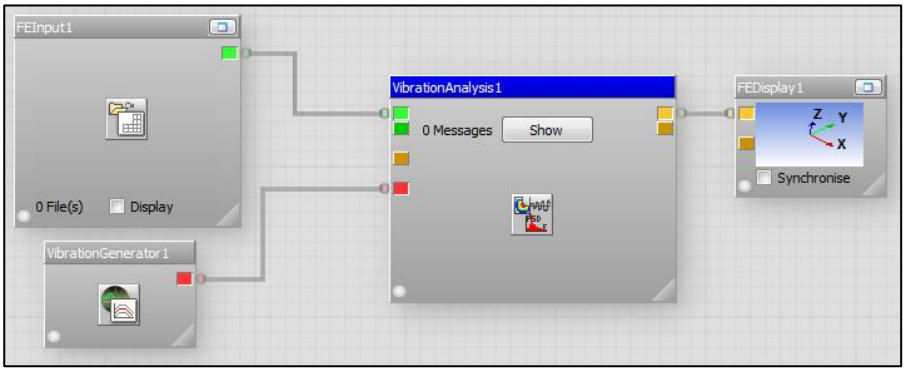

Figure 3-22: The workspace of the fatigue analysis of the nCode DesignLife

In Figure 3-22, the FEInput box is the input of finite element model which is the FRF of unit base vibration load. The VibrationGenerator box is the input PSD load which is the white noise type PSD. Figure 3-23 gives the PSD of the white noise profile which is used in the vibration fatigue analysis. As mentioned before, the frequency interval of the PSD profile is taken as 4-2000 Hz. Moreover, after few preliminary fatigue analysis iterations which are done in order to verify that the test time is reasonable, the amplitude of the white noise is taken as 100000 $(mm/s^2)^2/Hz$.

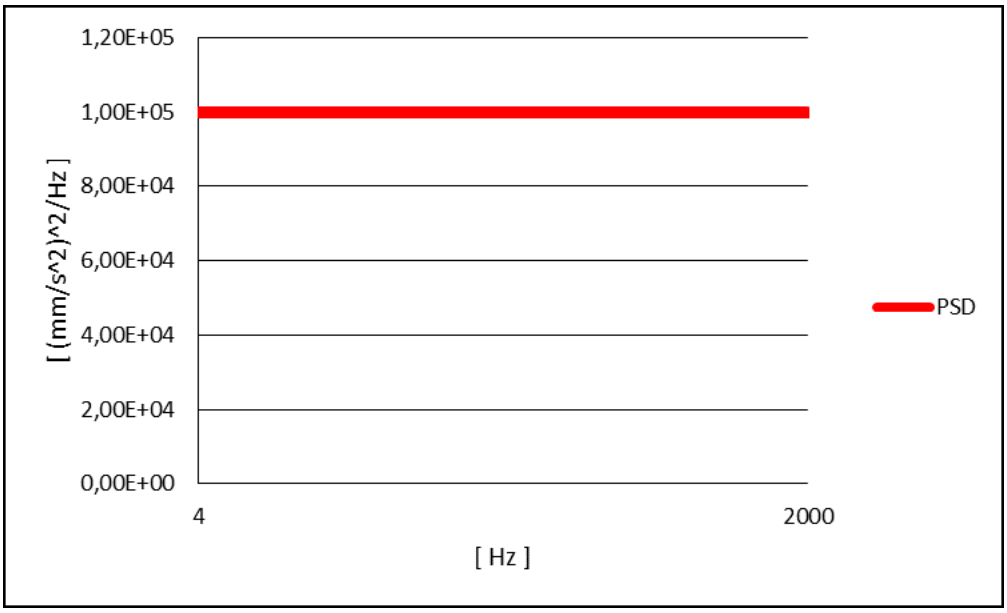

Figure 3-23: PSD profile of the vibration fatigue analysis

After supplying the FRF of the unit base vibration load and the PSD profile, VibrationAnalysis box of the nCode DesignLife program is edited. The detailed settings done in the VibrationAnalysis box section of the nCode DesignLife program is given in APPENDIX A.

The time setting of the analysis is set to 1 second and the PSD cycle count method is selected as the Dirlik method for the vibration fatigue analysis.

The material selection is done from the material library of the nCode DesignLife program. The nCode DesignLife has a material library from which one can select the ultimate tensile strength (UTS) for different alloys of aluminum. In this thesis study,

in order to select the appropriate aluminum UTS, the tensile strength test is conducted. Total of 7 specimens are tested in order to predict the UTS value of aluminum notched beams. The 2-D technical drawing of the specimens is given in Figure 3-24.

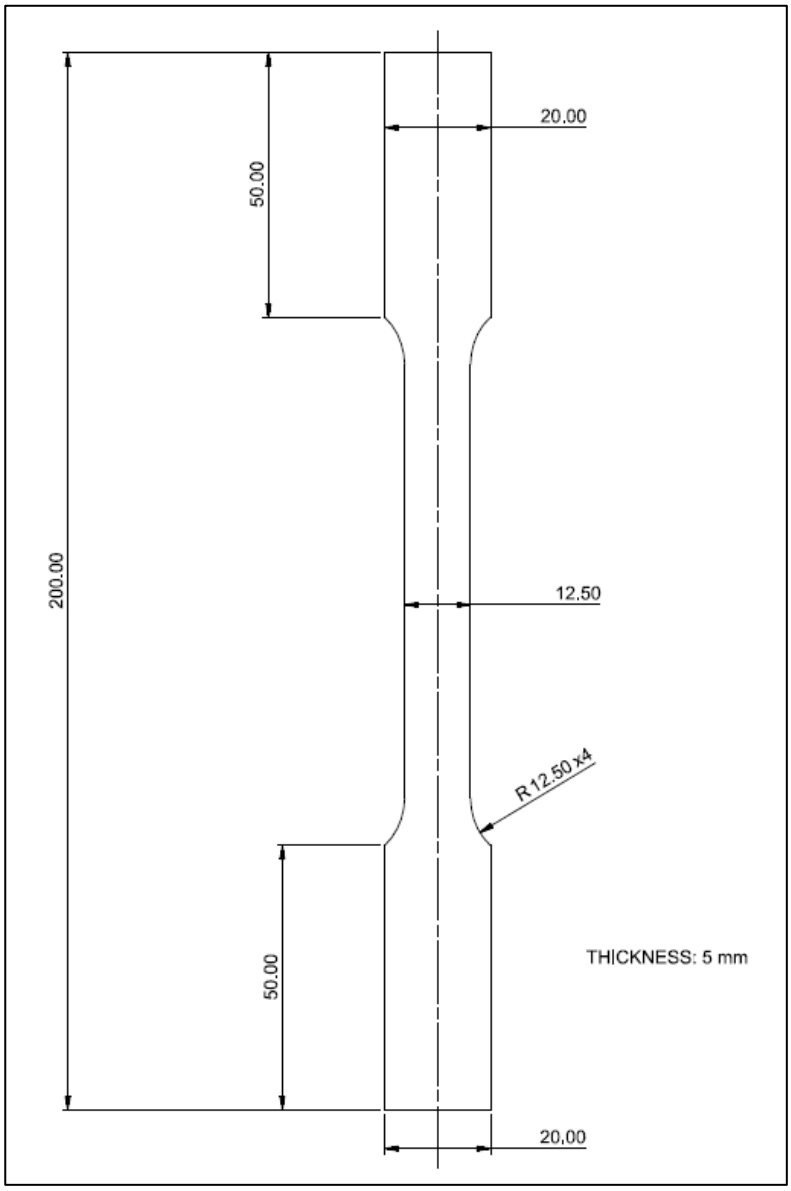

Figure 3-24: 2-D drawing of the aluminum tensile strength test specimens, [mm]

The tensile strength test is conducted with a strain rate of 0.5 min^{-1}. The resultant UTS values of specimens are given in Table 3-8.

Table 3-8: UTS values of aluminum specimens

Test #	1	2	3	4	5	6	7	Mean	Standard Deviation
UTS (MPa)	322.9	320.3	316.6	319.4	320.5	321.3	321.3	320.3	1.97

According to Table 3-8, the mean UTS value of the aluminum specimens is 320 MPa. However the nCode DesignLife material library has the option specifying the UTS in multiples of 100 MPa. Hence, 2 vibration fatigue analyses are conducted, the aluminum material with 300 MPa and 400 MPa UTS are selected as shown in Figure 3-25 and Figure 3-26. The roughness option is selected as polished because in order to observe the crack initiation properly, the notched region of the beam is polished in the present study.

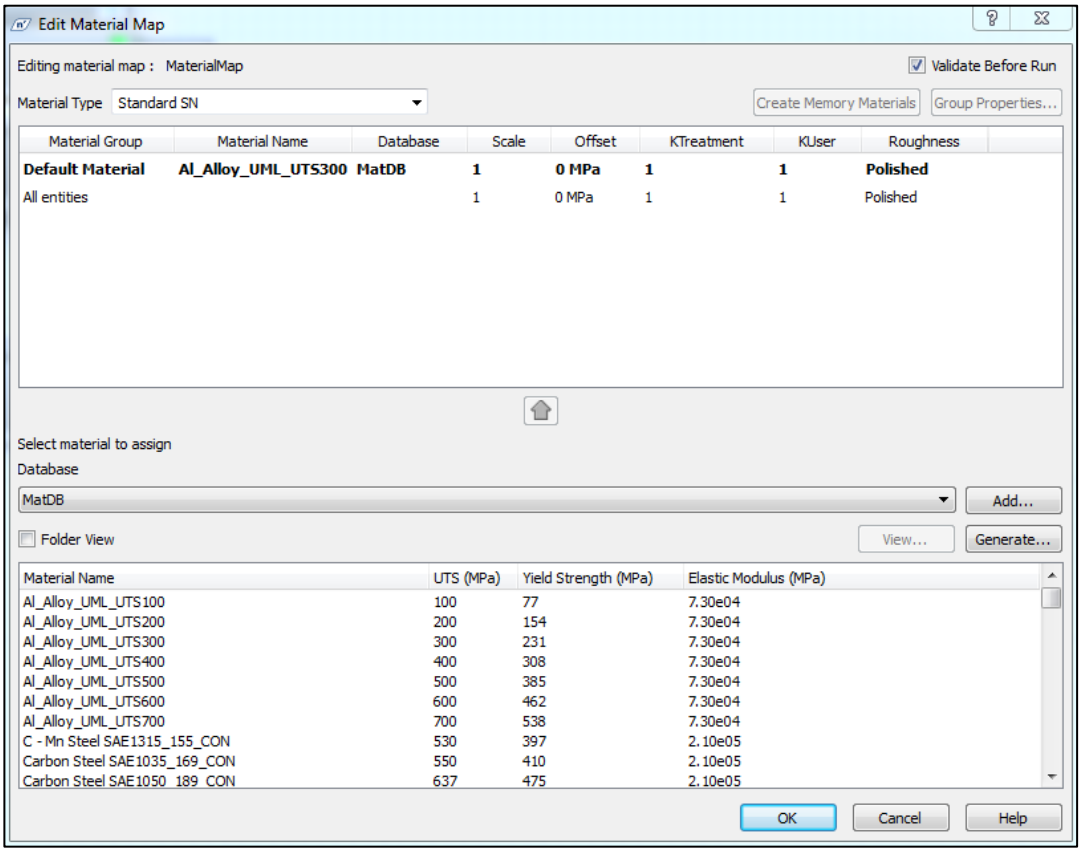

Figure 3-25: Material selection tool box in the nCode DesignLife program, 300 MPa UTS

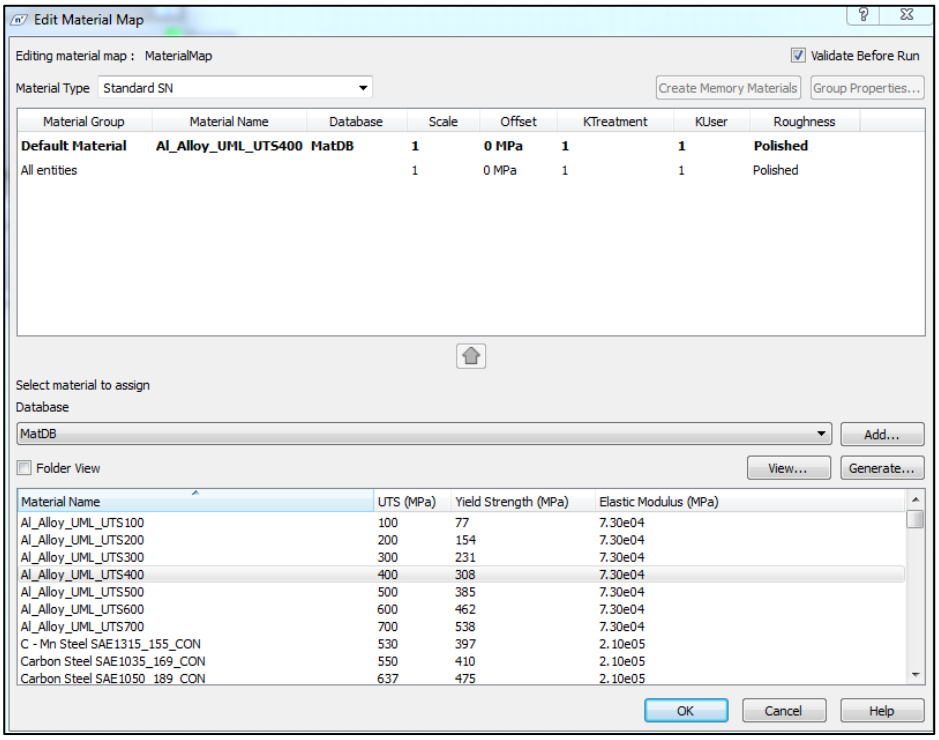

Figure 3-26: Material selection tool box in the nCode DesignLife program, 400 MPa UTS

The S-N graphs of the selected materials are given in Figure 3-27 and Figure 3-28.

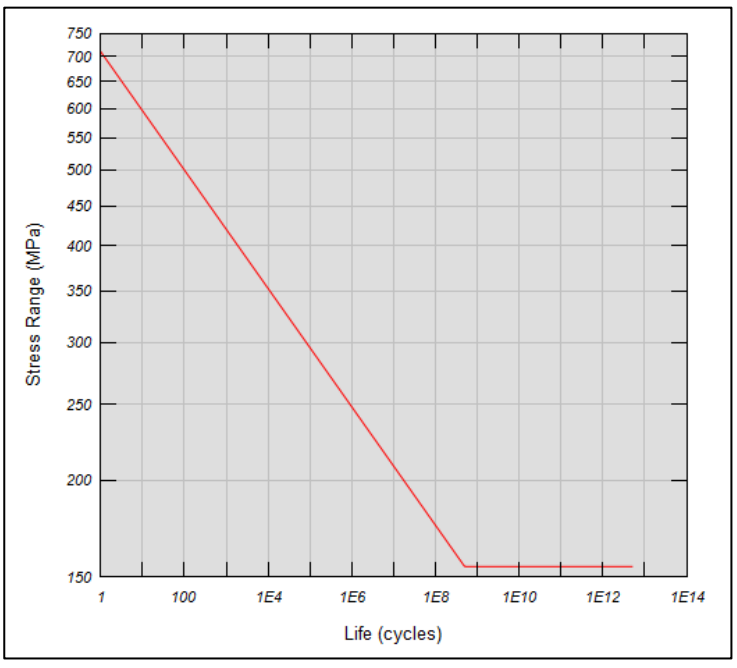

Figure 3-27: The S-N graph of Aluminum Alloy which has 300 MPa UTS

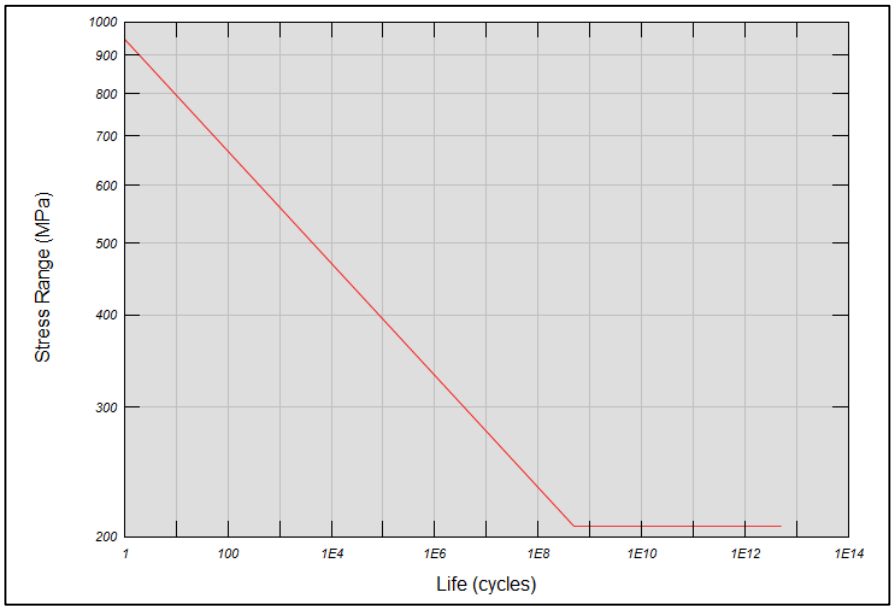

Figure 3-28: The S-N graph of Aluminum Alloy which has 400 MPa UTS

After providing the inputs and setting the options, the vibration fatigue analyses have been carried out.

The results shows that the node 33815 has the minimum fatigue life. However, the FRF graph of the node 4210 was used in the previous section to calculate the stress PSD. It is to be noted that the notch has 4 corner nodes in the finite element model which have the similar stress histories. The nodes 4210 and 33815 are shown in Figure 3-29.

The results of the 2 vibration fatigue analyses of the aluminum notched beam are given in Figure 3-30 and Figure 3-31 as the fatigue life in seconds.

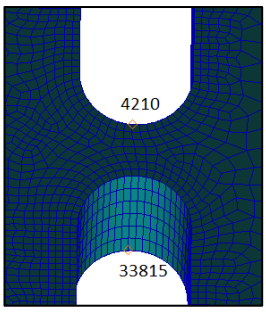

Figure 3-29: The node 4210 (upper) and the node 33815 (lower)

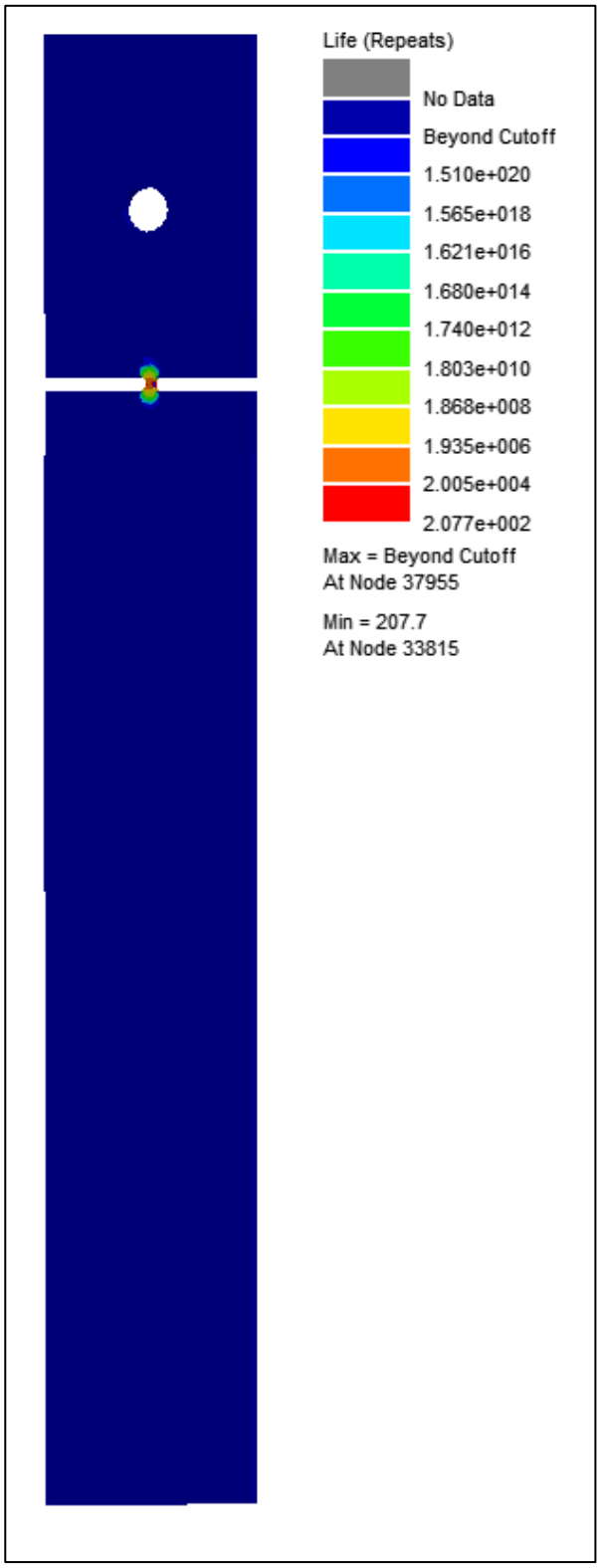

Figure 3-30: The vibration analysis result of the aluminum notched beam, 300 MPa UTS, life in seconds

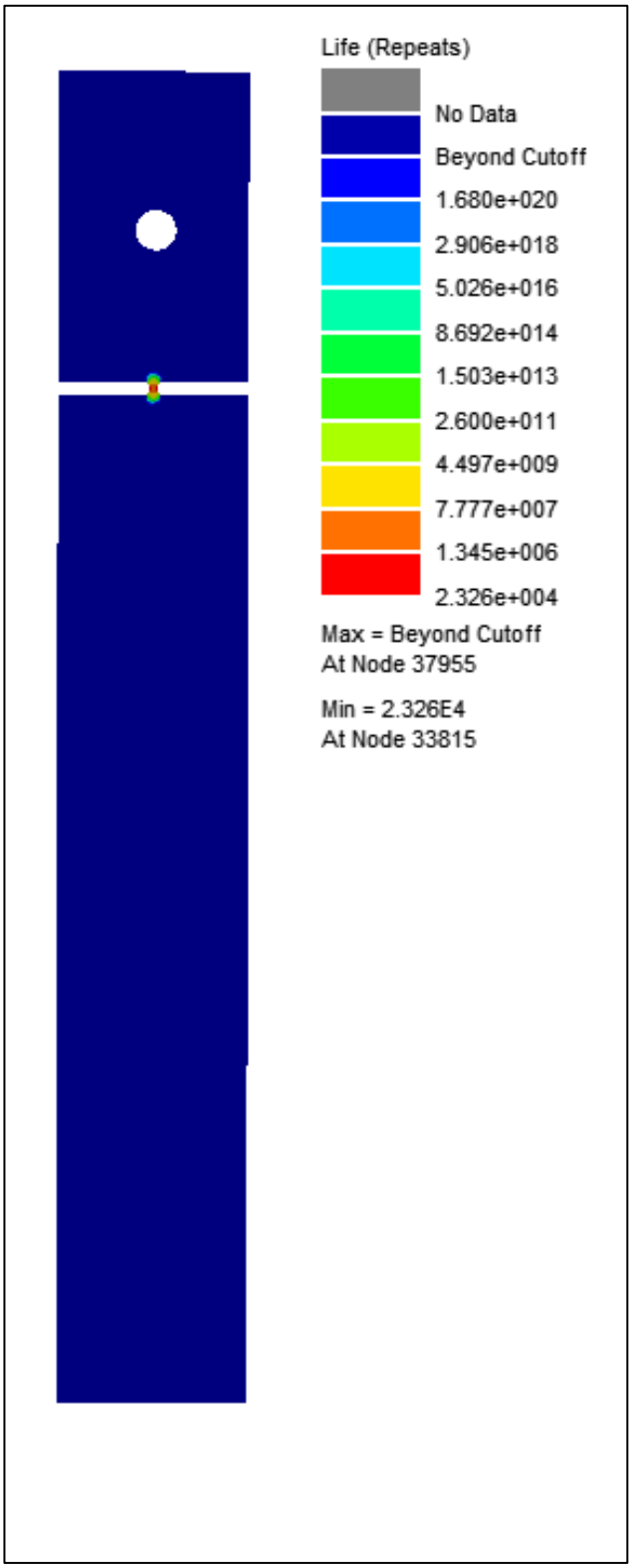

Figure 3-31: The vibration analysis result of the aluminum notched beam, 400 MPa UTS, life in seconds

The detailed views of the fatigue life results are given in Figure 3-32 and Figure 3-33.

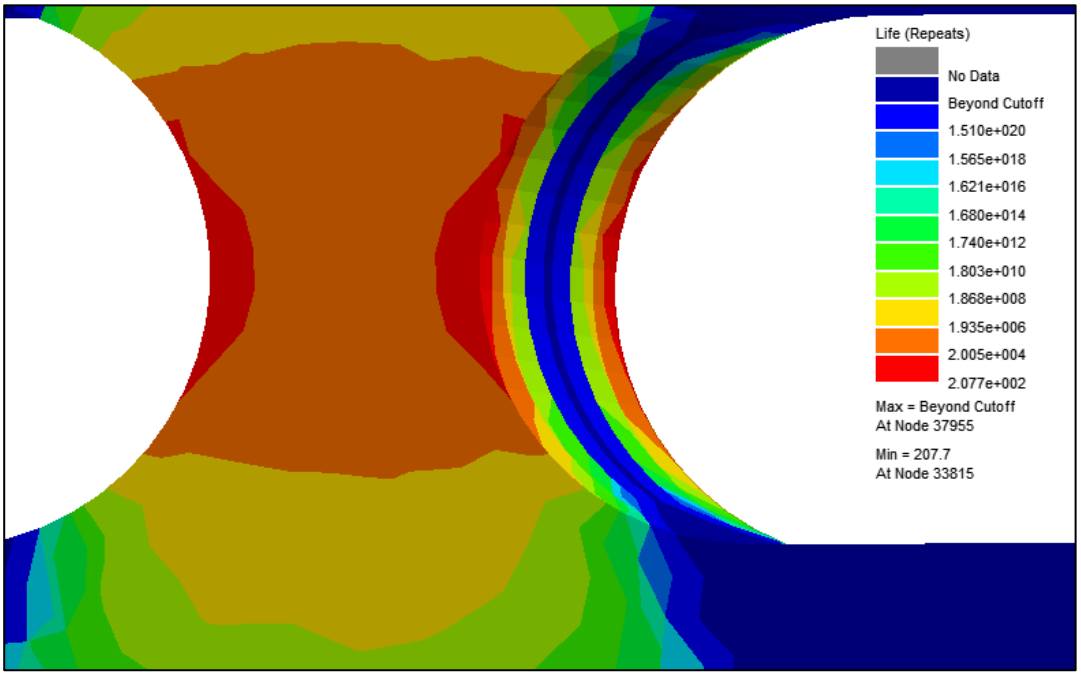

Figure 3-32: The detailed view of the result, 300 MPa UTS, [s]

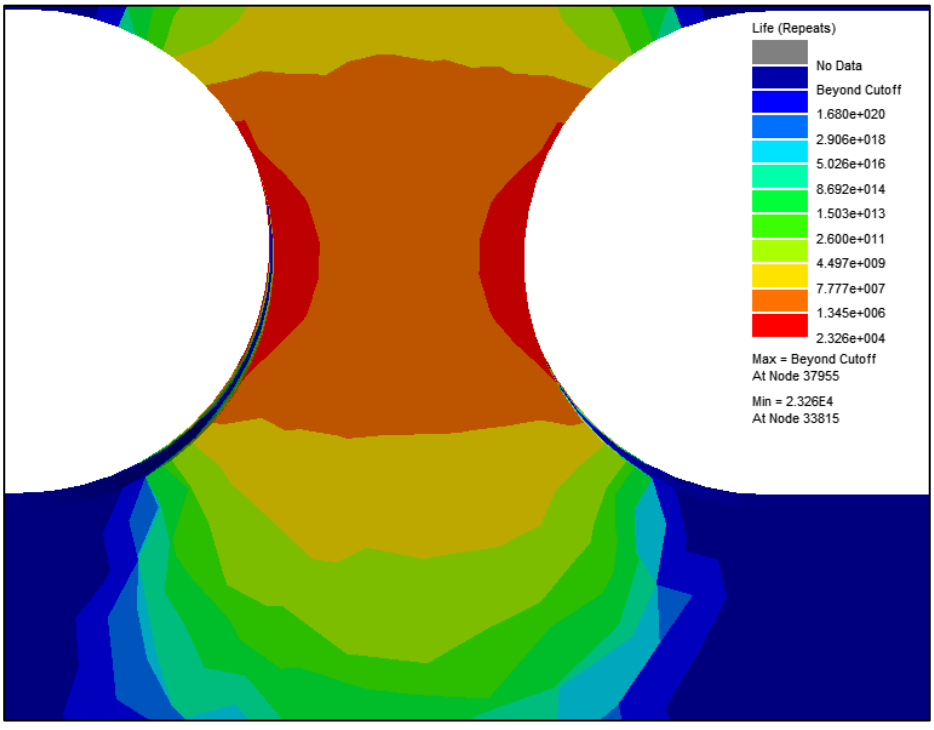

Figure 3-33: The detailed view of the result, 400 MPa UTS, [s]

According to the results, the life of the aluminum notched beam with 300 MPa UTS is 207.7 seconds or 3 minutes and 27.7 seconds around the corner of the notch and the life of the aluminum notched beam with 400 MPa UTS is 23260 seconds or 387 minutes and 40 seconds around the corner of the notch. The results are given in Table 3-9 in order to give a better visual comparison.

Table 3-9: Vibration fatigue analyses results of aluminum notched beam

	300 MPa UTS	**400 MPa UTS**
Time Results	207.7 seconds	23260 seconds
	3 min. 27.7 sec.	387 min. 40 sec.

3.6. Vibration Fatigue Test

In order to verify the fatigue analysis result of the aluminum notched beam, vibration fatigue test is conducted. The prepared test setup is given in Figure 3-34. The top accelerometer is chosen as the control accelerometer because it is the nearest one to the displacement constraint region of the aluminum notched beam.

The vibration table used in the vibration fatigue test, which is given in Figure 3-34, vibrates in the out-of-plane direction of the beam. Due to the internal resonance issues of the table, the frequency of interest is limited from 4 Hz to 2000 Hz in the present thesis study.

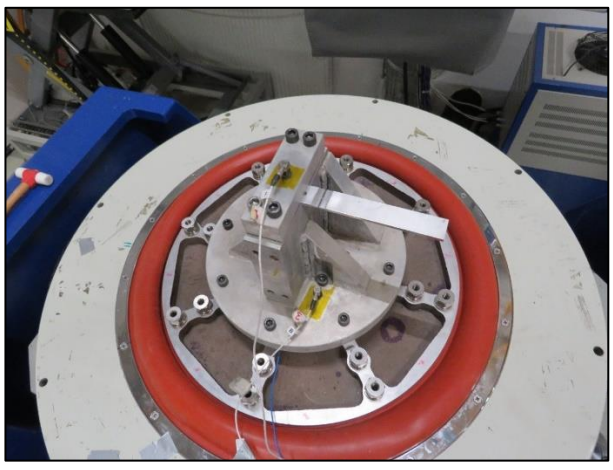

Figure 3-34: Test setup of the aluminum notched beam

The PSD profile of the test is set from 4 Hz to 2000 Hz due to the vibration table constraints as mentioned before. The experiment is conducted with 1 Hz increment. The white noise PSD load of the test is same as the analysis of the aluminum notched beams which is given in Figure 3-23.

For the data analysis of the vibration test LMS Test.Lab software is used. In LMS Test.Lab, the unit of PSD is g^2/Hz. Therefore, the white noise PSD load input is converted to g^2/Hz and the converted PSD is given in Figure 3-35.

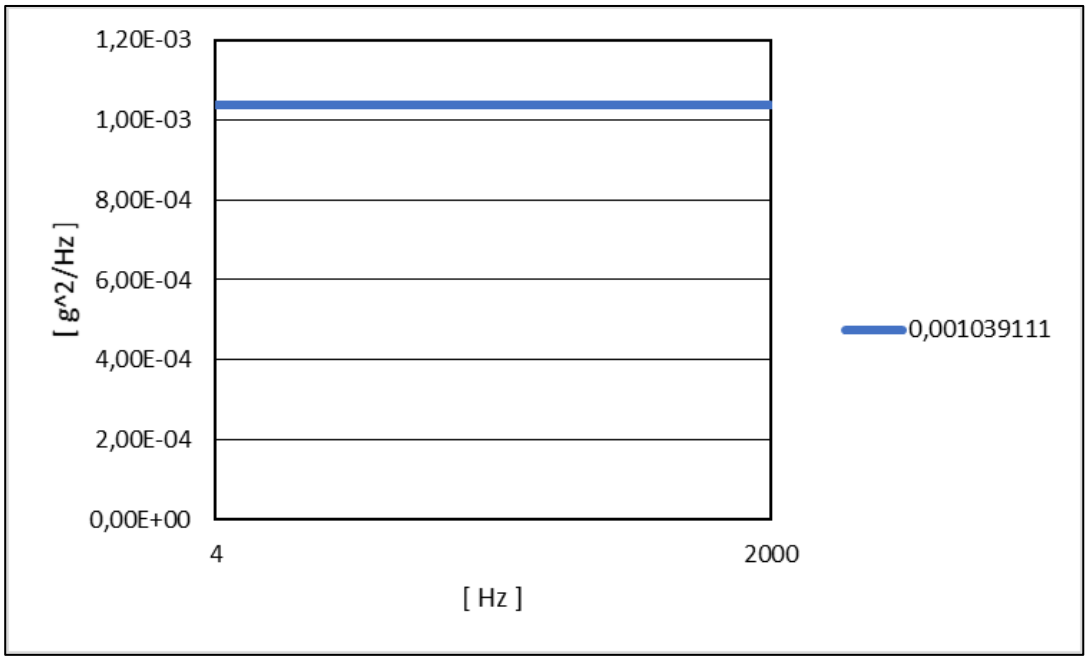

Figure 3-35: The input PSD profile of the vibration fatigue test in the units of g^2/Hz

Figure 3-36 gives one of the sample profile of the applied PSD load which is the output from reference accelerometer in the vibration fatigue test.

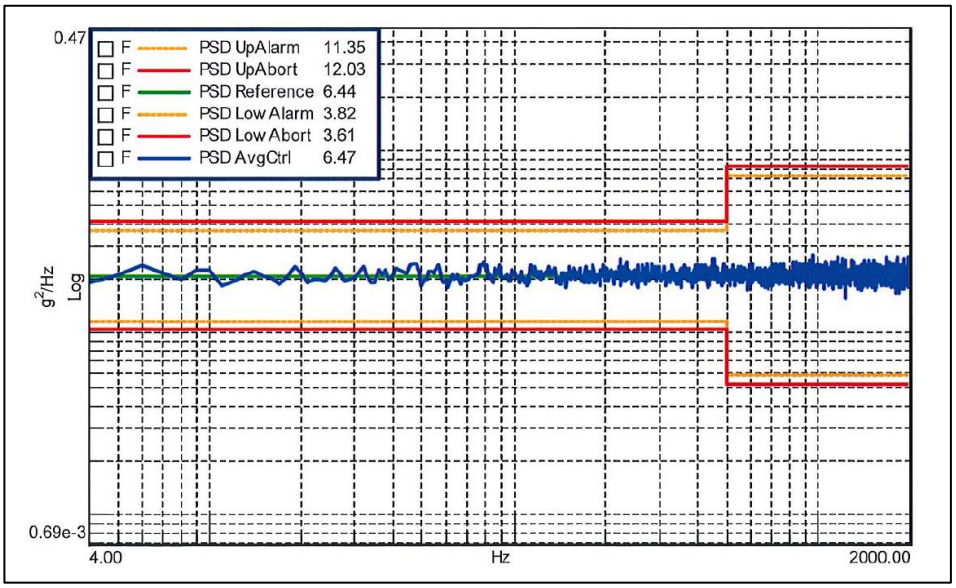

Figure 3-36: The sample applied output PSD load

Vibration fatigue tests are observed until the crack initiation occurs. The crack initiations are monitored with human eye. When the crack initiation occurs, the test is terminated and the time of the test is recorded. Total of 10 aluminum notched beams are tested. The times from the test beginning to observed crack initiation are given in Table 3-10.

Table 3-10: Crack initiation times of the aluminum notched beams

Specimen	Life (s)	Time
1	825	13 min 45 sec
2	840	14 min
3	895	14 min 55 sec
4	435	7 min 15 sec
5	730	12 min 10 sec
6	869	14 min 29 sec
7	876	14 min 36 sec
8	855	14 min 15 sec
9	1120	18 min 40 sec
10	880	14 min 40 sec
Mean	832.5	13 min 52.5 sec
Standard Deviation	170.4	2 min 50.4 sec

Pictures of some of the aluminum notched beams with cracks are given in Figure 3-37, Figure 3-38 and Figure 3-39.

The pictures are taken a little after the crack initiation. Since the crack monitoring method is human eye and when the crack initiation is observed, the vibration table is stopped. But during that time, the vibration table vibrates a little bit more. Hence, the cracks are photographed little after the real crack initiation time.

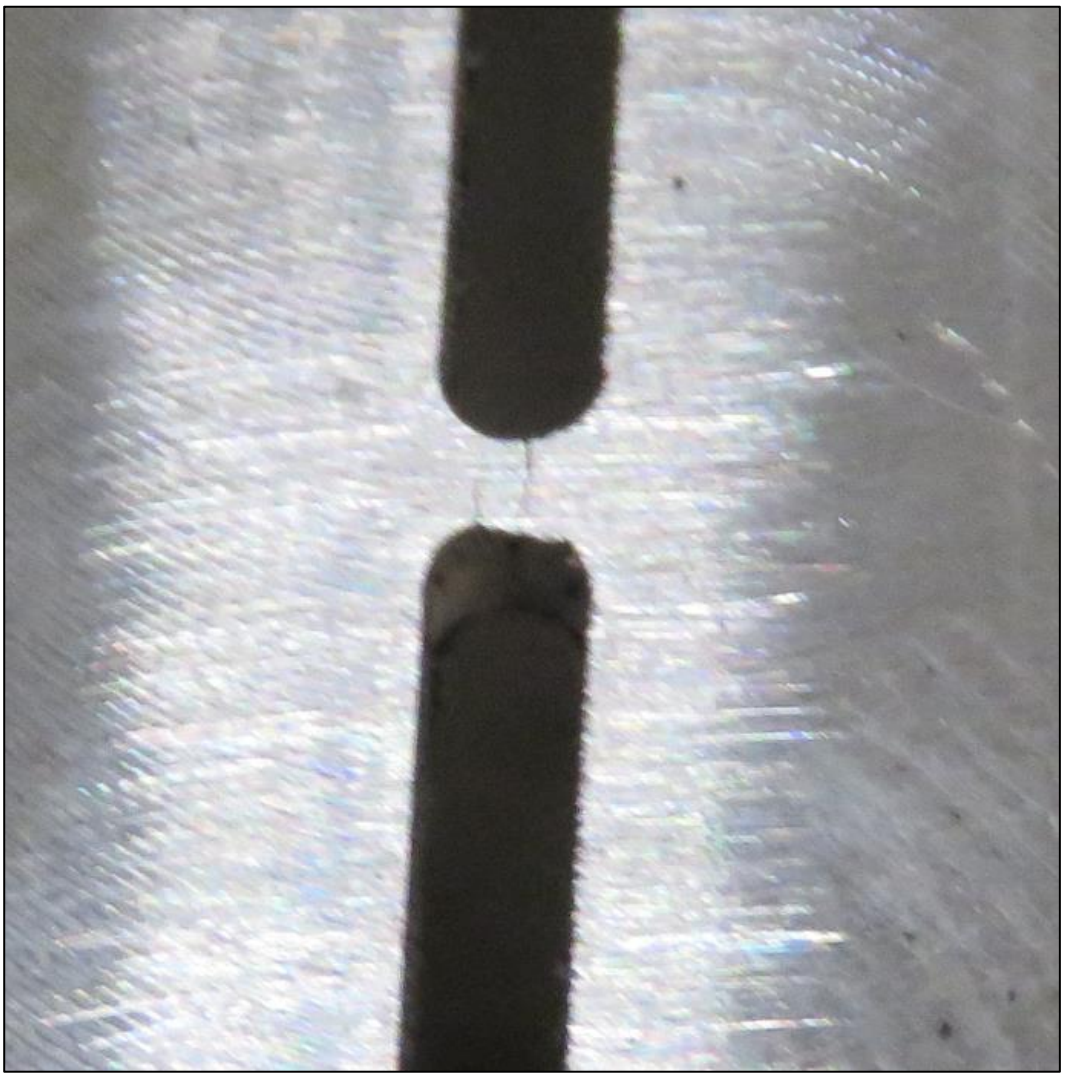

Figure 3-37: Aluminum notched beam with crack - Sample 1

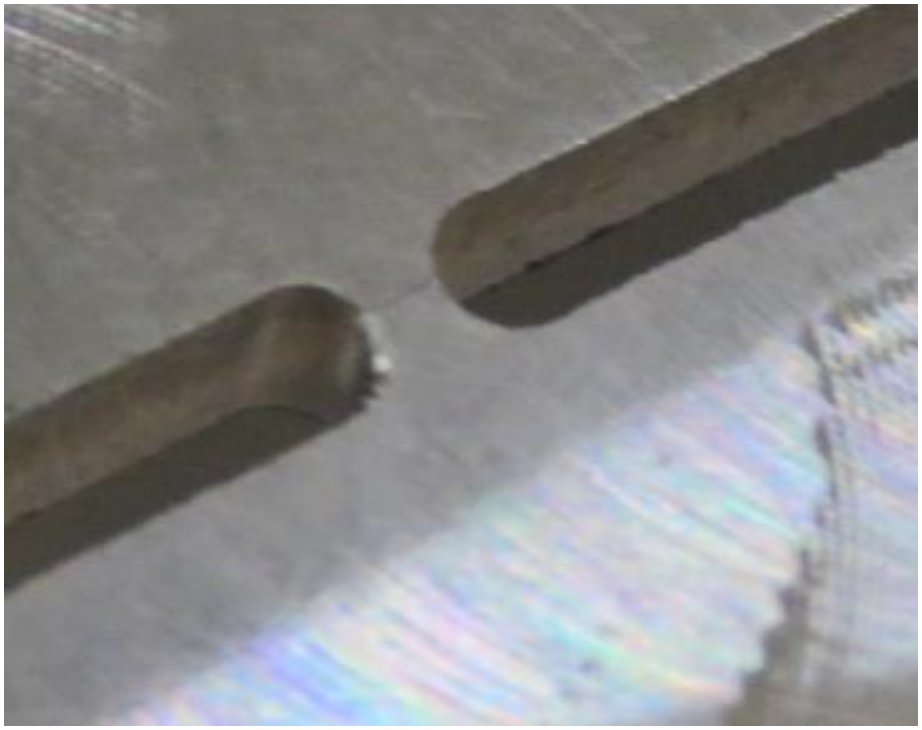

Figure 3-38: Aluminum notched beam with crack - Sample 2

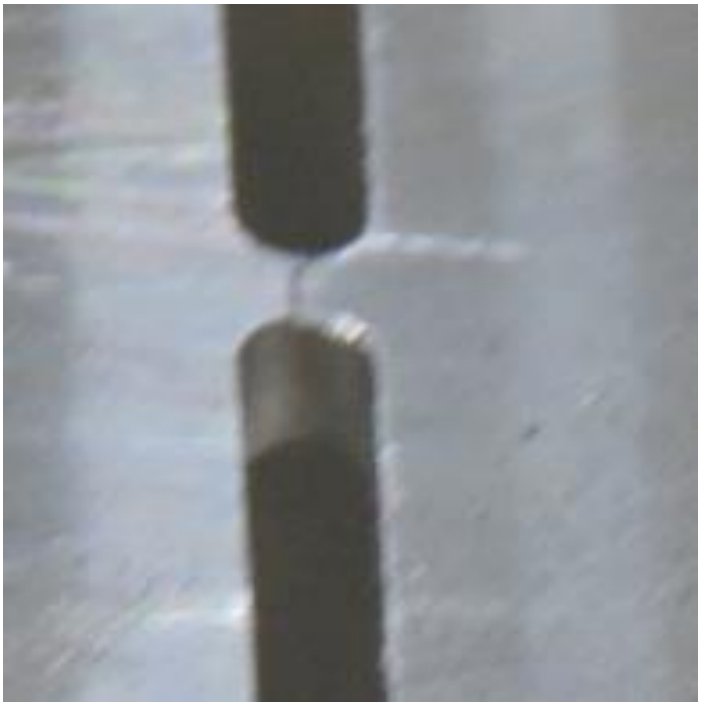

Figure 3-39: Aluminum notched beam with crack - Sample 3

CHAPTER 4

VIBRATION FATIGUE ANALYSIS AND TEST OF STEEL NOTCHED BEAMS

Steel notched rectangular cross-section beams are also designed in order to conduct the random vibration mechanical fatigue analysis and tests as in Chapter 3. Moreover, same analysis and test procedures is valid for steel notched beam as given in Chapter 3. Furthermore, in order to examine the effect of the different damping ratio values in the vibration fatigue analyses, 3 more analyses are conducted with different damping ratio values.

4.1. Steel Notched Beams

The same notched beam geometry is used as in Chapter 3. The geometry and 2-D drawing of the steel notched beam is given in Figure 3-1. The material properties of the material of the steel notched beam are given in Table 4-1.

Table 4-1: The mechanical material properties of Steel, [35]

Density	8000 kg/m^3
Elastic Modulus	200 GPa
Poisson's Ratio	0.27

4.2. Preliminary Modal Analysis

The modal analysis is performed using the MSC Nastran finite element solver and MSC Patran finite element pre-post processor. The used finite element types in the finite element model are the TET4 and HEX8 again as in Chapter 3. Figure 3-2 gives the description of the finite elements used in the finite element model.

Before starting the fatigue analysis, the same mesh refinement work has been performed again as in Chapter 3. The result of the mesh refinement work same as

Chapter 3 is given in Table 3-2 and Figure 3-4. According to the results of the mesh refinement study, the same finite element model of the Chapter 3 is used.

Figure 3-5 and Figure 3-6 give the finite element mesh of the aluminum notched beam, which is same as steel notched beam.

The same preliminary modal analysis is carried out as in Chapter 3. The modal effective mass fraction results of the modal analysis are given in Table 4-2.

Table 4-2: Modal effective mass fraction results for the out-of-plane displacement (z translation, T3)

Mode No.	Frequency (Hz)	Fraction	Cumulative
1	23.458	1.766E-09	1.766E-09
2	39.500	6.809E-01	6.809E-01
3	343.486	2.895E-09	6.809E-01
4	661.404	1.479E-01	8.289E-01
5	1908.914	5.752E-02	8.864E-01

According to Table 4-2, the same comments and remarks can be made again as in Chapter 3. Besides of it, same frequency interval is decided to be used as 4-2000 Hz as in Chapter 3.

The first 5 mode shapes of the steel notched beam are given in Figure 4-1, Figure 4-2, Figure 4-3, Figure 4-4 and Figure 4-5 respectively.

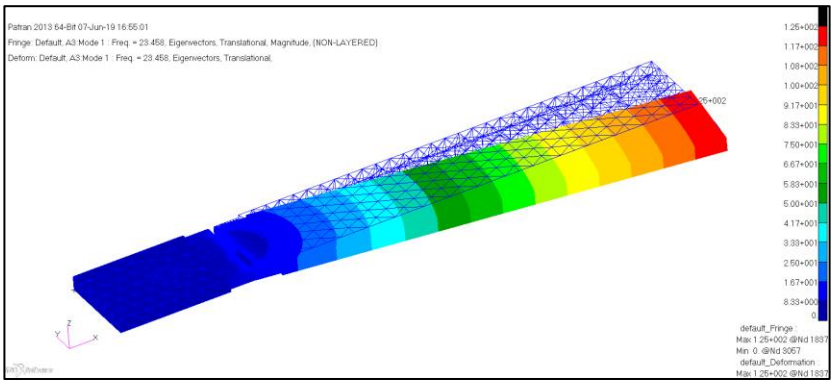

Figure 4-1: 1st mode shape of the beam- 1st in-plane bending

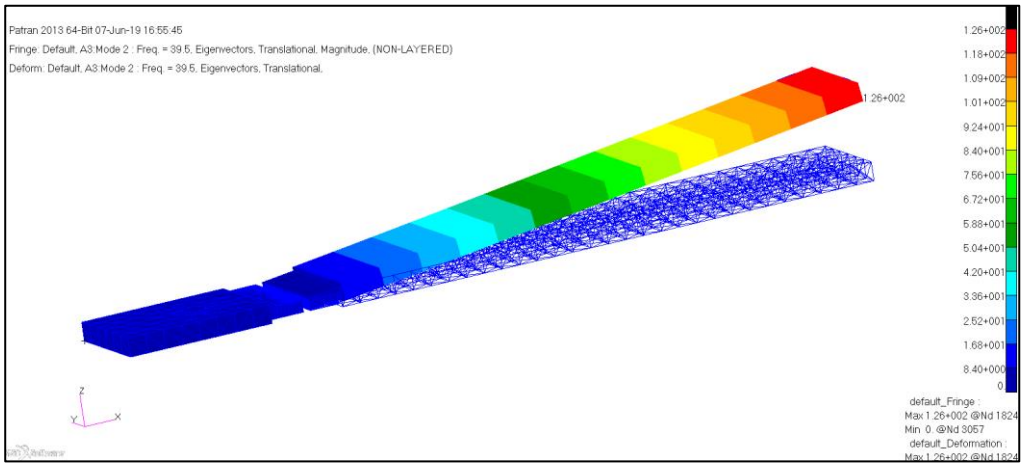

Figure 4-2: 2nd mode shape of the beam- 1st out-of-plane bending

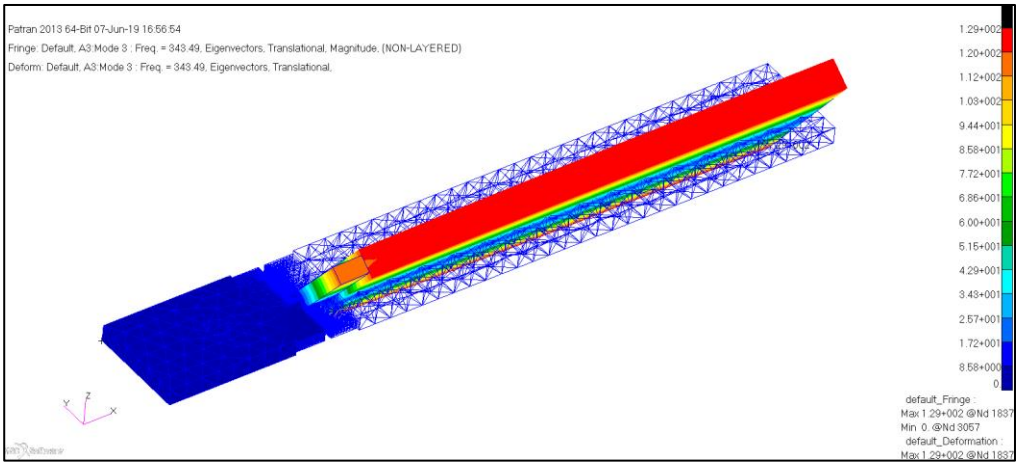

Figure 4-3: 3rd mode shape of the beam- 1st torsion

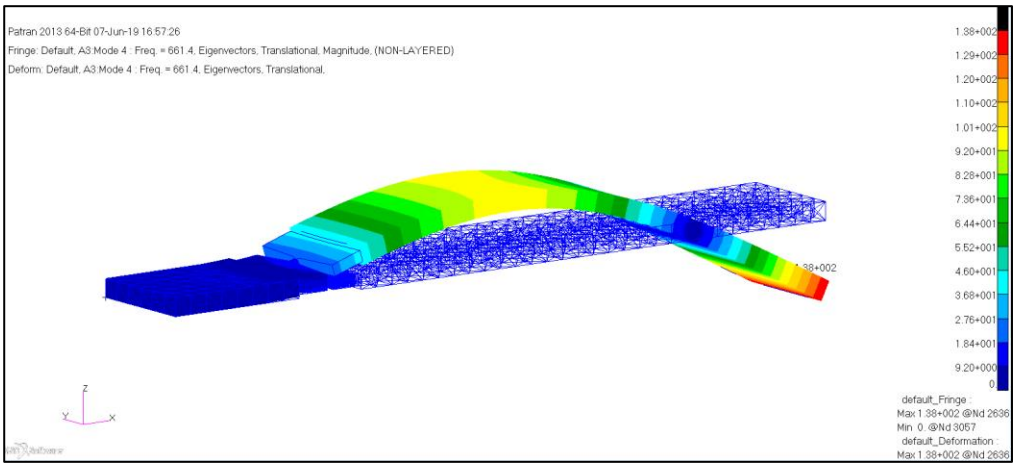

Figure 4-4: 4th mode shape of the beam- 2nd out-of-plane bending

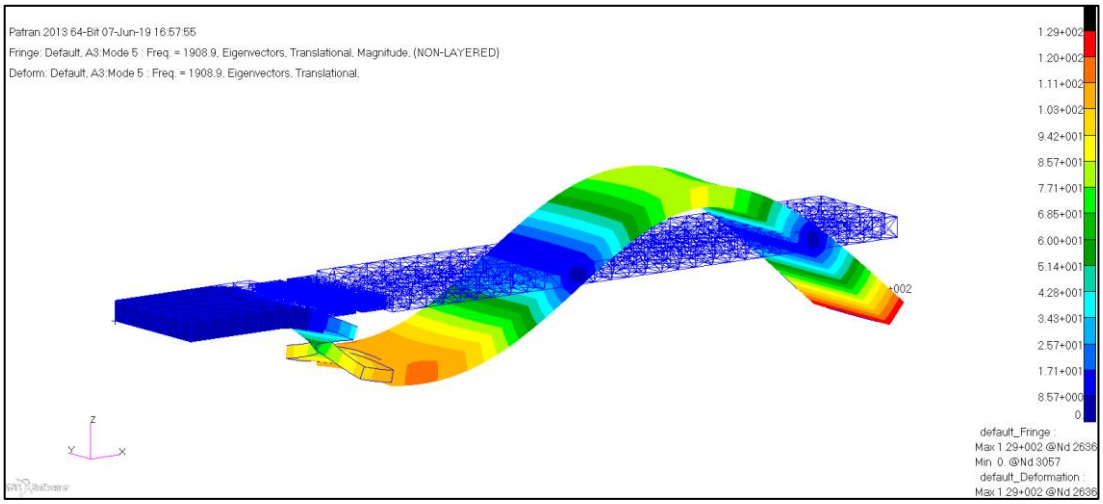

Figure 4-5: 5th mode shape of the beam- 3rd out-of-plane bending

Same as in Chapter 3, modes 1 and 3 of steel notched beam are ignored for the rest of this thesis study.

4.3. Modal Test of the Notched Beam

The same modal test procedure is carried out as in Chapter 3. The same test setup, same impact hammer and the same accelerometers used as in Chapter 3 and they are shown in Figure 3-14, Figure 3-15, Figure 3-16 and Figure 3-17.

The modal damping ratio result of the modal test is given in Table 4-3.

Table 4-3: The modal damping ratio results

Mode no.	Frequency, [Hz]	Damping ratio, (ζ), [%]
2	39.795	2.16
4	641.045	1.80
5	1746.366	1.12

Table 4-4 compares the modal analysis and test results. As Table 4-4 shows, modal analysis and test results are in agreement, below 10%, again as in Chapter 3.

Table 4-4: The deviations of analysis and test natural frequencies

Mode no.	Analysis Result [Hz]	Test Result [Hz]	Deviation [%]
2	39.500	39.795	0.741
4	661.404	641.045	3.078
5	1908.914	1746.366	8.515

4.4. Frequency Response Analysis of the Notched Beam

In order to perform the vibration fatigue analysis of the steel notched beam, same frequency response analysis procedure is carried out as in Chapter 3.

Table 4-5 gives the "Structural Damping" (G) values entered into the frequency response analysis.

Table 4-5: Structural Damping Ratios (G) of the notched beam

Mode no.	Natural Frequency	ζ [%]	G [%]
2nd	39.500	2.16	4.32
4th	661.404	1.80	3.60
5th	1908.914	1.12	2.24

The prepared finite element model of the steel notched beam and the applied load and boundary conditions are same as in Chapter 3 and they are given in Figure 3-19.

The frequency response analysis to unit acceleration load input is performed with the MSC Nastran solution sequence 111. The example stress frequency response of the notched beam to unit load is extracted from the same node as in Chapter 3, which is the middle node at the top element at the notched region, as shown in Figure 3-20.

The von Mises stress frequency response of the node 4210 in the analysis model is given in Figure 4-6. As expected, the resonance regions of the stress frequency response and the natural frequencies are consistent.

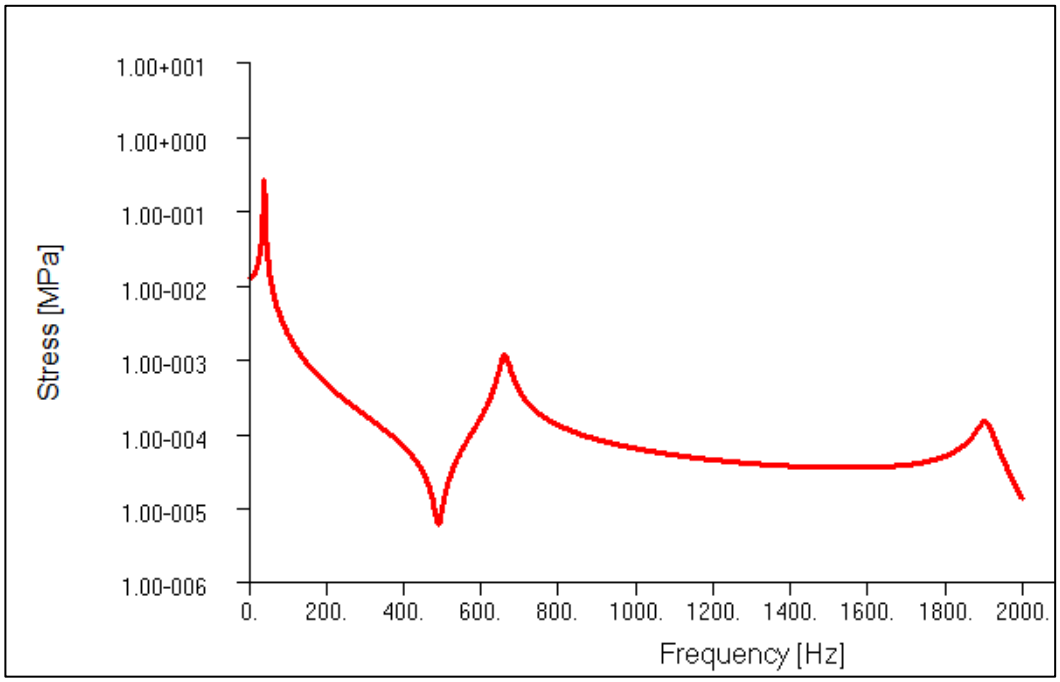

Figure 4-6: The von Mises stress response of the node 4210 to corresponding the unit load

4.5. Vibration Fatigue Analysis

Following the completion of the frequency response analysis corresponding to unit base vibration input, the same vibration fatigue analysis procedure as in Chapter 3 is conducted. As mentioned before, the frequency interval of the PSD profile is taken as 4-2000 Hz. Besides of it, after few same preliminary fatigue analysis iterations, the amplitude of the white noise is taken as 100000 $(mm/s^2)^2/Hz$ again as in Chapter 3. The PSD profile is given in Figure 3-23.

As in Chapter 3, after supplying the FRF of all nodes of the unit base vibration load and the PSD profile, same settings done in the VibrationAnalysis box section of the nCode DesignLife program which is given in APPENDIX A.

In order to select the appropriate material from the material library of nCode DesignLife program, same tensile strength test with same geometry, Figure 3-24, with same number of specimens is conducted.

The tensile strength test is conducted with a strain rate of 0.5 min^{-1} again. The resultant UTS values of specimens are given in Table 4-6.

Table 4-6: UTS values of steel specimens

Test #	1	2	3	4	5	6	7	Mean	Standard Deviation
UTS (MPa)	648.8	644.8	640.7	648.1	638.0	685.6	669.6	653.7	17.4

According to Table 4-6, the mean UTS value of the steel specimens is 653 MPa. Hence, the steel material with 600 MPa UTS and 700 MPa are selected as shown in Figure 4-7 and Figure 4-8. Again the roughness option is selected as polished because in order to observe the crack initiation properly, the notched region of the beam is polished in the present study as in Chapter 3.

The S-N graphs of the selected materials are given in Figure 4-9 and Figure 4-10.

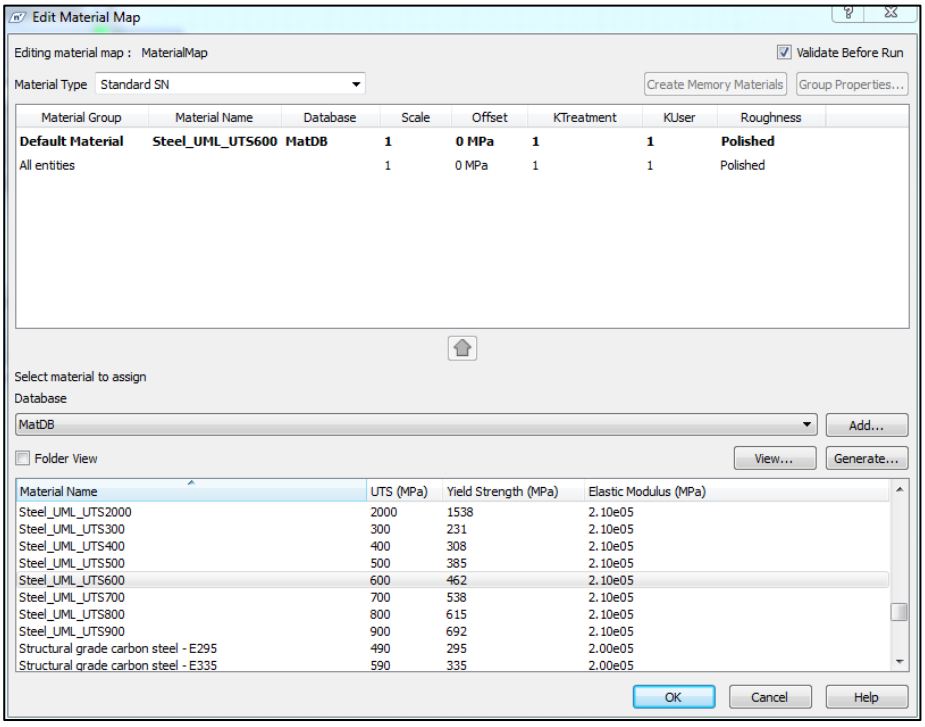

Figure 4-7: Material selection tool box in the nCode DesignLife program, 600 MPa UTS

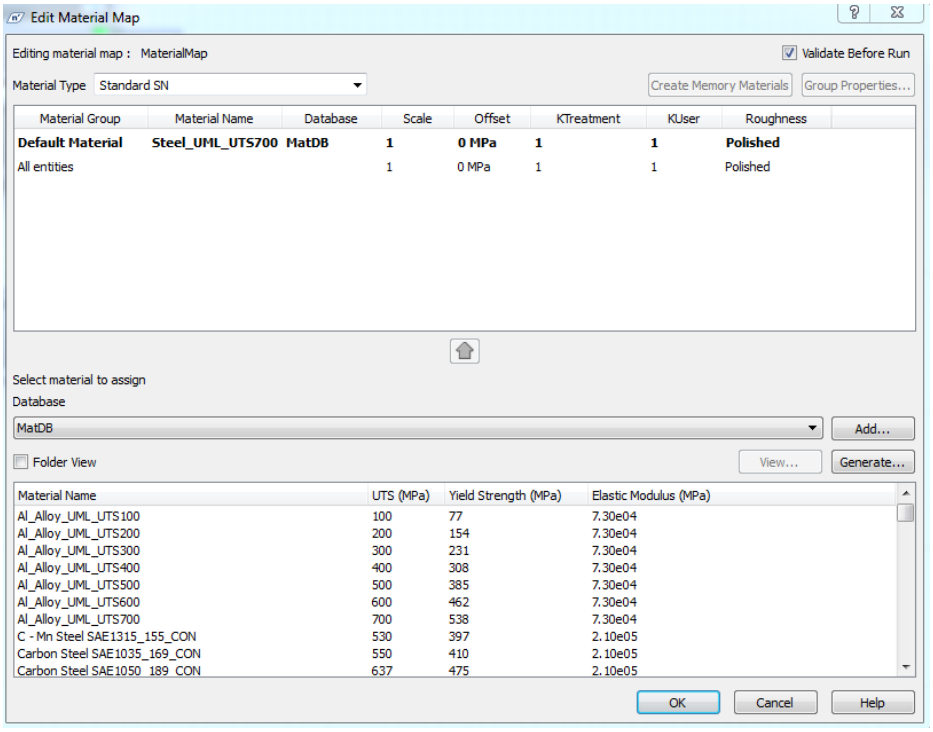

Figure 4-8: Material selection tool box in the nCode DesignLife program, 700 MPa UTS

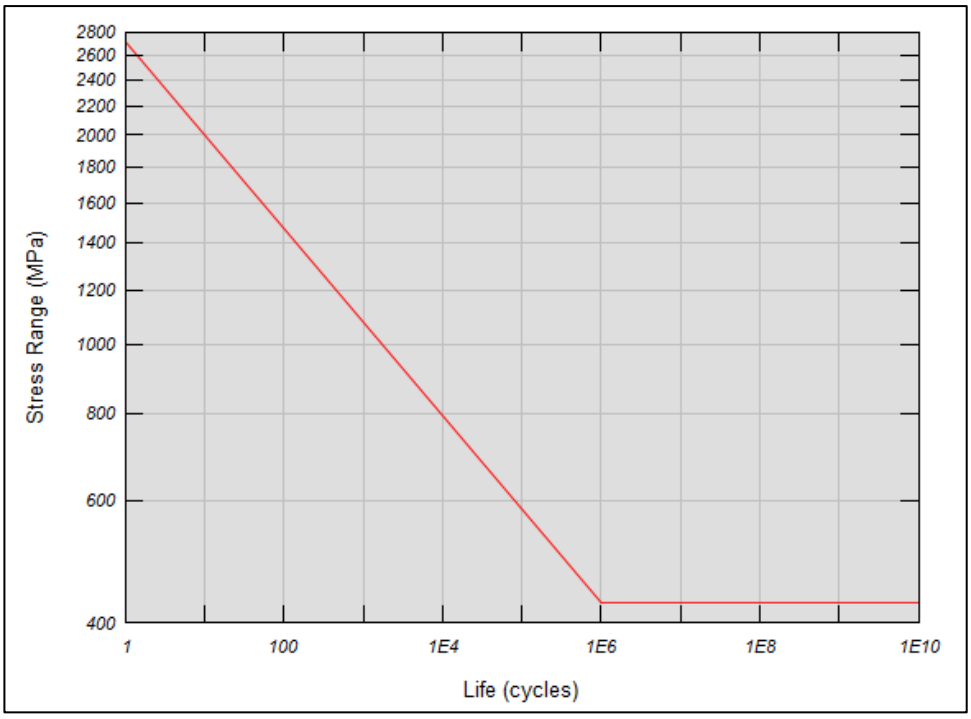

Figure 4-9: The S-N graph of Steel Alloy which has 600 MPa UTS

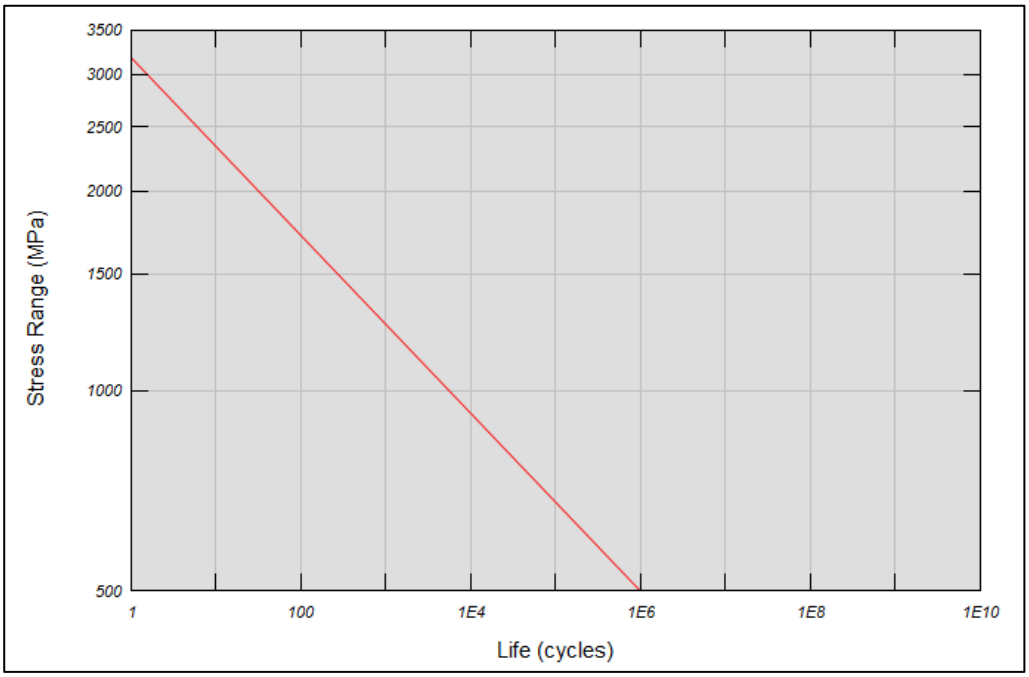

Figure 4-10: The S-N graph of Steel Alloy which has 700 MPa UTS

Again, as in Chapter 3, the results shows that the node 33815 has the minimum fatigue life. The results of the vibration fatigue analyses of the steel notched beam are given in Figure 4-11 and Figure 4-12 as the fatigue life in seconds. The detailed views of the fatigue life results are given in Figure 4-13 and Figure 4-14.

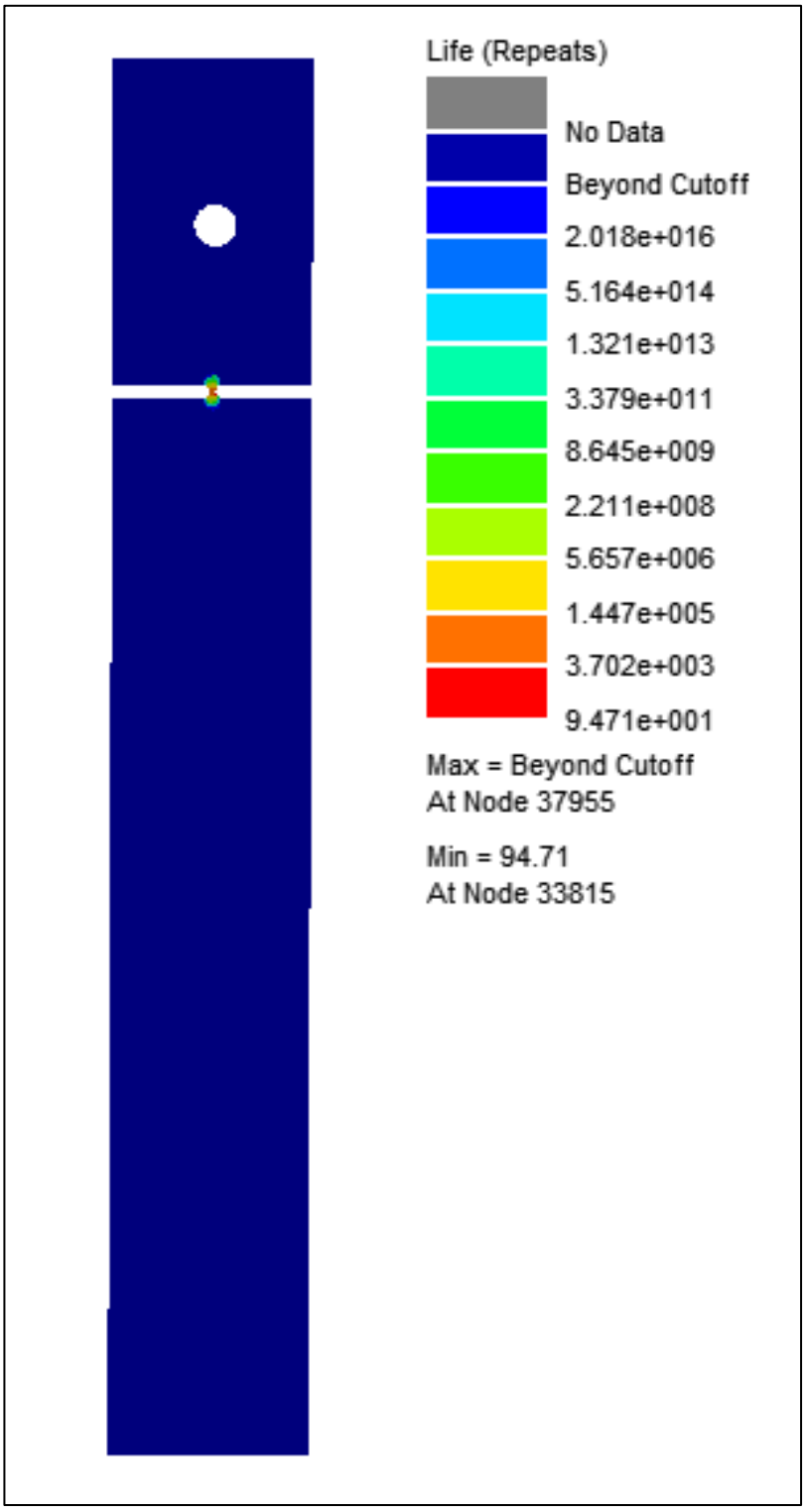

Figure 4-11: The vibration analysis result of the steel notched beam, 600 MPa UTS, life in seconds

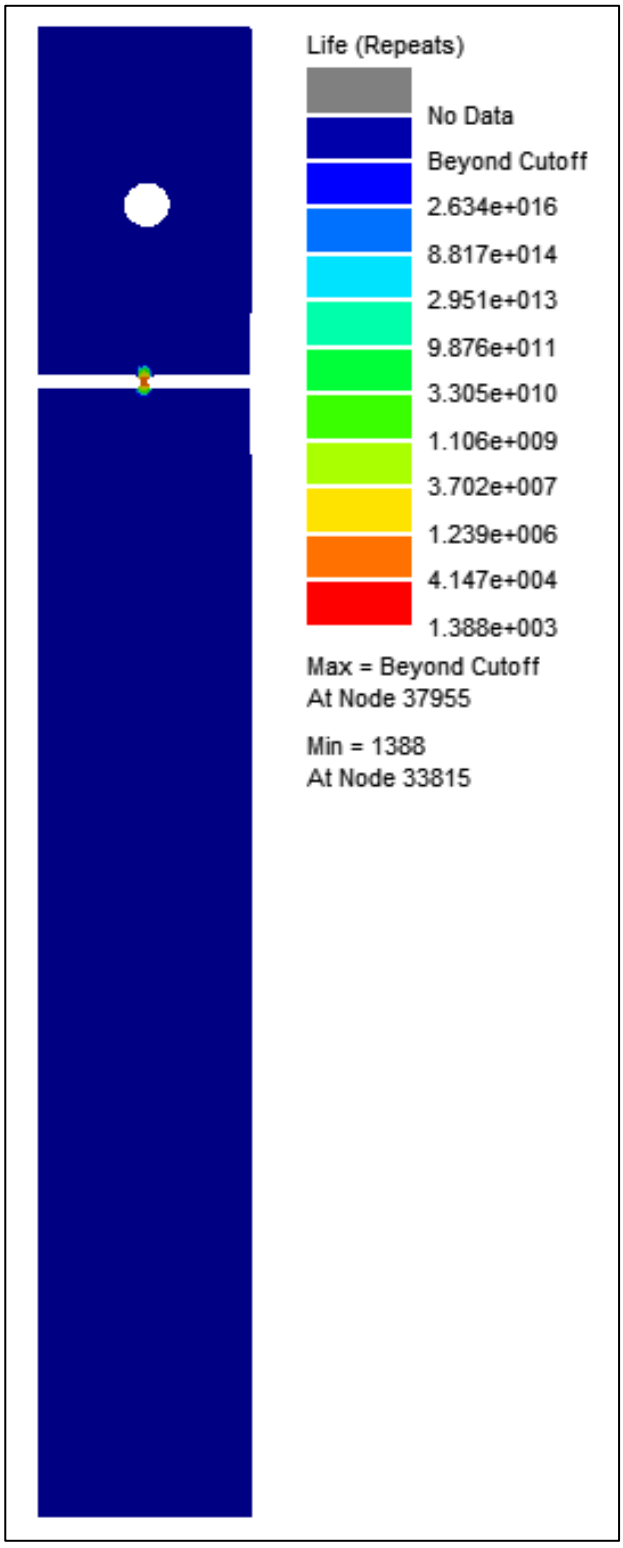

Figure 4-12: The vibration analysis result of the steel notched beam, 700 MPa UTS, life in seconds

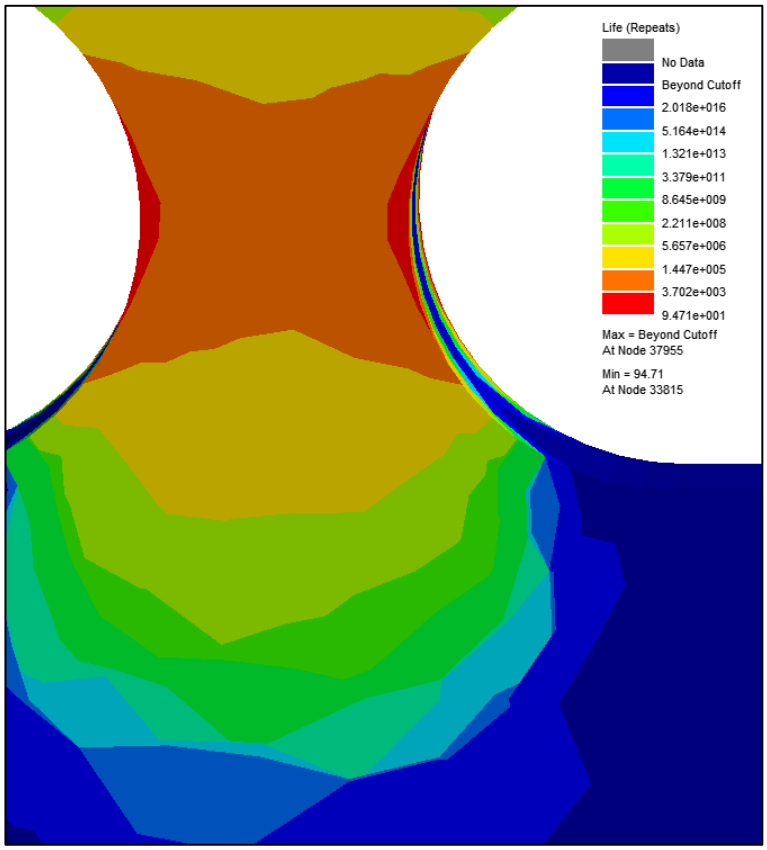

Figure 4-13: The detailed view of the result, 600 MPa UTS, [s]

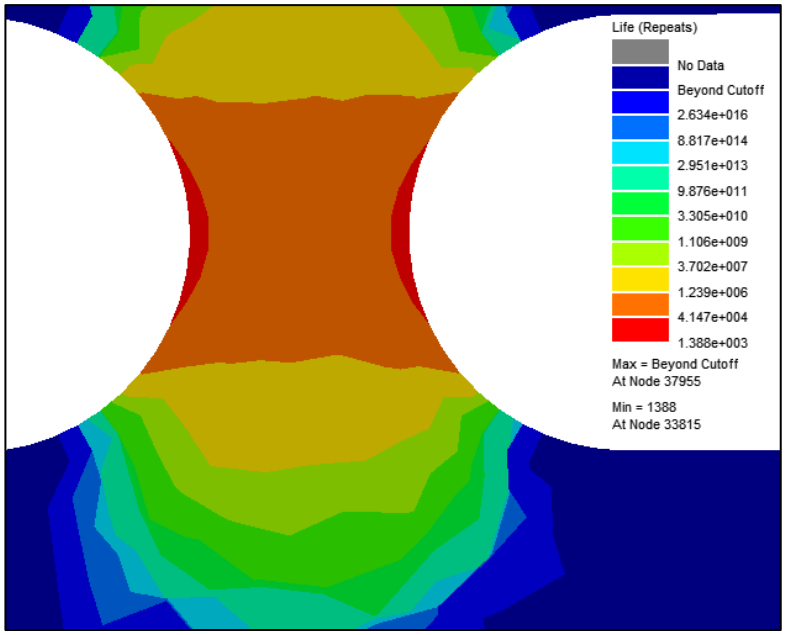

Figure 4-14: The detailed view of the result, 700 MPa UTS, [s]

According to the results, the life of the steel notched beam with 600 MPa UTS is 94.71 seconds or 1 minutes and 34.71 seconds around the corner of the notch and the life of the steel notched beam with 700 MPa UTS is 1388 seconds or 23 minutes and 8 seconds around the corner of the notch. In order to give a better visual comparison, Table 4-7 is given.

Table 4-7: Vibration fatigue analyses results of steel notched beam

	600 MPa UTS	700 MPa UTS
Time Results	94.71 seconds	1388 seconds
	1 min. 34.71 sec.	23 min. 8 sec.

4.6. Vibration Fatigue Test

In order to verify the fatigue analysis result of the steel notched beam, same vibration fatigue test is conducted as in Chapter 3. The prepared test setup is given in Figure 4-15.

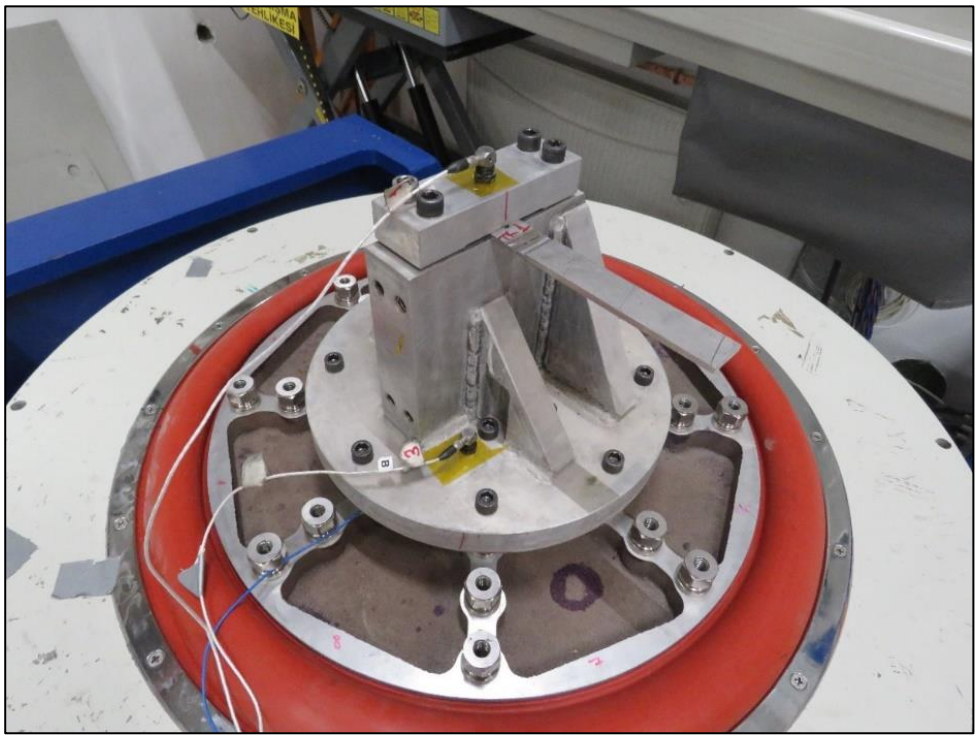

Figure 4-15: Test setup of the steel notched beam

The PSD profile of the test is set from 4 Hz to 2000 Hz due to the vibration table constraints as mentioned in Chapter 3. The experiment is conducted with 1 Hz increment again as in Chapter 3.

Again, as in Chapter 3, the crack initiations are monitored with human eye. When the crack initiation occurs, the test is terminated and the time of the test is recorded. Total of 13 steel notched beams are tested. The times from the test beginning to observed crack initiation are given in Table 4-8.

Table 4-8: Crack initiation times of the steel notched beams

Specimen	Life (s)	Time
1	480	8 min
2	398	6 min 38 sec
3	445	7 min 25 sec
4	673	11 min 13 sec
5	476	7 min 56 sec
6	500	8 min 20 sec
7	597	9 min 57 sec
8	521	8 min 41 sec
9	387	6 min 27 sec
10	475	7 min 55 sec
11	341	5 min 41 sec
12	408	6 min 48 sec
13	413	6 min 53 sec
Mean	470.3	7 min 50.3 sec
Standard Deviation	90.1	1 min 30.1 sec

Pictures of some of the steel notched beams with cracks are given in Figure 4-16, Figure 4-17, Figure 4-18 and Figure 4-19.

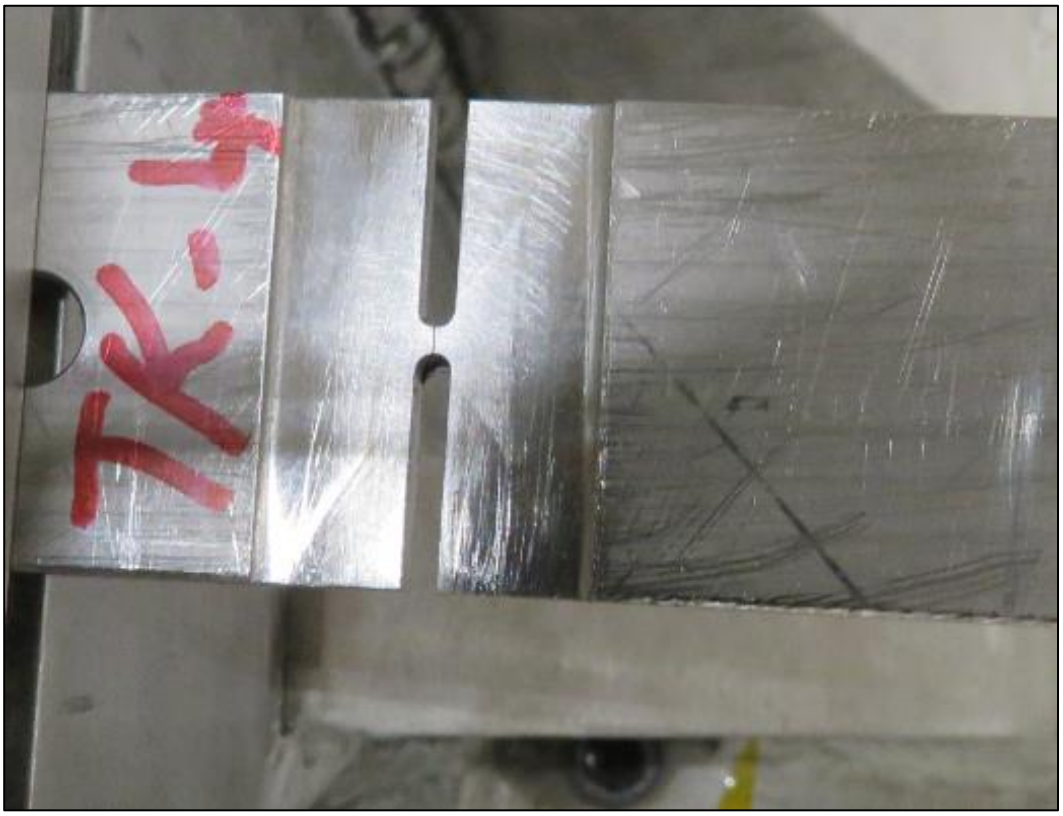

Figure 4-16: Steel notched beam with crack -Sample 1

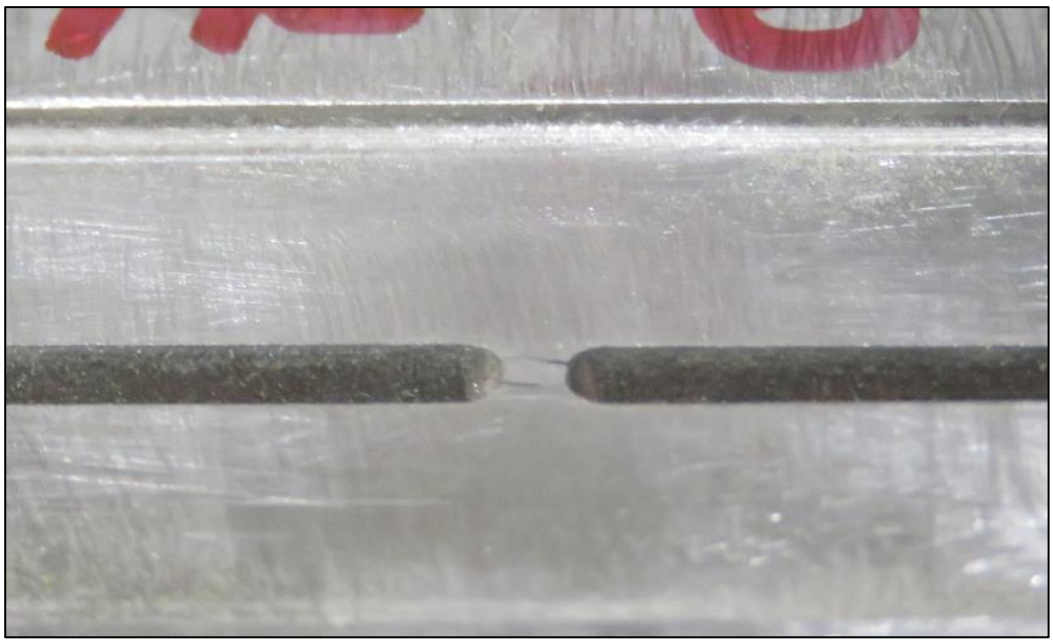

Figure 4-17: Steel notched beam with crack - Sample 2

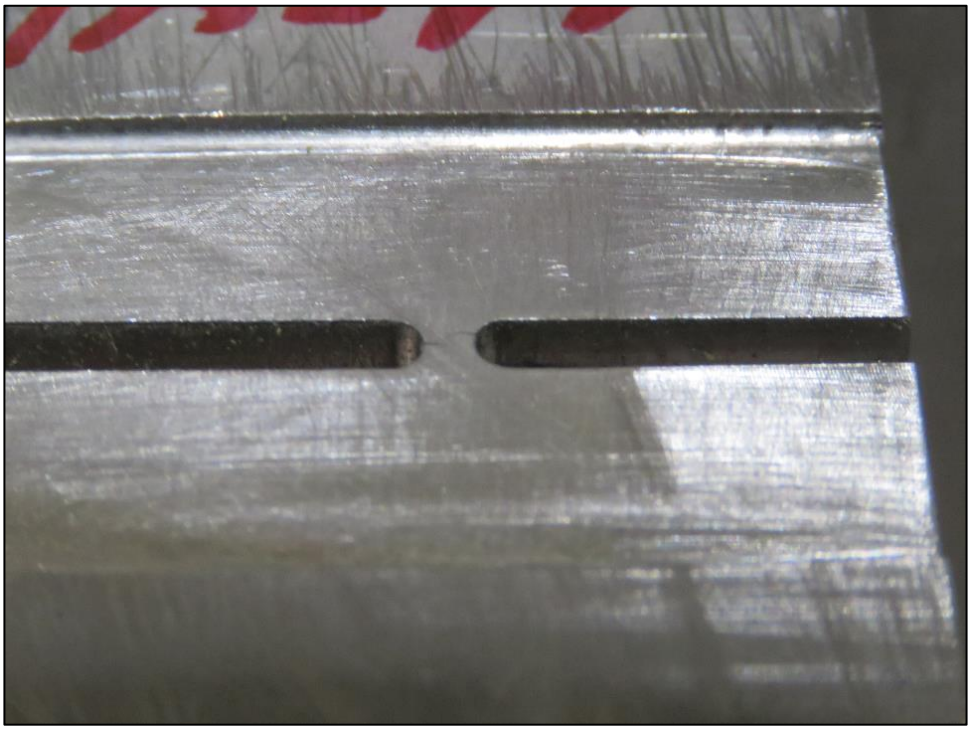

Figure 4-18: Steel notched beam with crack - Sample 3

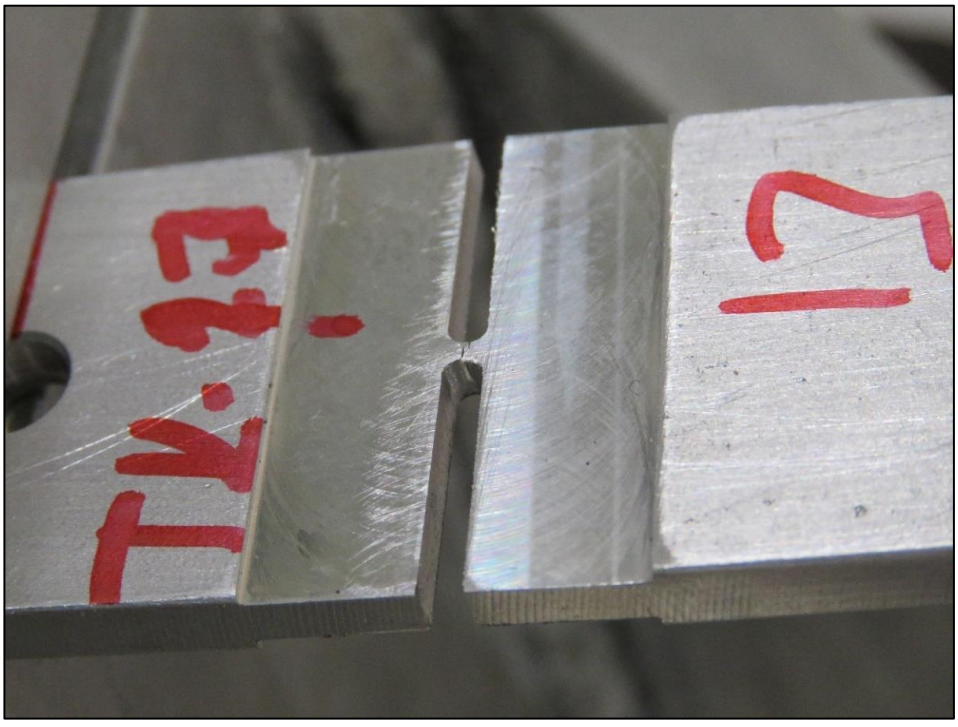

Figure 4-19: Steel notched beam with crack - Sample 4

4.7. Vibration Fatigue Analyses for Different Damping Ratio Values

In order to examine the effect of changing the damping ratio values, 0.03, 0.04 and 0.05 values are selected arbitrarily. Same analysis procedure, load and boundary conditions are carried out for the steel notched beams with 600 MPa UTS except for the damping ratio values. It should be noted that for the high participating modes 2, 4 and 5, the same damping ratio is given in MSC Patran environment for the frequency response analysis to study the effect of damping ratio on the fatigue life.

4.7.1. Vibration Fatigue Analysis Result for the Damping Ratio of 0.03

All the analysis procedures and load and boundary conditions are kept same and vibration fatigue analysis has been performed for a damping ratio of 0.03. Hence, in this section only the introduced damping ratio table and fatigue life result obtained from the analysis are presented. In the analysis, the applied damping ratio table is given in Table 4-9.

Table 4-9: Damping ratio table for the damping ratio of 0.03

Frequency [Hz]	Damping Ratio (%)
4	3
2000	3

The resultant fatigue life utilizing a damping ratio of 0.03 is obtained as 9.8 seconds and nCode DesignLife output page is given in Figure 4-20.

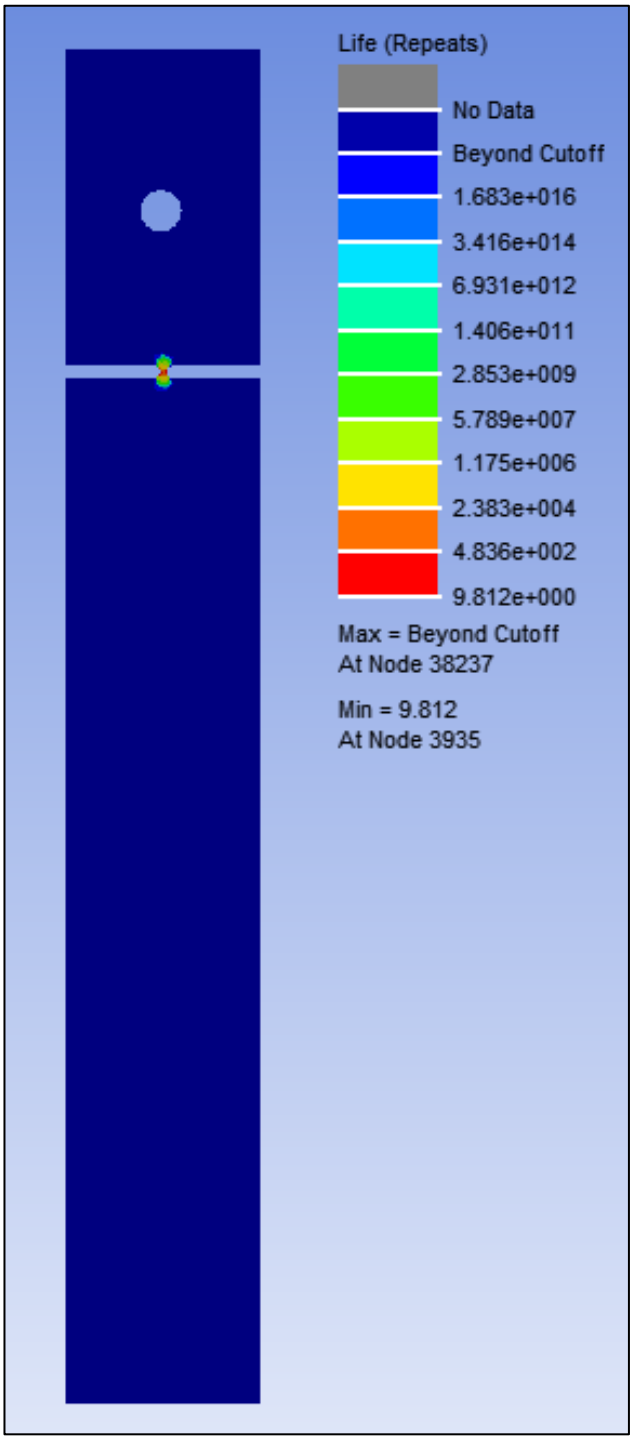

Figure 4-20: The fatigue life result with damping ratio of 0.03, life in seconds

4.7.2. Vibration Fatigue Analysis Result of Damping Ratio of 0.04

All the analysis procedures and load and boundary conditions are kept same and vibration fatigue analysis has been performed for a damping ratio of 0.04. Hence, in this section only the introduced damping ratio table and fatigue life result obtained from the analysis are presented. In the analysis, the applied damping ratio table is given in Table 4-10.

Table 4-10: Damping ratio table of 0.04

Frequency [Hz]	Damping Ratio (%)
4	4
2000	4

The resultant fatigue life utilizing a damping ratio of 0.04 is obtained as 57.1 seconds and nCode DesignLife output page is given in Figure 4-21.

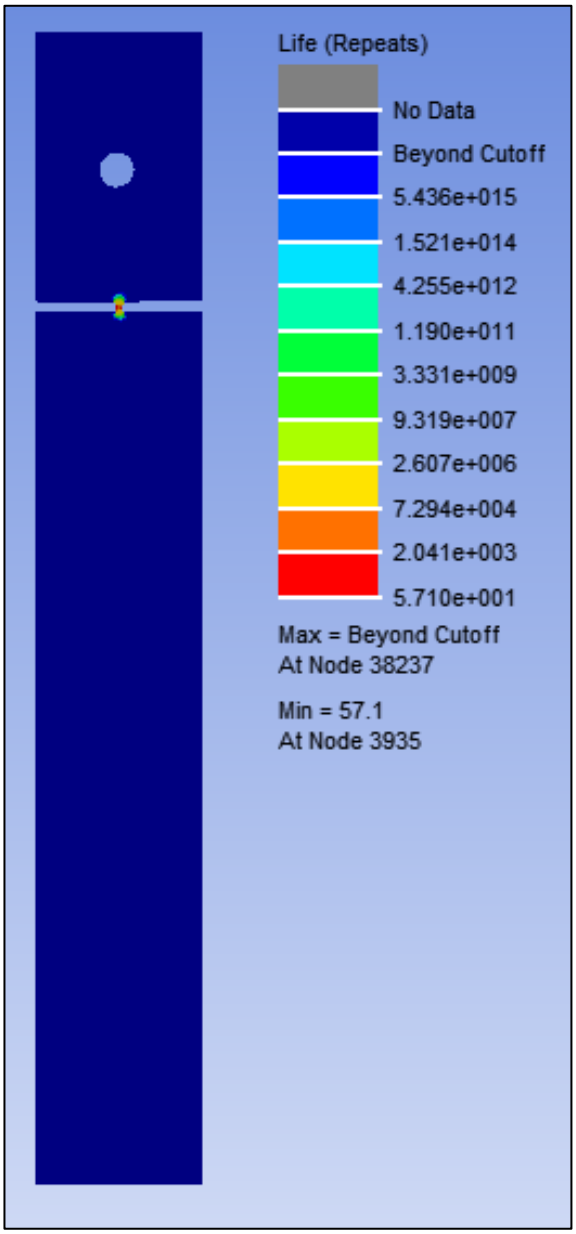

Figure 4-21: The fatigue life result with damping ratio of 0.04, life in seconds

4.7.3. Vibration Fatigue Analysis Result of Damping Ratio of 0.05

All the analysis procedures and load and boundary conditions are kept same and vibration fatigue analysis has been performed for a damping ratio of 0.05. Hence, in this section only the introduced damping ratio table and fatigue life result obtained

from the analysis are presented. In the analysis, the applied damping ratio table is given in Table 4-11.

Table 4-11: Damping ratio table of 0.05

Frequency [Hz]	Damping Ratio (%)
4	5
2000	5

The resultant fatigue life utilizing a damping ratio of 0.05 is obtained as 278.7 seconds and nCode DesignLife output page is given in Figure 4-22.

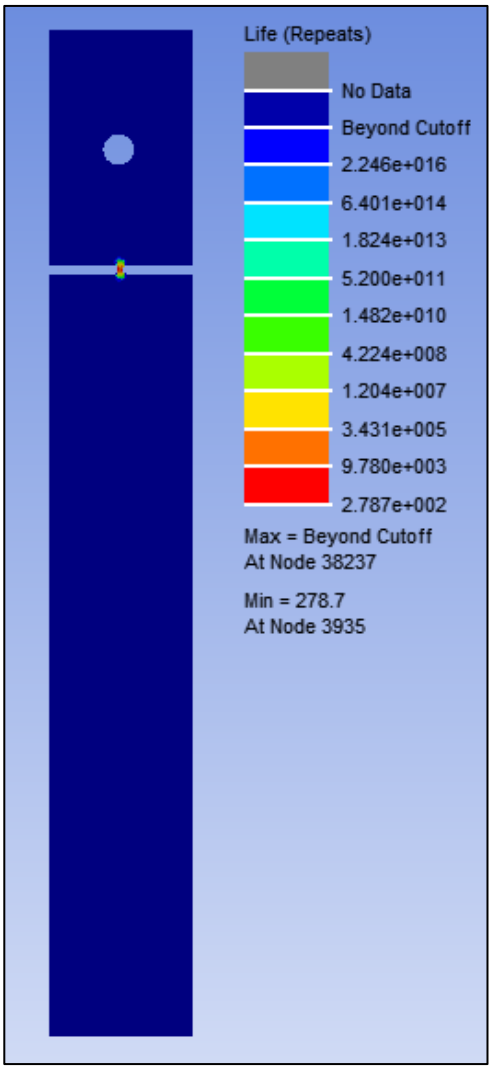

Figure 4-22: The fatigue life result with damping ratio of 0.05, life in seconds

4.7.4. The Comparison of Vibration Fatigue Analysis Results for Different Damping Ratios

The results of vibration fatigue analyses for different damping ratios are given in Table 4-12.

Table 4-12: The fatigue life results of the analyses

Damping Ratio (%)	Life (s)	Time
3	9.812	0 min 9.8 sec
4	57.1	0 min 57.1 sec
5	278.7	4 min 38.7 sec

As seen in Table 4-12, the result of the vibration fatigue analysis highly depends on the damping ratios. When the damping ratio is increased, fatigue life also increases drastically because the stress peak in the resonance regions decrease, as also indicated in [29]. Hence, when the stresses in the resonance regions decrease, the fatigue damage (D) decreases and the fatigue life (1/D) increases.

CHAPTER 5

RESULT AND CONCLUSION

5.1. Notched Beams Analyses and Test Results

In this thesis study, the vibration induced mechanical fatigue analyses and tests of aluminum and steel notched beams are conducted. The summary of the results are given in Table 5-1.

Table 5-1: Results summary

	Aluminum			**Steel**		
	Analyses		**Test**	**Analyses**		**Test**
Time Results	**300 MPa UTS**	**400 MPa UTS**	13 min. 52.5 sec.	**600 MPa UTS**	**700 MPa UTS**	7 min. 50.3 sec.
	3 min. 27.7 sec.	387 min. 40 sec.		1 min. 34.7 sec.	23 min. 8 sec.	

According to the Table 5-1, the results seems to be not matching however in fatigue discipline, these type of results, lower UTS value results, are accepted because the analyses stay in the safe side. The lower UTS value results of the analyses are shorter than the results of the tests as expected. The reasons for the difference between the vibration fatigue tests and analysis are attributed to the following:

- As seen from Table 5-1, the selected UTS value is highly effective on the results. During the vibration fatigue analyses, the UTS values selected as multiplies of 100 MPa. However, the real UTS values are 320.3 MPa for aluminum and 653.7 MPa for steel.
- During the vibration fatigue tests, crack initiation is spotted by the eye inspection. Since the formation of micro cracks cannot be detected accurately

with eye inspection, the real crack initiation time and observed crack initiation time may differ. It is highly probable that the real crack initiation times in vibration fatigue tests are much earlier. To remedy this, it is recommended to use high speed camera to catch the start of the crack initiation.

- The material properties of the notched beams used in the analyses and material properties of tested beams can be slightly different.
- In the nCode DesignLife program, for both aluminum and steel specimens, the available material UTS values are selected lower than the actual UTS values determined by the tensile tests. Hence, the corresponding fatigue strengths used in the vibration fatigue analysis are also lower than actual fatigue strengths of the aluminum and steel materials. This has a lowering effect on the fatigue life as determined by the vibration fatigue analysis.
- In the vibration fatigue analysis, structural damping calculated from the modal damping which is obtained by the modal testing is used. Calculation of modal damping is highly sensitive to the experimental setup and it is very critical that the damping ratio values should be determined accurately. In this thesis study, the modal test and the vibration fatigue test setups that are used are different because of the busy workload of the vibration table. This may have also caused deviations in the actual damping ratios to be used in the vibration fatigue testing. In Chapter 4, the effect of damping on the fatigue life is studied. It is seen that modal damping value is highly effective on the fatigue life. Hence, it is recommended to repeat the modal damping tests in the same test setup as the vibration fatigue test setup, if possible by alternative means, to ensure that the experimentally determined damping values are reliable.

5.2. Conclusion

In this thesis study, the vibration induced fatigue is studied both numerically and experimentally.

In the present thesis study, in chapter 1, description of mechanical fatigue, some history of mechanical fatigue, literature survey and damage theories of mechanical fatigue are given. In chapter 2, theory of random vibration fatigue and used methods are given. Chapter 3 consists of vibration fatigue analysis and tests of aluminum notched beams. Chapter 4 consists of vibration fatigue analysis and tests of steel notched beams.

In the broadband frequency intervals, the resonance frequencies or natural frequencies of the structures are likely to be disturbed or excited. When the resonance regions are disturbed, the time domain analysis become short and there is necessity to do the analysis in frequency domain. Due to that necessity, in this thesis, the frequency domain mechanical fatigue analysis is studied.

It is obvious that the numerical fatigue life analysis highly depends on the stress results of the finite element model. Little increase of the stresses causes a big decrease in the fatigue life. Moreover, in the analyses, the predicted damping ratios affect the stress amplitudes of the resonance regions significantly. Hence, one should determine the damping ratios accurately for each natural frequency.

In order to verify the vibration fatigue analysis methodology, the aluminum and steel notched beams are designed, analyzed and tested. Firstly, in order to decide the frequency range of interest, preliminary modal analyses are conducted. Secondly, the modal tests are carried out in order to determine the damping ratios associated with the resonance regions. Then, in order to extract the response of the beams to unit base acceleration load, the frequency response analyses are carried out. Then, vibration fatigue analyses are carried out. In the fatigue analyses, in order to select the proper material, the tensile testing of the beam material are carried out. Finally the vibration fatigue tests are conducted in a vibration table.

It is noticed that the eye inspection method of crack initiation falls short in vibration fatigue testing. Since, the real time eye monitoring is insufficient to detect crack initiation in vibrating parts, another method should be implemented in order to determine the accurate crack initiation time. One option is to use high speed camera to catch the start of the crack initiation when beam is still vibrating. Or, the test could be stopped at frequent intervals and the notched region could be checked for the onset of crack initiation. Vibration based crack initiation detection can be also a reasonable option. By means of a highly sensitive accelerometer mounted on the notched beam, vibration amplitudes can be monitored to detect the crack initiation. However, this study requires many tests and cross check for reliability. Other options could be to use non-destructive inspection (NDI) methods. For instance, periodic penetrant testing, acoustic emission testing, electromagnetic testing, infrared and thermal imaging testing, optical microscopy testing with stereoscopic microscope etc. can be implemented. However, the use of these NDI methods make the tests longer because to perform the NDI tests, vibration tests have to be paused frequently.

5.2.1. Future Work

As for the future work, the method of monitoring the crack initiation time can be improved. In this thesis study, the eye inspection method is used and it is obvious that this method falls short while determining the crack initiation time on the vibrating parts. Moreover, time domain and frequency domain analyses can be compared for a sample application. Also, different PSD cycle counting methods other than Dirlik such as Lalanne, NarrowBand and Steinberg etc. can be investigated. Furthermore, whether or not the vibration fatigue analysis can be applicable for the non-metal materials such as solid rocket propellants could be investigated as a future work.

REFERENCES

1. American Society for Testing and Materials, *"Standard Definitions of Terms Relating to Fatigue Testing and Statistical Analysis of Data",* ASTM E 206-72, 1972.
2. B. KOÇER, "*Vibration Fatigue Analysis of Structures Under Broadband Excitation",* MSc Thesis submitted to Mechanical Engineering Department, METU, June 2010.
3. S. ARIDURU, "*Fatigue Life Calculation by Rainflow Cycle Counting Method"*, MSc Thesis submitted to Mechanical Engineering Department, METU, December 2004.
4. R. A. SMITH, "*The Versailles railway accident of 1842 and the first research into metal fatigue*", Fatigue '90 MCE Publications, vol. 4, pp. 2033–2041, Birmingham, 1990.
5. "Versaille rail accident", Last Edit: 19/07/2017, [online], Accessed on 28/08/2017, Accessible: https://en.0wikipedia.org/index.php?q=aHR0cHM6Ly9lbi53aWtpcGVkaWEub3JnL3dpa2kvVmVyc2FpbGxlc19yYWlsX2FjY2lkZW50
6. C. LALANNE*, "Fatigue Damage"*, Volume 4, 2nd Edition, Chapter 1, ISTE Ltd., 2009.
7. Y. ELDOĞAN, "*Vibration Fatigue Analysis of Structures Installed on Air Platforms"*, MSc Thesis submitted to Mechanical Engineering Department, METU, February 2012.
8. "5 Disasters Caused by Material Fatigue and What We Learned From Them", Last Edit:10/06/2016, [online], Accessed on 05/04/2018, Accessible: https://www.element.com/nucleus/2016/06/10/5-disasters-caused-by-material-fatigue-and-what-we-learned-from-them
9. J. OUELLETTE, "*Incredible physics behind the deadly 1919 Boston Molasses Flood*", Last Edit:24/11/2016, [online], Accessed on 05/04/2018,

Accessible: https://www.newscientist.com/article/2114116-incredible-physics-behind-the-deadly-1919-boston-molasses-flood/

10. A. RIBERIO, J. CORREIA, A. DE JESUS, "*Evolution of Fatigue History"*, 21st Brazilian Congress of Mechanical, October 24-28, 2011.
11. "The remarkable salvage of BOAC's lost Comet", Last Edit:19/09/2011, [online], Accessed on 05/04/2018, Accessible: https://www.lookandlearn.com/blog/13348/the-remarkable-salvage-of-boacs-lost-comet/
12. A. ALMAR-NAESS, P. J. HAAGENSEN, T. MOAN, T. SIMONSEN, "*Investigation of the Alexander L. Kielland Failure—Metallurgical and Fracture Analysis"*, Journal of Energy Resources Technology, January, 1982.
13. "Friday March 30,2012", Last Edit: 30/03/2012, [online], Accessed on: 05/04/2018, Accessible: http://kalw.org/post/friday-march-302012#stream/0
14. G.S. CAMPBELL, R. LAHEY, "A survey of serious aircraft accidents involving fatigue fracture", International Journal of Fatigue, Vol 6 No 1, January, 1984.
15. "Aloha Airlines Flight 243", Last Edit:08/08/2017, [online], Accessed on 28/08/2017, Accessible: https://en.0wikipedia.org/index.php?q=aHR0cHM6Ly9lbi53aWtpcGVkaWEub3JnL3dpa2kvQWxvaGFfQWlybGluZXNfRmxpZ2h0XzI0Mw
16. B. O'CONNOR, "*Eschede Train Disaster",* Leadership ViTS Meeting, NASA, May 7, 2007, Accessed on 05/04/2018, Accessible: https://sma.nasa.gov/docs/default-source/safety-messages/safetymessage-2007-05-01-eschedetraindisaster-vits.pdf?sfvrsn=aea91ef8_6
17. "Eschede, Germany ICE High Speed Train Disaster", [online], Accessed on: 05/04/2018, Accessible on: http://danger-ahead.railfan.net/features/eschede2.htm

18. “Dynamic Tests: What, When and Why?”, 13/04/2014, R. TREHAN, [online], Accessed on 28/08/2017, Accessible: https://www.cati.com/blog/2014/04/dynamic-tests-what-when-and-why/
19. N. W. M. BISHOP, “*Vibration Fatigue Analysis in the Finite Element Environment”*, XVI Encuentro Del Grupo Español De Fractura, Spain, 1999.
20. H.Y. LIOU, W.F. WU, C.S. SHIN, “*A Modified Model for The Estimation of Fatigue Life Derived from Random Vibration Theory”*, Probabilistic Engineering Mechanics, 1999, Vol.14, pp.281-288.
21. M. AYKAN, *“Vibration Fatigue Analysis of Equipments Used in Aerospace”,* MSc Thesis submitted to Mechanical Engineering Department, METU, June 2005.
22. A. FATEMI, L. YANG, “*Cumulative Fatigue Damage and Life Prediction Theories: a Survey of the state of the Art for Homogeneous Materials”*, International Journal of Fatigue, Vol.20, no. 1, page 25, 1998.
23. A. HALFPENNY, “*A Frequency Domain Approach for Fatigue Life Estimation from Finite Element Analysis”*, Whitepaper, [online], nCode International Ltd., Sheffield UK, Accessed on 30/08/2017, Accessible: http://www.ncode.com/fileadmin/mediapool/nCode/downloads/Whitepaper_nCode_frequency_domain_fatigue-Halfpenny.pdf
24. N. BISHOP, A. WOODWARD, “Fatigue Analysis of a Missile Shaker table Mounting Bracket”, RLD Limites, UK, MSC Software, UK, Accessbile: https://www.academia.edu/1058168/Fatigue_Analysis_of_a_Missile_Shaker_Table_Mounting_Bracket?auto=download
25. C. LALANNE, *“Mechanical Vibration & Shock, Fatigue Damage”*, Volume IV, Taylor and Francis Books, Inc., 1999.
26. C. GENÇ, *“Mechanical Fatigue and Life Estimation Analysis of Printed Circuit Board Components”,* MSc Thesis submitted to Mechanical Engineering Department, METU, August 2006.
27. G. PETRUCCI, B. ZUCCARELLO, “*On the estimation of the fatigue cycle distribution from spectral density data*”, Proceedings of the Institution of

Mechanical Engineers, Part C: Journal of Mechanical Engineering Science, vol. 213, no. 8, 1999.

28. N. W. M. BISHOP, F. SHERRATT, "*Finite Element Based Fatigue Calculations*", 1st Edition, NAFEMS LTD., UK, 2000.
29. G.İ. DEMİREL, A. KAYRAN, *"The Effect of Modal Damping on Random Vibration Metal Fatigue Analysis"*, AIAC-2017-044, 9th Ankara International Aerospace Conference, METU , TURKEY, 2017.
30. T. DİRLİK, "Application of Computers in Fatigue Analysis", Ph.D. Thesis submitted to Engineering Department, University of Warwick, January 1985.
31. S. ÖZSOY, *"Vibration Induced Stress and Accelerated Life Analyses of an Aerospace Structure",* MSc Thesis submitted to Mechanical Engineering Department, METU, January 2006.
32. MIL-STD-810E, "*Environmental Test Methods and Engineering Guidelines*", Department of Defense Test Method Standard, USA, 1989.
33. *International Test Operations Procedure* (ITOP) 1-1-050, Development of Laboratory Vibration Test Schedules, 1993.
34. Y. LEE, J. PAN, R. B. HATHAWAY, M. E. BARKEY, *"Fatigue Testing and Analysis (Theory and Practice),* 2005, Elsevier, USA.
35. United States., & William J. Hughes Technical Center (U.S.). (2012). MMPDS-07: Metallic materials properties development and standardization (MMPDS). Washington, D.C.: Federal Aviation Administration.
36. "Finite Element Model Supported File Types", [online], Accessed on 21/12/2017, Accessible: https://www.efatigue.com/fem/background/filetypes.html
37. MSC. Software, Dynamic Analysis User's Guide, MSC Nastran 2013.1 Documentation, Chapter 4-Frequency Response Analysis, November 2013.
38. M. ÇELİK, M. AYKAN, "Vibration fatigue analysis and multi-axial effect in testing of aerospace structures", Mechanical Systems and Signal Processing 23 (2009) 897–907, Elsevier.

39. C. BRACCESI, F. CIANETTI, L. TOMASSINI, “An innovative modal approach for frequency domain stress recovery and fatigue damage evaluation”, International Journal of Fatigue 91 (2016) 382–396, Elsevier.
40. C. BRACCESI, F. CIANETTI, L. TOMASSINI, “Random fatigue. A new frequency domain criterion for the damage evaluation of mechanical components”, International Journal of Fatigue 70 (2015) 417–427, Elsevier.
41. A. CARPINTERI, G. FORTESE, C. RONCHEI, D. SCORZA, A. SPAGNOLI, S. VANTADORI, “Fatigue life evaluation of metallic structures under multiaxial random loading”, International Journal of Fatigue 90 (2016) 191–199, Elsevier.
42. E. A. AL-BAHKALI, H. ELKENANI, M. SOULI, “Fatigue life estimate of landing Gear’s leg using modal analysis”, Int. Jnl. of Multiphysics Volume 8, Number 2, 2014.
43. M. M. RAHMAN, A. K. ARIFFIN, N. JAMALUDIN, C. H. C. HARON, R. A. BAKAR, “Fatigue Life Prediction of Two-Stroke Free Piston Engine Mounting Using Frequency Response Approach”, European Journal of Scientific Research, ISSN 1450-216X Vol.22 No.4 (2008), pp.480-493.
44. M. MRSNIK, J. SLAVIC, M. BOLTEZAR, “Vibration fatigue using modal decomposition”, Mechanical Systems and Signal Processing 98 (2018) 548–556, Elsevier.
45. A. R. KUMAR, S. R. BALAKRISHNAN, S. BALAJI, “Design Of An Aircraft Wing Structure For Static Analysis And Fatigue Life Prediction”, International Journal of Engineering Research & Technology (IJERT), Vol. 2 Issue 5, May – 2013.
46. S. VANTADORI, I. ITURRIOZ, C. RONCHEI, “Discussion on fatigue life estimation under multiaxial random loading: Comparison between time- and frequency-domain approach”, Theoretical and Applied Fracture Mechanics 96 (2018) 134–145, Elsevier.

47. G. A. PAPAGIANNOPOULOS, G. D. HATZIGEORGIOU, “On the use of the half-power bandwidth method to estimate damping in building structures”, Technical Note, Soil Dynamics and Earthquake Engineering 31 (2011) 1075–1079, Elsevier.
48. A. FLAGA, J. SZULEJ, P. WIELGOS, “Comparison of determination methods of vibration’s damping coefficients for complex structures”, Budownictwo i Architektura 3 (2008) 53-61.

APPENDICES

A. VibrationAnalysis Box of nCode DesignLife Program

Name	Value	Description
General		
LoggingLevel	Info	The amount of detail to output to the message window during the run
ResultsUpdateInterval	10	Time interval between processing result output
AnalysisGroup		
AnalysisGroup_GroupNames	*	Groups to process
AnalysisGroup_MaterialAssignmentGroup	SelectionGroup	Sets the grouping type to be used for material mapping
AnalysisGroup_SelectionGroupType	FEInput	Sets the grouping type to be used for extracting results
AnalysisGroup_ShellLayer	Top	Shell layer to use
AnalysisGroup_SolutionLocation	AveragedNodeOnElement	Solution location
AnalysisGroup_StressUnits	MPa	The units to use for stress values
Compressed results (for display)		
Compressed results (for display)_ChannelPerEvent	False	Whether to create a channel for each duty cycle event
Job		
Job_NumAnalysisThreads		The number of simultaneous analysis threads to use for this job
SNEngine		
SNEngine_CertaintyOfSurvival	50	Required confidence level on damage results
SNEngine_CombinationMethod	CriticalPlane	The method used to combine component stresses/strains
SNEngine_MeanStressCorrection	None	The method used to correct the damage calculation for mean stress
SNEngine_OutputEventResults	False	Whether to output results per event or not for duty cycle processing
VibrationLoad		
VibrationLoad_ExposureDuration	1	Exposure duration in seconds
VibrationLoad_FrequencySelectionMethod	LoadingAndFRFFrequencies	Method used for selecting frequency points
VibrationLoad_InterpolationMethod	LogLog	Method to use when interpolating the loading spectra
VibrationLoad_LoadingMethod	PSD	Vibration loading method
VibrationLoad_PSDCycleCountMethod	Dirlik	PSD cycle count method
VibrationLoad_SweepRate	1	Sweep rate applied in terms of the sweep type
VibrationLoad_SweepType	LinearHzPerSec	Sweep type using sweep rate provided

Figure A-0-1: The detail settings of VibrationAnalysis box